POLITECNICO DI MILANO
DEPARTMENT OF CIVIL AND ENVIRONMENTAL ENGINEERING
DOCTORAL PROGRAMME IN STRUCTURAL, SEISMIC AND GEOTECHNICAL
ENGINEERING

Structural Health Monitoring of Offshore Structures using Data-Based Methods

Doctoral Dissertation of:
Masoud Salar

Supervisors:
Prof. Luca Martinelli
Prof. Carlo De Michele

Tutor:
Prof. Luca Martinelli

The Chair of the Doctoral Program:
Prof. Stefano Mariani

11 April 2022 - XXXIII Cycle

Acknowledgements

I would like to highly thank all the individuals who have supported and encouraged me throughout my Ph.D. period to accomplish this work.

*First and foremost, my deepest and warm gratitude is addressed to my supervisors, **Prof. Luca Martinelli** and **Prof. Carlo De Michele**, for all the support, guidance, patience, and invaluable suggestions they gave me during this research period.*

*I would also like to express my sincere thanks to the committee members, **Prof. Costas Papadimitriou** from the University of Thessaly, **Prof. Stefano Mariani** from Politecnico di Milano, **Prof. Saeed Eftekhar Azam** from the University of New Hampshire for their valuable advice, suggestions, and comments on this dissertation.*

Special thanks to Dr. Alireza Entezami, for sharing his extensive knowledge in the structural health monitoring field and data-driven techniques and for his guidance during this study.

Additionally, since this research study has focused on datasets acquired from some well-known benchmark structures, I would like to appreciate the Los Alamos National Laboratory in the USA, the Earthquake Engineering Research Laboratory at the University of British Columbia in Canada, and the SMC Group at the Harbin Institute of Technology in China for accessing those datasets. Moreover, I express my sincere gratitude to Prof. Mohammad Reza Tabeshpour from the Department of Mechanical Engineering at the Sharif University of Technology in Iran for accessing their experimental datasets.

Last but not least, I would like to give my profound appreciation to my lovely family for everything they have done for me. More specially, I appreciate my parents who always support and encourage me during my studies and life.

Masoud Salar

I

Abstract

STRUCTURAL Health Monitoring (SHM) is a growing and interesting topic in the offshore industry. The oil and gas industries are dealing with aging infrastructure and are looking for possible and reliable ways to extend the life span of these structures, whereas the wind energy industry is significantly investing in such structures. This makes a lot of unique challenges for health monitoring of offshore structures, which all come together with a significant concept known as uncertainty. These kinds of structures are highly prone to failure risk due to their uncertain environment and severe environmental variability. Moreover, many existing structures have not been monitored yet, and those have experienced various loading and operational conditions during their operational life, which are unknown. Due to the inaccessibility of many wind farms, typical inspection procedures are costly and, in some circumstances, dangerous. On this basis, SHM seeks to overcome these concerns by establishing technologies that enable an automated online evaluation of the state of structures to improve decision-making.

The main aim of SHM is to assess the integrity of these structures for early damage detection, damage localization, and damage quantification. In recent years, data-based techniques based on statistical approaches present efficient ways to diagnose damage by using measured vibration responses of structures. These approaches are generally based on two main steps, including feature extraction and statistical decision-making. Time series analysis and novelty detection approaches are effective tools for these steps. Despite the advantages of data-based damage detection methods, those may give unreliable results of damage diagnosis in terms of false alarm and false detection errors. These errors may lead to some challenging issues including inappropriate feature extraction, inaccurate feature classification for damage detection due to the adverse effects of environmental and operational variability as well as high-dimensional features. To overcome these challenges, this dissertation proposes data-based methods in the feature extraction and classification steps. The proposed data-based approaches are related to an iterative time series-based method for feature extraction, a robust multidimensional scaling-based method, and a clustering-based novelty detection approach for early damage detection, damage localization, and damage quantification.

Eventually, experimental and real structures are investigated to validate the efficacy and accuracy of the proposed approaches. The results indicated that the methods described in this study are reliable and effective solutions for SHM of civil and offshore structures under ambient excitations and environmental and operational variability.

Abbreviations

Abbreviation	Full Form
ACF	Autocorrelation Function
AIC	Averaged Integrations of Coherence
AR	AutoRegressive
ARMA	AutoRegressive-Moving Average
ARMAX	AutoRegressive Moving Average with eXogenous
ARX	AutoRegressive with eXogenous
BM	Block Maxima
CMSE	Cross-Modal Strain Energy
CNN	Convolution Neural Networks
COMAC	Coordinate Modal Assurance Criterion
DSF	Damage-Sensitive Feature
ERA	Eigensystem Realization Algorithm
EVT	Extreme Value Theory
FE	Finite Element
GEV	Generalized Extreme Value
GOF	Goodness-Of-Fit
GP	Generalized Pareto
IMSE	Iterative Modal Strain Energy
LAF	Linear Adaptive Filter
LSTM	Long and Short-Term Memory
MAC	Modal Assurance Criterion

Abbreviation	Full Form
MSECR	Modal Strain Energy Change Ratio
MSED	Modal Strain Energy Decomposition
MSF	Modal Scale Factor
NExT	Natural Excitation Technology
PACF	Partial Autocorrelation Function
PCA	Principal Component Analysis
PLS	Partial Least Square
POT	Peak-Over-Threshold
PP	Peak Picking
RD	Relative Difference
RDT	Random Decrement Technique
SHM	Structural Health Monitoring
SPR	Statistical Pattern Recognition
SVM	Support Vector Machine
VAR	Vector AutoRegressive

Contents

List of Figures

List of Tables

Introduction

D UE to the fact that numerous offshore jacket structures around the world have already exceeded their expected lifespan, there is an increasing interest in implementing structural health monitoring (SHM) to extend the lifetime of the jackets to guarantee structural integrity, safe operation, failure prevention, and control of further degradation. Although performing SHM to existing and old jackets bears the cost of purchase and installation, the outcome in the long term will optimize operation and maintenance costs. This could be one of the main reasons that SHM has received great attention in recent decades, both in academic study and in industry [1].

1.1 Structural Health Monitoring

Structural health monitoring is the procedure of gathering data from the structure of interest; understanding the condition of that structure by utilizing the collected data; and assisting and updating the process of decision-making concerning the structure's operation [2].

Detection of damage is a part of the larger issue of damage identification. The aim of a monitoring system should be to gather *sufficient* information about the damage to perform proper remedial action so as to return the system to a high-quality operation or at least to ensure safety. Furthermore, efficiency indicates that the monitor should return only the *necessary* information. In this regard, it is useful to consider the identification problem and evaluation of the fault as a hierarchical structure [3].

Accordingly, Rytter [4] categorized *"damage detection"* for SHM of a system into four levels:

Level 1. Detection

Level 2. Localization

Level 3. Assessment

Level 4. Consequence or Prediction

However, Worden and Dulieu-Barton [3] introduced a new level and defined the process of damage detection into five levels with the following structure:

Level 1. Detection: The technique provides a qualitative indication that damage might be present in the structure.

Level 2. Localization: The technique provides information about the probable location of the damage.

Level 3. Classification: The technique provides information about the type of damage.

Level 4. Assessment: The technique provides a prediction of the severity or extent of the damage.

Level 5. Prediction: The technique provides information about the safety of structure like remaining useful life of the system.

It should be noted, success at a particular hierarchical level is mainly dependent on success at lower levels; it is impossible to assess the extent of damage without first defining the location of the damage, and it is also impossible to predict the future severity of damage without first identifying the type of damage that has happened. When attempting to implement SHM approaches, determining the level of desirable identification is a critical choice that will have a significant impact on the methodology taken [5].

Reaching these damage detection levels in the above-mentioned order indicates an increasing knowledge of the damage state. Statistical approaches are widely employed to diagnose the occurrence (and potentially the location) of damage when an unsupervised learning method is performed. However, statistical approaches can be utilized to better assess the type and severity of damage when a supervised learning method combined with analytical models is used. Prediction of remaining useful life is more challenging, as it typically necessitates precise physical models of the damage processes of interest, and accurate estimates of the future loading regime of the system [6].

1.2   Structural Health Monitoring Approaches

There is broad agreement in the literature that there are two main approaches to dealing with SHM problems: the 'model-based' or 'inverse-problem' approach and the 'data-based' approach [7]. The model-based method is typically achieved by developing a physics-based model of the structure through a Finite Element (FE) model, while the data-based method is established on the utilization of vibration data without any physics-based model.

1.2.1 Model-Based Techniques

The model-based method is mainly accomplished by obtaining a law-based or physics-based model of a real structure using an FE model, although other modeling approaches can be applied. The dynamic characteristics (stiffness, mass and damping) of the FE model are updated using recorded vibration data of the real structure under dynamic test so as to provide an analytical model, which more accurately describes the real structure [7]. Accordingly, identification, localization, and quantification of damage can be achievable by solving an inverse-problem utilizing vibration data obtained from the structure of interest under test [5].

The model-based methods are especially valuable for estimating system response to new loading conditions and/or new system configurations (damage states). Nevertheless, model-based methods are usually more intensive in terms of computation than data-based methods [8].

There are some challenging issues while implementing model-based methods. First, building an accurate model of a real structure based on first physical principles is extremely difficult. For instance, lack of information in many areas; and material characteristics may not be determined with high accuracy [7]. To overcome this problem, the FE model is adjusted with the data from the structure of interest by model updating methods [9–17]. Another issue arises from the ill-posedness of the inverse problem which needs to apply suitable regularized solution methods such as Tikhonov regularization [18–21] and truncated singular value decomposition [22] in order to address this issue [23, 24]. Moreover, conditioning can be improved by decreasing the dimension of the inverse-problem via subset selection [25].

1.2.2 Data-Based Techniques

As the name implies, the data-based method does not follow a physics-based model. The data-based method is built by implementing statistical pattern recognition or machine learning methods to acquire vibration data from undamaged and damaged states of the structure of interest [7, 26–31]. Given that the data-based method depends mainly on data; hence, the need to build a physics-based model can be eliminated. Besides, numerous uncertainties which are deriving from measurement variability, noise, environmental and operational variability during SHM task can be accommodated using data-based methods [5].

However, physics-based models may still be used effectively in the data-based method to set up proper features for damage detection. Considering the advantages and disadvantages of data-based and model-based methods, it is believed firmly that the data-based approach is more convenient for SHM purposes [7].

1.3 Statistical Pattern Recognition paradigm

Pattern recognition using machine learning techniques is a well-established field. In general, the theory provides a mathematical method for associating measured data with specified class labels. In the SHM context, the aim is to associate the measured data to a damaged state, the simplest – and possibly most essential – issue is to distinguish whether a structure is in the 'healthy' or 'damaged' state. In terms of mathematics, there are several different approaches to pattern recognition, the most important of

which are *statistical*, *neural*, and *syntactic* approaches [32]. Considering that almost all engineering problems involve numerous degrees of uncertainty, the statistical method in the context of pattern recognition seems to be a promising method for SHM purposes. Furthermore, neural network methods could also be evaluated in statistical terms and also provide a reliable solution to SHM issues [7].

   Four steps can be combined to establish a general statistical pattern recognition (SPR) paradigm for an SHM system [33]. These steps include:

1. Operational evaluation,

2. Data acquisition,

3. Feature selection and

4. Statistical modeling for feature discrimination.

The four mentioned steps of the SPR paradigm for SHM are briefly discussed below [7]:

1.3.1   Operational Evaluation

The purpose of the *operational evaluation* is to answer several key questions about the application of an SHM technique for detecting damage in a structure:

- What are the justifications for performing the SHM in terms of life safety and/or economics?

- How is damage defined for the system under investigation, as well as for numerous damage scenarios?

- What are the operational and environmental conditions in which the system to be monitored operates?

- What are the limitations of data acquisition in an operational environment?

   Operational evaluation attempts to establish limits on what will be monitored and how the monitoring will be carried out. Additionally, operational evaluation aims to adjust the damage detection procedure to features that are unique to the monitored system, as well as to exploit unique features of the damage to be identified [7].

1.3.2   Data Acquisition, Normalization and Cleansing

The excitation techniques, type and number of sensors, sensor locations, and data acquisition/storage/transmittal hardware are parts of the *data acquisition* in the SHM process. The data acquisition in this process will be application-specific. Decisions on the data acquisition hardware to be employed for the SHM system will be strongly influenced by economic considerations. Another factor that must be taken into account is the time interval at which data should be collected [7, 34, 35].

   Since data may be measured in different environmental and operational conditions, the capability to normalize collected data is critical to the damage detection process. *Data normalization*, in the context of SHM, is the process of distinguishing between sensor measurement variations caused by damage and those induced by changing environmental and operating conditions. It is also worth mentioning that normalizing

the measured responses by the measured inputs is one of the most popular methods. When environmental and/or operational variability is a challenge, it may be necessary to normalize the data in some temporal fashion in order to compare data collected at similar points in the environmental and/or operational period. Variability can originate from variations in ambient and test conditions, modifications in the data reduction procedure, and unit-to-unit discrepancies [6]. Data normalization problems are usually major challenges to implementing a reliable SHM system in the field [7].

The process of selecting data to pass on to or remove from the feature selection process is known as *data cleansing*. The information obtained by persons who are directly associated with data acquisition is often used in the process of data cleansing. It can be noted, filtering and resampling are examples of signal processing approaches that can be considered data cleansing processes [7].

Eventually, the data acquisition, normalization, and cleansing in the process of structural health monitoring should not be static. The process of data acquisition can be improved using knowledge obtained from the feature selection and statistical model development processes which will constantly give information concerning changes [7]. Several studies considered different aspects of the data acquisition and data normalization issues in the context of SHM [36–40].

1.3.3 Feature Extraction and Data Condensation

Feature extraction is the process of converting the measured data into a different form which allows the correlation with the damage to be discovered more easily. The process of feature extraction in vibration-based SHM is mainly based on fitting some model, either model-based or data-based, to the measured vibration data. Furthermore, the process of selecting which feature to apply in the damage detection process is known as *feature selection* [7].

A *damage-sensitive feature* is some quantity derived from the obtained vibration data that is utilized to express the presence (or not) of damage in the structure of interest. Determining features that can correctly identify a damaged state from an undamaged one is the primary concern that is tackled in most of the SHM research [41, 42]. Therefore, if the features are chosen carefully, the pattern recognition and machine learning process for feature classification can become slightly easier and the existence of damage can be identified by a simple evaluation of the variations in the features. On the contrary, if selected features are not correlated with the damage, even the most powerful pattern recognition and machine learning algorithms will fail to detect the damage in the SHM process.

The *data condensation* is referred to the procedure of decreasing the dimension of the collected data. Since the practical application of the measurement technologies in SHM generates a huge amount of data; data condensation task is essential and beneficial when comparing many feature sets acquired during the lifetime of the structure are intended [7].

1.3.4 Statistical Model Development for Feature Discrimination

Statistical model development is associated with the development of techniques that apply to the extracted features in order to estimate the damage states of the system.

Machine learning algorithms are employed to develop the statistical models because establishing a functional relationship between the extracted features and the damaged state of the structure based on physics-based approaches is usually difficult. In the context of SHM, these machine learning algorithms which are utilized in developing the statistical models are divided into two categories:

1. Supervised learning algorithms: when data from both the undamaged and damaged states of the structure are available for training. *Group classification* and *regression analysis* are primary examples of these algorithms.

2. Unsupervised learning algorithms: when only data from the undamaged states of structure are available for training. *Outlier* or *novelty detection* approaches are primary class of such algorithms.

The statistical models are built in such a manner to minimize false diagnoses. There are two types of false diagnoses: (1) *false-positive* damage indications (i.e. identifying damage while the structure is undamaged) and (2) *false-negative* damage indications (i.e. no indication of damage while the structure is damaged). In addition, diagnostic systems can be designed to weigh/assess the costs of the two types of errors differently.

Two types of structural health monitoring are performed using statistical models. (1) *Protective monitoring* is when damage-sensitive features are utilized to detect an approaching failure and to shut down and/or change the system's use in some way before catastrophic failure occurs. In such circumstances the statistical models are applied to define thresholds on acceptable levels of feature change. (2) *Predictive monitoring* is the process of identifying patterns in data features and using them to estimate when damage will exceed the threshold level. This kind of monitoring is required in order to establish cost-effective maintenance strategies. In this situation statistical modeling is employed to evaluate uncertainty in predictions of the feature's time rate of change [7].

1.4 Structural Health Monitoring of Offshore Structures

The offshore structures industry has experienced rapid growth during the last decades. It is claimed that the marine industry was born in 1947 when a steel platform was placed in 20 feet (6.10 m) of water offshore the coast of Louisiana. Before this date, most *"offshore"* activities were built on wooden piled decks which were linked to the shore through trestles. Moreover, other types of offshore platforms were installed in oil-producing areas such as in the Caspian Sea in the early 1900s [43].

It is worth mentioning that one of the first investigators for the implementation of Structural Health Monitoring in practice was the offshore industry. Due to the fact that offshore structures are faced with a harsh marine environment, there is a demand for structural assessment especially when traditional inspections were either impossible or too expensive [2]. Structural Health Monitoring is focused on the integrity of the structures so as to decrease costs, increase the operational lifetime, and enhance safety [44]. Hence, SHM is even more crucial for the case of offshore structures.

During two decades of the 1970s and 1980s, the offshore oil & gas industry put significant efforts to develop vibration-based damage detection techniques for offshore platforms. Nevertheless, because of several practical issues (e.g., measurement challenges due to platform machine noise, instrumentation challenges in hostile environ-

ments, changing mass due to marine growth and variation fluid storage levels, temporal variability of foundation conditions, and the inability of wave motion to excite higher vibration modes), which arise in the marine environment, the efforts to develop SHM technology for the offshore industry were mainly abandoned in the early 1980s [45]. To date, some techniques have been developed in order to detect, quantify and localize the damage in offshore structures [46].

There are some reasons which make offshore structures a challenging issue in order to implement Structural Health Monitoring [2].

- The nature of working on offshore platform structures involve many open problems and questions in the field of SHM at one time. These systems are constructed in environments with severely changing operational conditions, which operators are mostly unable to quantify these variabilities [47–49]; specifically, where the structural models are uncertain [50, 51] and based upon output-only analyses, which suffers from a high incompleteness in the monitoring information [52] and modal expansion techniques [53, 54].

- Alternatively, direct fatigue load analysis, as a potential damage that occurs inside of a structure, could be considered, which requires estimating the input loads [55–58].

- The mentioned problems are become more complicated by taking into account the inherent structural nonlinearity in such systems, coming from both nonlinear fluid structure interactions [59] and foundation conditions [60–63]. These nonlinearities contribute greatly to a very uncertain environment with high challenges for both system identification and SHM due to the high number of unknowns and confounding effects.

- It is also an environment where there is tangible cost benefit for implementation of SHM strategies due to the high maintenance and inspection cost.

These factors motivate researchers to keep their study in order to apply developing technologies for SHM of offshore structures.

1.5   Contribution and Outline of This Dissertation

In this dissertation some possible and capable techniques based on machine learning and statistical methods are presented and applied to various kinds of structures in order to diagnose probable damages and their severity in these structures.

This dissertation is organized into 7 chapters. In Chapter 2, an important literature review related to the data-based Structural Health Monitoring (SHM) techniques relies on statistical pattern recognition paradigm focusing on feature extraction and classification methods, especially for offshore structures is discussed. Chapter 3 presents an iterative method for feature extraction via time series analysis using vibration responses. Chapter 4 proposes some statistical methods as a combination of data analysis techniques and time-invariant linear models. A new machine learning method in an unsupervised learning manner by using the k-medoids clustering algorithm for damage diagnosis is proposed in Chapter 5. The applications and results of proposed damage

detection techniques on different monitoring data acquired from numerical, experimental, and real (large-scale) structures are given in Chapter 6. Finally, Chapter 7 points out conclusions, which are derived from this study and perspectives for future research.

CHAPTER *2*

Literature Review

$\mathbf{I}$N this chapter, some contributions from the literature related to SHM of structures are presented. SHM studies for offshore structures have been arisen by both economic and life-safety concerns. There have been various examples where the failure of these structures led to the death of everyone on the platform. Fig. 2.1 depicts fires that caused from damage to an offshore platform [7].

The offshore structures are encountered with a large number of damage scenarios. Corrosion damage, fatigue damage accumulation, and ship impact on the structural elements are some examples of damage cases. However, the majority of numerical studies for damage detection in offshore structures modeled a crack in a structural element or completely removed the element. Several tests were accomplished on in situ platforms [64–68]. Moreover, experiments were carried out on scale-model platforms in laboratory settings [69–72].

Due to the fact that only a small part of offshore structures is located above the water surface, it leads to some limitations and difficulties implementing *in situ* monitoring scheme. However, reaching to these places could be quite difficult and risky. In case divers are employed to take measurements below the water surface, it becomes highly expensive and extremely dangerous. Instead, below the water surface, data can be acquired by installing appropriate sensors and wiring into structural components, such as tubular truss members, during construction period. It is worth mentioning that the corrosive saltwater environment can adversely impact sensors and associated wire systems when used for long-term monitoring [7].

Vandiver [73] by considering changes in the natural frequencies of a welded steel offshore pile-supported tower detected subsurface structural damage. In addition, a technique based on statistical energy analysis for predicting the dynamic response of a wide range of floating and fixed offshore structures to random wave forces is presented.

Figure 2.1: *Damage to an offshore oil platform in the Gulf of Mexico causing fires (Credit: US Coast Guard via Getty Images).*

Loland and Dodds [74] measured the responses of three platforms in the North Sea during nine months. Since, natural frequencies of the offshore structure are dependent on the stiffness, mass and geometry of the structure and are independent on the excitation, therefore, the response is most noticeable at the natural frequencies. Accordingly, it is observed, minor structural modification to the test platforms caused changes of 10% to 15% at the natural frequencies. The corresponding mode shapes need to be identified in order to track these natural frequencies.

Wojnarowski [75] presented a method for structural integrity evaluation and early damage detection of offshore structures using vibration measurements. Numerous parameters (mass, corrosion, entrained water, marine growth, soil support conditions, etc.) which affect the lower-mode vibration characteristic of the structure were studied separately and their quantitative effect on the natural frequencies was calculated.

Yang et al. [70] applied the random decrement method in order to identify induced cracks in a model of a welded-steel offshore platform. It is found that complete severance mostly affects low-frequency modes and to a limited extent, higher-frequency modes.

To evaluate the structural integrity of steel offshore platforms in the Gulf of Mexico, Duggan et al. [64] explored the use of ambient surface vibrational measurements. The study was planned to realize if the vibrational behavior of the platforms is stable under various environmental and operational circumstances, but pertaining to structural changes. First, data was collected during 7 months from platforms with different structural configurations, environmental loading and operating conditions. During the monitoring period, on the Ship Shoal 247A platform, repairs on two legs and the replacement of three bracing members were made. Subsequently, autospectral and cross-spectral analysis techniques were used to analyze selected data. The results indicated that ambient surface vibration methods could not detect the elimination of bracing ele-

ments on the Ship Shoal platform, and in order to correctly distinguish changes in the platform, it is necessary to identify the mode in addition to the natural frequency.

Coppolino and Rubin [76] measured structural responses from ambient vibrations of a producing Shell Platform SP-62C which is located in a water depth of 100 m in the Gulf of Mexico during its normal producing operation. These measured modal responses were used to build an FEM of the platform, and several damage scenarios were defined in the model. It is shown that based on the location of damage, natural frequencies change from 1% to 2% compared to their undamaged states.

The ability of structural response measurements for detecting damage in the West Sole (WE) platform was investigated by Kenley and Dodds [65]. For this purpose, before removing the platform, it was intentionally and progressively damaged by cutting members. To measure the dynamic response of the platform to ambient excitation in undamaged and damaged states, several accelerometers were placed above and below water. It was concluded that overall measurements above water can identify the full severance of an element, whereas local measurements underwater can detect flooding and part severance of a member.

Lepert et al. [77] based on numerous experimental tests on an offshore platform model, and modal analysis theory indicated that there is a relation between the incidence of failure and the variation of dynamic characteristics of the structure, which is dependent on the size and location of the damage. Moreover, the Vibro-detection method was introduced as an effective alternative to traditional nondestructive testing techniques for the assessment of offshore structures.

Nataraja [67] in order to develop and prove the feasibility of monitoring systems for identifying structural damage, measured the ambient vibration responses of three fixed steel platforms located in the North Sea over a two-year period. According to the results, only the lowest natural frequencies could be detected without difficulty, and these frequencies remained consistent during the monitoring interval. Besides, temporary changes in frequencies due to the variation in deck mass related to drilling activities could be detected. Therefore, in order to distinguish frequency changes due to the deck mass from structural damage and foundation stiffness changes, it is crucial to monitor the deck mass. Furthermore, it was mentioned that vibration monitoring using accelerometers on the surface and deck can only detect global changes in these structures.

Kim and Stubbs [78] examined a method for damage localization and estimating the severity of damage in a numerical offshore platform model when only modal parameters of damaged state for a few modes of vibration are known.

Roitman and Viero [79] considered the performance of Modal Assurance Criterion (MAC), Coordinate Modal Assurance Criterion (COMAC), Modal Scale Factor (MSF), mode shape Relative Difference (RD) method, and Change in Modal Vector Perpendicular to Predominate Modal Direction techniques which are using mode shapes, for damage detection and localization of a scaled fixed platform. It is found that the MAC and MSF methods were sensitive to the damage when higher modes were evaluated. In addition, despite the sensitivity of the COMAC and model shape Relative Difference methods to damage, they were unable to accurately identify the location of the damage. Moreover, since the Change in Modal Vector Perpendicular to Predominate Modal Direction was able to detect damage in structure by using only deck sensors, it could play

an important role in diagnosing damage in offshore structures.

Nichols [44] proposed a technique using ambient excitation in order to detect damage in offshore structures. For this purpose, the output of a stochastic process confirming the ambient Pierson-Moskowitz wave distribution is used to excite the offshore models. Subsequently, the response of a damaged structure is predicted using structural response data from an undamaged state.

Yang et al. [80] employed the natural excitation technology (NExT), eigensystem realization algorithm (ERA), and peak picking (PP) techniques in the frequency domain for output-only modal identification as a reference model for damage identification purposes. Given that, the ambient vibration test in the field on a steel jacket-type offshore platform under wave-induced and wind force was performed.

Wang et al. [81] introduced a modal strain energy index for diagnosing damage in a simulated offshore jacket platform utilizing modal information. It was shown that the damage detection technique only requires a few lower modes and a partial degree of freedom of the entire model to detect the location of damage due to the changes in deck mass.

Shi et al [82] described a damage detection algorithm based on statistical treatment for damage localization of a numerical model of the offshore platform using a few lower modes of vibration in both undamaged and damaged states. Modal parameters which were derived from eigenvalue analysis on the model were used to evaluate the effectiveness of the method using variations in partial mode shapes and its robustness against identification error of baseline structure. Afterward, modal parameters were identified using an Autoregressive-moving average (ARMA) method for dynamic responses of the offshore platform. Eventually, the proposed method was employed with the aid of statistical methods for modal parameters to define the location of damage in the platform.

Cheng and Wang [83] presented a method for detecting damage in a simplified offshore platform using time-domain responses data under random excitation. First, the time-domain of noise data was used to construct a time series model. Accordingly, based on time-domain response data, a sensitivity matrix consisting of the first differential of autoregressive coefficient of the time series models with regard to the structural stiffness was calculated. Finally, the location and severity of damage in the structure were determined through solving damage vector.

Asgarian et al. [84] utilized modal strain energy for damage detection, damage localization, and estimating the severity of damage in a numerical offshore platform model. In this study, modal strain energy change ratio (MSECR) was obtained for each structural member in order to detect the location of the damage. In addition, cross-modal strain energy (CMSE) was employed to estimate damage severity in each suspected damaged member.

Elshafey et al. [85] investigated a combination approach using random decrement signature and neural networks in order to identify damage in an experimental model of a real fixed offshore jacket structure. The model was equipped with accelerometers and strain gauges on the legs and deck to record responses of the experimental model which was excited by random loads. It is shown that the proposed method uses a limited number of vibration data and, it was successful in diagnosing damage using vibration data excited by the Pierson-Moskowitz spectrum.

The application of the bicoherence function for damage detection of a simulated offshore platform using acceleration responses was studied by Hillis et al. [86]. The proposed technique used only natural environmental excitation, and it was able to detect small changes in stiffness of single structural elements employing measurements of global structural motion.

Diao et al. [87] utilized the acceleration time-history responses of a numerical model of a four-story steel frame under white noise to compute the vibration transmissibility, and for dimensionality reduction, principal component analysis (PCA) was carried out on the amplitude of vibration transmissibility. The variations of the principal component before and after damage were determined and combined as damage characteristic vectors, which were input into the Back-propagation neural network to identify the location of the damage. During the damage detection process, the effects of various noise intensities were examined, and it was conducted that the method is capable of detecting structural damage, however, it was easily affected by the noise.

Wang [88] to detect and quantify damage in offshore platform structures, while limited modal data are existing, implemented iterative modal strain energy (IMSE) technique. It is worth mentioning that the technique uses both modal frequencies and spatially incomplete mode shapes, and it is not necessary for the modal frequencies to be paired one by one with the mode shapes.

Wang et al. [46] considered the performance of a traditional modal strain energy (Stubbs index) method and modal strain energy decomposition (MSED) method for damage localization of an offshore platform.

The applicability of vibration-based algorithms based on stochastic subspace identification (SSI) in the time domain for stability and structural change monitoring of offshore wind turbines was investigated by Kraemer and Friedmanna [89]. As a result, the sensitivity of the technique for monitoring purposes was evaluated through long-term monitoring of a large-size test rig of an offshore wind turbine at a scale of 1:10 under various structural states.

Yi [90] using strain response data collected by FBG sensors, proposed a local damage detection method for offshore platforms by principal component analysis (PCA) and linear adaptive filter (LAF) methods based on statistical techniques. Furthermore, the impacts of changes in temperature and external loading on a scaled tidal current power plant structure were considered and using the nonparametric PCA and LAF techniques an effective remedy was suggested.

Kim et al. [91] developed an SHM system for identifying damage in the hybrid offshore wind and tidal current turbine using measured acceleration responses. Accelerometers were mounted at four different levels of the experimental model from the base to the top. To detect damage in the structure, first, the coherence function between two sets of acceleration data was performed, then the averaged integrations of coherence (AIC) function with frequency were applied.

Oliveira et al. [92] in order to identify structural changes in wind turbines, developed a vibration-based method according to the determination of the modal features of the most important vibration modes. To consider the effect of environmental and operational changes on the natural frequencies, data was collected for more than 1 year from a 2-MW wind turbine. Then, the impact of environmental and operational variety over the features was reduced by using a statistical technique based on regression models to

identify structural changes in the structure.

Vidal et al. [93] developed a data-based method for identifying damage in offshore jacket-type wind turbines utilizing only accelerometer data. The wind excitation was modeled as Gaussian white noise and vibrational responses of the wind turbine as raw data, pre-processed by means of mean-centered group-scaling. Then, for the sake of dimensionality reduction and computing time of the next step, principal component analysis (PCA) was employed. Eventually, the quadratic kernel support vector machine (SVM) was applied as a classifier.

Due to the fact that the accuracy of damage detection is dependent on the locations of damages as well as the location and number of sensors, a sensitivity analysis was carried out by Jiang et al. [94] to vary the number and location of sensors, and damage severity. It is denoted that when locations of sensors are closer to the locations of damages, the results of damage detection improve, and these results are more sensitive to sensor locations when damages are present in the upper structures. Moreover, the detection results are more sensitive to the severity of damage than to the incidence of several damages.

A data-based strategy by employing accelerometer data and applying principal component analysis and machine learning algorithms for damage detection and localization on a laboratory-scale of a jacket-type offshore wind turbine was developed by Vidal et al. [95]. In addition, structural health monitoring based on vibration-response for an experimental model of a steel jacket-type offshore wind turbine using Convolution Neural Networks (CNN) was performed by Puruncajas et al. [96]; which converted accelerometer data into gray-scale images and classified these images by the deep CNN for predicting possible damages.

Bao et al. [97] investigated the use of one-dimensional convolutional neural network (CNN) technique for damage detection of an offshore platform. Damage-sensitive features were automatically extracted from raw strain response data. The method was able to identify and localize the damage for both single and multiple full element damage scenarios, while the minor multiple damages on local elements of the platform were hard to localize. In addition, the one-dimensional CNN method through a linear regression model, can also accurately estimate the damage severity to the members.

Bao et al. [98] by a combination of the random decrement technique (RDT) with long and short-term memory (LSTM) networks proposed the so-called RDT-LSTM method for the localization and severity assessment of structural damage for offshore jacket platform using measured vibration response. First, RDT was used for preprocessing the noisy random data, and then LSTM was applied to identify damage. The RDT-LSTM method was able to accurately detect and localize the structural damage under random excitation.

Feijóo et al. [72] proposed an unsupervised damage detection approach using an autoencoder neural network model for offshore jacket wind turbine foundation. The presented method only employed the healthy data of the structure and it performed under various environmental and operational changes using only output data obtained by accelerometer sensors.

Bao et al. [99] considered the feasibility of using deep learning methods (CNN, LSTM, and CNN-LSTM) for determining the location and estimating the severity of damage for the offshore platforms using vibration response data. The results demon-

strated that deep learning methods, in combination with the RDT technique for data preprocessing offer outstanding structural damage detection performance for offshore structures.

Data-Based Methods for Feature Extraction and Classificaiton

TIME series analysis takes into account as the most applicable feature extraction technique in such a way that statistical characteristics of time series models are chosen as damage-sensitive features (DSFs). Based on time series analysis, one can fit a mathematical model with appropriate and specific orders to the vibration time-domain data and extract coefficients and residuals of the model [100–106].

The coefficients of AutoRegressive (AR) model as the DSFs were extracted by Sohn et al. [107] in order to use them in statistical control charts for the damage identification process. In another study, the residuals of AR model, which quantify the difference between the prediction from the AR model and the actual measured time-domain, were employed by Fugate et al. [108] as the damage-sensitive features in the statistical control charts for the damage identification. A new methodology associated with the feature extraction process by combining the AR and AutoRegressive with eXogenous input (ARX) models was established by Sohn et al. [109]. In that approach [109], the residuals of AR model were employed as the input of the ARX model and then the coefficients of this model were applied as the DSFs. An AutoRegressive Moving Average (ARMA) model was used by Nair et al. [110] for the feature extraction procedure by applying the first three AR coefficients as the damage-sensitive features. An ARX model with a new sensor clustering method was exploited by Gul and Necati Catbas [111] for the feature extraction process. In their methodology [111], the output of each sensor in a cluster was utilized as an input to the ARX model to predict the output of the reference channel of that sensor cluster. A damage identification methodology by applying the AutoRegressive Moving Average with eXogenous input (ARMAX) model was proposed by Ay and Wang [112] to quantify the acquired set of vibration signals. A novel

sensitive damage feature extraction based on measuring the distance of the coefficients of vector autoregressive (VAR) models by Mahalanobis distance method was proposed by Mosavi et al. [113].

Even though the time series models are widely employed in the context of SHM in order for extracting the DSFs, there are some limitations in using these models such as making sure of the adequacy and accuracy of models. From a statistical viewpoint, a time series model should produce uncorrelated residuals to make sure the model accuracy and adequacy [114]. Any model that does not satisfy this requirement should be modified [115]; thus, choosing an appropriate order plays a crucial role in the accuracy and adequacy of any time series model. Furthermore, most of the researchers did not sufficiently clarify the main reasons of choosing and using the time series models in their studies [116, 117]. In statistics, there are many time series models with different specifications, which can be applied to the vibration time-domain data. It is important to identify the best time series model with optimal orders to make sure the model accuracy and adequacy. In this study, an iterative feature extraction technique based on time series modeling is proposed with the special focuses on identifying the best time series model, choosing the optimal orders for the identified model.

The statistical decision making refers to use statistical methods for the classification of DSFs. This step of the statistical pattern recognition framework is concerned with the implementation of algorithms that operate on the extracted features to quantify the damage state of the structure. The algorithms used in the statistical decision making are normally carried out by machine learning methods that are broken into unsupervised and supervised learning classes. Both of them are intended to train a model from the extracted features in an effort to discriminant the undamaged state from the damaged one. The unsupervised learning class only needs the DSFs of the undamaged condition for training the model, whereas in the supervised learning class the trained model is composed of the extracted features of the undamaged and damaged conditions. An statistical classification algorithm was presented by Carden and Brownjohn [118] based on analyzing the dynamic responses of structures in the time domain. In their method [118], the parameters of ARMA model were used in the classifier to learn an unsupervised learning algorithm for damage identification. Two supervised learning algorithms, namely nearest neighbor classification and learning vector quantization were employed by de Lautour and Omenzetter [116] in order to detect damage based on using the coefficients of AR model as the damage-sensitive features. The health of structures by a multivariate statistical process control method, called Hotelling's T^2 control chart, based on extracting the parameters of AR model was evaluated by Wang and Ong [119]. A new statistical process control approach was proposed by Zapico-Valle et al. [120] to classify the state of structure applying signal lengths as new damage-sensitive features. In addition, Mahalanobis distance-based outlier detection algorithm by using the coefficients of AR model was used by Gul and Catbas [121] in order to detect and locate structural damage in the different laboratory structures. In another area, the crack length for damage diagnosis in the plate-like structures using the guided wave-based technique and a novel ellipse-based binary damage imaging algorithm were assessed by Zima and Rucka [122].

One of the important problems in the context of SHM is the effect of operational and environmental variability on the results of damage detection. They are linear changes

in the structures resulting from either environmental conditions such as temperature, wind loading, and moisture or operational conditions including live loads, operation speed and changing the source of excitations [123]. Such variations often alter the physical properties of the structure such as mass and stiffness and lead to Type I error (known as false-positive or false alarm error). This error occurs when the structure is declared damaged, while it is in fact undamaged. Sohn et al. [124] presented a damage classification approach under varying operational and environmental conditions using a unique combination of time series analysis, neural networks, and statistical inference techniques. Kullaa [125] applied factor analysis to eliminate the effects of these conditions on the measured features. In that study [125], linear and nonlinear models were established to indicate the relationship between temperature and four natural frequencies without measuring environmental quantities. Oh and Sohn [126] proposed nonlinear principal component analysis based on unsupervised support vector machine. The proposed nonlinear PCA characterized the nonlinear relationship between the extracted DSFs from AR-ARX model and unmeasured environmental and operational parameters. Some efficient machine learning methods were presented by Figueiredo et al. [123] in order to remove the operational and environmental variability from the features of AR model. In the global health monitoring, it is essential to apply powerful and reliable statistical methods for identifying damage without any false-positive errors.

3.1 Time Series Analysis

In statistics, time series analysis is a method that makes an attempt to fit a mathematical model to time series data in order to find out meaningful statistical characteristics of the data [115]. On the other hand, time series is a sequence of data points that typically consists of successive measurements at a specific time interval. In the time series modeling, the stochastic structure of time series is captured by identifying an appropriate model. Since there are various types of time series, it is necessary to select an adequate model to estimate parameters included in the model, depending on the characteristics of the time series and the objective of the time series analysis.

3.1.1 Time Series Models

There are three class types of time series models, autoregressive, integrated, and moving average, which are mostly used in time series analyses. AR model is known as a simplest linear time series model that is linearly related to the output (response) data. When the input data such as the excitation force is available, ARX model can be constructed. It is possible to combine AR and ARX models to the moving average and produce ARMA model for the output-only data and ARMAX model for the input-output data [114].

The selection of time series model depends on the type of data and data acquisition system. A total formulation of a time series model along with input, output, and error terms can be expressed in the following equation [114]:

$$
\begin{aligned}
y(t) + a_1 y(t-1) + ... + a_{n_a} y(t-n_a) = b_1 u(t-1) + ... \\
+ b_{n_b} u(t-n_b) + e(t) + d_1 e(t-1) + ... + d_{n_b} e(t-n_b)
\end{aligned}
\tag{3.1}
$$

where $u(t)$ and $y(t)$ denote the input and output data at the specific time t; $e(t)$ is the error or discrepancy term between the measured time series data and predicted one via the model. The unknown parameters of the model are shown by a, b, and d, which refer to the coefficients of model. Moreover, the orders of the time series model are represented by n_a, n_b, and n_d. It is possible to compact Eq. (3.1) as follows:

$$A(q)\mathbf{y}(t) = B(q)\mathbf{u}(t) + D(q) + \mathbf{e}(t) \tag{3.2}$$

In Eq. (3.2), $A(q)$, $B(q)$, and $D(q)$ are the polynomials by using the backshift operator q [127], which can be formulated as:

$$A(q) = 1 + a_1 q^{-1} + a_2 q^{-2} + ... + a_{n_a} q^{-n_a}$$
$$B(q) = 1 + b_1 q^{-1} + b_2 q^{-2} + ... + b_{n_b} q^{-n_b} \tag{3.3}$$
$$D(q) = 1 + d_1 q^{-1} + d_2 q^{-2} + ... + d_{n_d} q^{-n_d}$$

As a note, it would be interested in to know that Eq. (3.1) represents the general formulation of the ARMAX model. In other words, any changes in the terms of this model lead to obtaining the other type of the time series models. If $n_d = 0$ or removing the error term $D(q)$ from Eq. (3.1), for example, the model becomes ARX so that the polynomials of input and output data will be enough for the model construction. Thus, the formulation of ARX model is written as follows:

$$A(q)\mathbf{y}(t) = B(q)\mathbf{u}(t) + \mathbf{e}(t) \tag{3.4}$$

The ARMA model is obtained by setting n_b to zero as:

$$A(q)\mathbf{y}(t) = D(q)\mathbf{e}(t) \tag{3.5}$$

Finally, the AR model is generated by $n_b = n_d = 0$, that is:

$$A(q)\mathbf{y}(t) = \mathbf{e}(t) \tag{3.6}$$

The AR model is a linear stationary model, which is widely used in analysis of the stationary time series data. As shown in Eq. (3.6), this model only requires the output data and its polynomial; therefore, it is more suitable for the vibration-based applications when the input data or excitation forces applied to the structures are immeasurable or unknown.

3.1.2   Model Identification by Box-Jenkins Methodology

The time series models should be compatible with the time series data. In other word, the selection of an appropriate time series model depends strongly on the nature of time series data. For instance, in the non-stationary data, an integrated time series model such as autoregressive integrated moving average (ARIMA) may be better than an ARMA model due to the nature of non-stationary data. One applicable way for identifying the most proper time series model for the stationary time series data is to use Box-Jenkins methodology [114]. This approach relies on using autocorrelation function (ACF) and partial autocorrelation function (PACF) that are statistical tools for measuring the correlation of time series data.

Under the Box-Jenkins methodology, if the ACF tails off with an exponential decay or a damped sine wave, and the PACF becomes zero after a lag, the time series conforms to the AR model. On the contrary, if the PACF tails off with an exponential decay or a damped sine wave, and the ACF cuts off after a lag, the MA representation can be selected. Eventually, if both the ACF and the PACF tail off with an exponential decay or a damped sine waves, ARMA can be chosen as the most proper model [114].

3.2 A New Iterative Feature Extraction Technique

As mentioned in the introduction, the parameters and residuals of time series models can be used as the DSFs. During the damage occurrence in a structure, the parameters of the identified time series model decrease due to their relations to the physical characteristics of structure. The process of extracting the model parameters under both undamaged and damaged conditions is based on (1) fitting an appropriate time series model to vibration response data acquired from each sensor and (2) extracting its parameters as the DSFs. By contrast, the process of feature extraction by the model residuals consists of using an appropriate model along with its parameters estimated from the undamaged condition to predict the responses of the damaged condition. The fact beyond this procedure is that the model used in the undamaged condition will no longer correctly predict the response of the damaged structure; therefore, the uncorrelated residuals regarding the damaged state will increase.

The proposed iterative feature extraction is intended to extract these features from the correlated residuals of model. This technique is based on choosing the best time series model compatible with the raw vibration time-domain data and extracting the uncorrelated residuals as the major criterion of adequacy and accuracy of time series models. In this technique, the model identification procedure is carried out by Box-Jenkins methodology [114]. Each iterative method needs a stopping condition to terminate the iterations and a maximum amount to determine the number of iterations. The stopping criterion in the proposed iterative feature extraction technique is based on the residual analysis of the identified model. To determine the maximum number of iterations, the residual analysis using Ljung-Box test is employed in an iterative manner as shown in Fig. 3.1 The maximum number of iterations ensures that the iterative technique will finally terminated in a quantity (order) that makes the model possible to produce uncorrelated residuals. On the basis of Ljung-Box test, if p-value of the model residuals is larger than 0.05, one can infer that the model can produce uncorrelated residuals in the sense that it is an adequate and correct model.

Once the maximum orders of model are obtained, a minimum arbitrary number is chosen to begin the iterative algorithm. On this basis, the order of model is started with the minimum number to examine the correlation of the residual of the model through autocorrelation function. In most cases, the model residuals gained by the minimum order are correlated; thus, the iterative step continues in such a way that the correlated residuals of the model with the minimum order are utilized as the input data in the algorithm of the proposed iterative technique. Fig. 3.2 depicts the flowchart regarding the feature extraction by the proposed iterative technique.
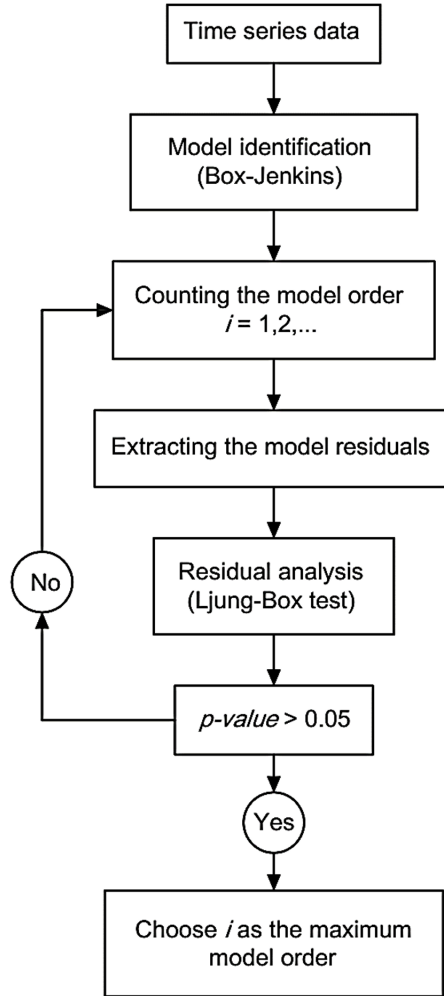
Figure 3.1: *The flowchart of the iterative algorithm for determining the maximum order.*

3.3 Global Health Monitoring Strategy

The aim of machine learning algorithms is to build or train a model that makes decisions based on the features extracted from the feature extraction step in the statistical pattern recognition framework. An important factor in the machine learning algorithms is to select training and test data sets for learning the model. In the context of SHM, the extracted features from the normal (undamaged) condition are typically chosen as the training data set, while the test data set consists of features that come from the normal and abnormal (damaged) conditions.

Assume that $\mathbf{X} \in \Re^{m \times n}$, with m-dimensional feature vectors from n different normal structural states, is the parameters (coefficients) of the identified model under the undamaged conditions extracted from the proposed iterative feature extraction technique. The matrix $\mathbf{X}$ is selected as the training data set to learn a model and detect any probable damage in the structure. In contrast, $\mathbf{Z} \in \Re^{m \times k}$, where k is the number of feature vectors from the undamaged and/or damaged conditions, takes into account as

22
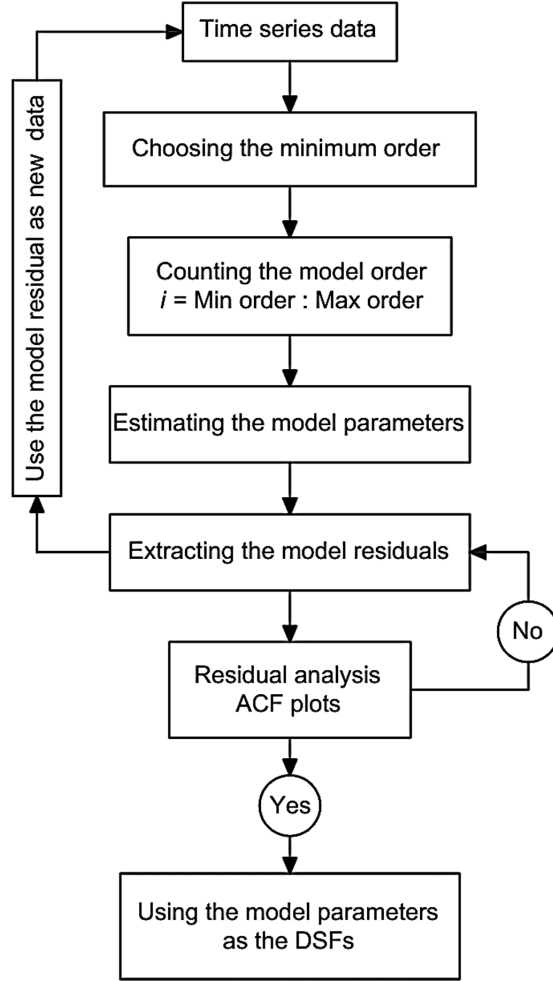
Figure 3.2: *The flowchart of the proposed iterative feature extraction technique.*

the test data set. As a result, any deviation of the features under the damaged conditions (test data) from the trained model constituted by the training data is an indication of damage occurrence.

3.3.1 Machine Learning Algorithms

3.3.1.1 Mahalanobis-Square Distance

Mahalanobis-square distance (MSD) is a well-known distance metric [128] that measures the distance between two points in the feature space composed of two or more variables. Considering the training matrix $\mathbf{X}$ with multivariate mean vector $\bar{\mathbf{x}} \in \Re^{m \times 1}$ and covariance matrix $\mathbf{\Sigma} \in \Re^{m \times m}$, MSD between the feature vectors of the training data and the feature vector of test data $\mathbf{z}$ is defined as:

$$DI_{\mathrm{MSD}} = (\mathbf{z_j} - \bar{\mathbf{x}})^T \mathbf{\Sigma}^{-1} (\mathbf{z_j} - \bar{\mathbf{x}}) \tag{3.7}$$

where $\bar{z}_j$ is the jth vector of the test data matrix $\mathbf{Z}$. In this methodology, the trained model consists of the mean and covariance matrices computed by the training data set. The main assumption in MSD is that the feature vector of the damaged condition (test data) with the source of environmental and operational variability will be further from the mean of the normal condition. Therefore, any deviation of MSD values in the test data from the training data or trained model implies that the damage has occurred in the structure.

3.3.1.2 Factor Analysis

Factor analysis is a multivariate statistical method used to describe variability among observed, correlated variables in terms of a potentially lower number of unobserved variables called factors. Mathematically speaking, the linear factor model in the matrix form can be expressed as:

$$\mathbf{X} = \mathbf{\Lambda}\mathbf{F} + \mathbf{E} \tag{3.8}$$

where $\mathbf{\Lambda} \in \Re^{m \times f}$ is a constant matrix of factor loadings, $\mathbf{F} \in \Re^{f \times n}$ represents a matrix of factor scores, and $\mathbf{E} \in \Re^{m \times m}$ is a matrix of unique factors or error terms. The error variable $j = 1, 2, ..., m$ are assumed to be independent with ψ_j specific variances. Note that f is a small number of the unobserved independent variables that should be less than the number of variables or features ($f < m$). In the SHM community, the factor model in Eq. (3.8) can be used to train a model by determining the factor loadings and specific variance matrices in the following form:

$$\mathbf{\Sigma} = \mathbf{\Lambda}\mathbf{\Lambda}^T + \mathbf{\Psi} \tag{3.9}$$

where $\mathbf{\Psi}$ is a diagonal matrix with the specific variances. There are several methods to estimate $\mathbf{\Lambda}$ and $\mathbf{\Psi}$ such as maximum likelihood estimation [129] and principal factor analysis [130]. Eq. (3.9) is the trained model based on the factor analysis method using the training data set. In the same manner to MSD method, the covariance matrix $\mathbf{\Sigma}$ is a square matrix with m elements concerned with the training data $\mathbf{X}$.

In order to compute the values of factor model for the global health monitoring, it is necessary to estimate the factor scores. To achieve this goal, some methods such as linear regression, Thomson, and Bartlett can be applied to determine the factor score matrix $\mathbf{F}$ considering the test data set $\mathbf{Z}$. For the linear regression method, the factor score matrix is determined as:

$$\mathbf{F} = \mathbf{\Lambda}^T(\mathbf{\Psi} + \mathbf{\Lambda}\mathbf{\Lambda}^T)^{-1}\mathbf{Z} \tag{3.10}$$

For Thomson's method:

$$\mathbf{F} = (\mathbf{I} + \mathbf{\Lambda}^T\mathbf{\Psi}^{-1} + \mathbf{\Lambda})^{-1}\mathbf{\Lambda}^T\mathbf{\Psi}^{-1}\mathbf{Z}^T \tag{3.11}$$

where $\mathbf{I} \in \Re^{f \times f}$ is the identity matrix. Eventually, the factor score matrix $\mathbf{F}$ by Bartlett's method is given by:

$$\mathbf{F} = (\mathbf{\Lambda}^T\mathbf{\Psi}^{-1} + \mathbf{\Lambda})^{-1}\mathbf{\Lambda}^T\mathbf{\Psi}^{-1}\mathbf{Z}^T \tag{3.12}$$

After computing the factor loadings and factor score matrices, a damage index for the global health monitoring is formulated by using Euclidean norm in the following equation:

$$DI_{\text{FA}} = \left\| (\mathbf{Z}^T - \boldsymbol{\Lambda} \cdot \mathbf{F})^T \right\|_2 \tag{3.13}$$

3.3.1.3 Principal Component Analysis

Principal component analysis (PCA) is a multivariate statistical process that is utilized to convert a set of observations of possibly correlated variables into a set of values of linearly uncorrelated variables named as principal components [131]. In the SHM community, PCA contributes to several applications such as dimensionality reduction, feature extraction [132, 133], data normalization for removing the effect of operational and environmental variability from the DSFs [134], and feature classification for damage detection problem [135].

Mathematically speaking, PCA is described as an orthogonal linear transformation that transforms data to a new coordinate system such that the greatest variance by some projection of the data represents the first coordinate, called the first principal component, the second greatest variance on the second coordinate, and so on.

In this study, PCA is used as a machine learning algorithm to detect damage in the structure using the features extracted from the proposed iterative feature extraction technique. Before establishing a damage indicator by PCA, it is necessary to implement a standardization process in the training data set with the aid of its mean and variance. Considering the parameters of the identified time series model gained by the proposed iterative feature extraction technique, the standardization of training data matrix is given by:

$$\tilde{x}_{ij} = \frac{x_{ij} - \mu_j}{\sigma_j} \tag{3.14}$$

where $\tilde{x}_{ij}$ denotes the ith sample at the jth variable in the matrix of training data. Moreover, μ_j and σ_j are the mean and standard deviation of the training data $\mathbf{X}$, at which $i = 1, 2, ..., n$ $j = 1, 2, ..., m$. Once the training data set is standardized, its covariance matrix is decomposed by singular value decomposition to determine the eigenvalues and eigenvectors (principal components) in the following form:

$$\tilde{\boldsymbol{\Sigma}} = \mathbf{V} \boldsymbol{\Lambda} \mathbf{V}^T \tag{3.15}$$

where $\boldsymbol{\Lambda}$ is a diagonal matrix containing the ranked eigenvalues λ_j, and $\mathbf{V}$ is the matrix containing the corresponding eigenvectors v_j. To determine the damage index of PCA, the test data set $\mathbf{Z}$ is normalized by the mean and standard deviation of the training data set $\mathbf{X}$. In fact, these statistical moments along with the principal components of the training data make a model based on PCA. Therefore, any deviation from this model is representative of damage occurrence. The PCA-based damage indicator can be written as follows:

$$DI_{\text{PCA}} = \left\| (\mathbf{Z} - \mathbf{S} \cdot \mathbf{V})^T \right\|_2 \tag{3.16}$$

where $\mathbf{S} = \mathbf{ZV}$.

3.3.1.4 Auto-Associative Neural Network

The auto-associative neural network (AANN) is a machine learning method that is employed to evaluate the global state of structure by training a neural network model. Applying the features extracted from the undamaged state, AANN is trained to characterize the underlying dependency of the identified features on the unobserved operational and environmental variations by treating this unobserved dependency as hidden intrinsic variables in the neural network. The structure of AANN consists of three hidden layers: (1) the mapping layer, (2) the bottleneck layer, and de-mapping layer as shown in Fig. 3.3.
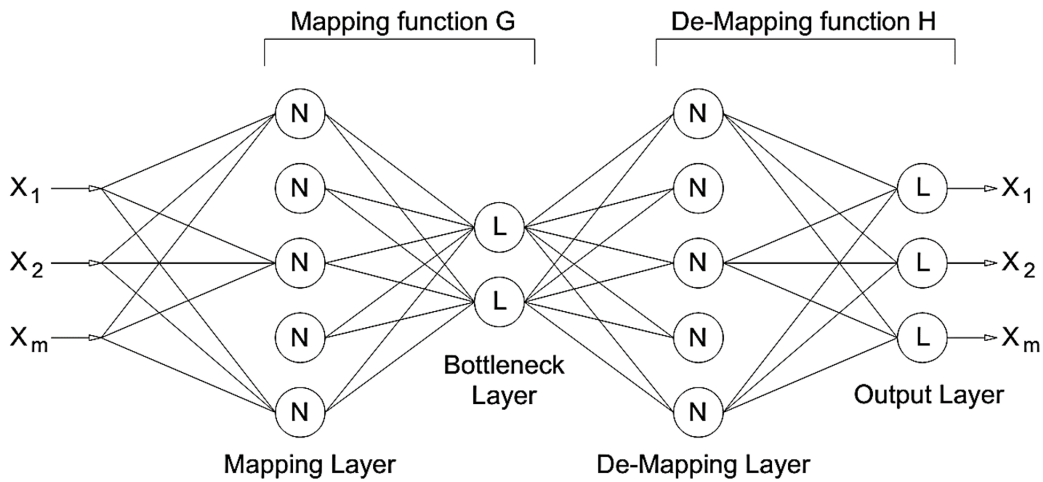
Figure 3.3: *Network structure of an AANN.*

For the applications of SHM, the network is initially trained to learn the correlations between features; therefore, it can reveal the unobserved sources of variability that influence the structural response. This correlation is represented at the bottleneck output, where the number of nodes depends on the number of unobserved independent variables that influence the structural response.

In AANN, a model regarding the machine learning algorithm is trained as a neural network using the training data set, the numbers of nodes in bottleneck, mapping, and de-mapping layers. Subsequently, the test data sets are applied to this model to calculate the output of the network concerning the test data. On this basis, a damage index based on AANN can be expressed as:

$$DI_{\text{AANN}} = \left\| \bar{\mathbf{Z}} - \mathbf{Z} \right\|_2 \tag{3.17}$$

In this equation, $\mathbf{Z}$ is the test data, and $\bar{\mathbf{Z}}$ represents the output of the network.

3.3.2 Threshold Level

In order to detect the global state of the structure and classify the undamaged and damaged conditions, it is significant to define a threshold value. Determining this threshold value is very critical and needs careful efforts to calculate an accurate amount. Any

deviation from the threshold level in the process of SHM is indicative of damage occurrence. Depending on the class of machine learning algorithms, the calculation of threshold value depends only on the training data set, the number of observations, and the number of dimensions in the training data.

In this study, a simple method is presented to define the threshold level. Under this method, the only training data is applied to the machine learning methods or their damage indices without using the test data. For example, suppose that $\mathbf{x}$ is a feature vector of the training data set $\mathbf{X}$; therefore, instead of using $\mathbf{z}$ in Eq. (3.7), the values of MSD using the training data set is simply computed as:

$$DI_{\mathrm{MSD}} = (\mathbf{x_j} - \bar{\mathbf{x}})^T \mathbf{\Sigma}^{-1}(\mathbf{x_j} - \bar{\mathbf{x}}) \tag{3.18}$$

Arranging the absolute values of MSD in ascending form, where it begins with $DI_{\min}$ and ends by $DI_{\max}$, the threshold value is given by:

$$t = DI_j|_{j=0.95r} \tag{3.19}$$

In this equation, r is the number of data points in the values of MSD using the training data set, and the scalar amount 0.95 denotes 95% cut-off over the training data. This process can simply be conducted for the other machine learning methods presented in this study. Table 3.1 represents the step-by-step levels of determining the threshold value.

Table 3.1: *The step-by-step levels of determining the threshold value.*

Step 1:	Specify the training data set $\mathbf{X} \in \Re^{m \times n}$ and the test data set $\mathbf{Z} \in \Re^{m \times k}$
Step 2:	Apply the only training data set in the damage index (DI) of the machine learning algorithms without using the test data
Step 3:	Arrange the quantities of damage indices obtained from the previous step in the ascending form
Step 4:	Choose the threshold value based on Eq. (3.19)

3.4 Summary

The main objective of this chapter is to present a global health monitoring strategy by proposing an iterative feature extraction technique and some capable machine learning methods. The proposed iterative algorithm is based on time series modeling with the special focuses on selecting the best time series model and extracting uncorrelated residuals. In this technique, Box-Jenkins methodology is applied to choose a model compatible with the raw vibration data. Residual analysis using Ljung-Box test is then employed to determine a maximum amount as a stopping criterion in the proposed iterative method. In order to extract the parameters of the identified model, it is essential to have uncorrelated residuals. On this basis, an iterative algorithm is established in such a way that the initial correlated residuals obtained from the minimum arbitrary order are used as the input data instead of the raw vibration responses. The machine learning methods are Mahalanobis-square distance (MSD), factor analysis (FA), principle component analysis (PCA), and auto-associative neural network (AANN). The most important ability of these methods is to remove the influence of environmental

and operational variability from the DSFs leading to an appropriate global health monitoring. The major contribution of this study is to propose an iterative feature extraction technique using time series modeling in order for dealing with some limitations and drawbacks such as extracting uncorrelated residual with sufficient orders from vibration time domain responses. Another novelty of this study is to compare the features extracted from the proposed iterative feature extraction technique by some applicable and reliable machine learning approaches under varying the operational and environmental variability.

Robust Multidimensional Scaling Method for High-Dimensional Vibration Data

D UE to directly applying measured data, feature extraction and feature classification are two key parts of any data-driven method. The process of feature extraction discovers meaningful information (features) from raw vibration measurements [7]. For the SHM applications, such features should be sensitive to damage; hence, those are usually known as damage-sensitive features (DSFs). Depending upon the nature and type of vibration data, advanced signal processing techniques provide powerful and effective approaches to extracting diverse DSFs from vibration signals [136]. Time series analysis by time-invariant linear representations is one of the robust feature extraction methods [137]. Several research studies have utilized various time-invariant linear models for feature extraction such as AutoRegressive (AR) [138], AutoRegressive with eXogeneous input (ARX) [139], AutoRegressive Moving Average (ARMA) [140], and AutoRegressive Moving Average with eXogenous input (ARMAX) [112]. Using these models, it is possible to use the AR coefficients and the model residuals as the main DSFs [141]. However, the extraction of features sensitive to damage from measured vibration responses under unpredictable and unknown ambient excitations may be problematic.

The process of feature classification utilizes the DSFs extracted from the normal (known) and current (unknown) states of the structure so as to evaluate the global structural condition and detect any potential damage [7, 142–144]. Hence, this process compares two different states of a structure in order to recognize the status of the current state, which can be either undamaged or damaged. Some effective and well-known feature classification methods include Mahalanobis distance [145, 146], artificial neural networks [147, 148], and clustering [149, 150]. One of the major challenging issues

in feature classification is concerned with the emergence of high-dimensional DSFs. The main limitation is that the implementation of early damage detection by such features may be troublesome and time-consuming. On the other hand, when the high-dimensional DSFs are obtained from unmeasurable and unknown ambient excitations, those may cause unreliable results of damage detection.

The initial solution is to reduce the size of data or DSFs by various dimensionality reduction techniques such as principal component analysis (PCA) [151, 152], random projection [153], deep auto-encoders [154–156], etc. to convert such features into low-dimensional spaces. However, the loss of important information is the main concern about dimensionality reduction techniques [157]. Mujica et al. [158] compared four techniques including PCA, partial least square (PLS), and some extensions called multiway PCA and multiway PLS to reduce the dimension of data for damage identification. They concluded that the multiway approaches are very useful in systems that involve several sensors since those decrease drastically the computation cost. The other comparative study on the problem of dimensionality reduction in the context of SHM can be found in the article of Rebillat and Mechbal [159], who applied several methods including simple direct regression, PCA, PLS, canonical correlation analysis, and autoencoders. They concluded that among the mentioned techniques, PCA, PLS, and canonical correlation analysis are all able to discover a low-dimensional space in their problem.

The other challenging issue in feature classification for any data-driven SHM method is to determine a reliable threshold limit that should be able to distinguish the damaged state from the normal condition. The threshold limit determination is a crucial process because an inaccurate choice increases false alarm (false positive) and false detection (false negative) errors that cause confusing results [160]. In reality, the information of the current state of the structure is usually unknown. Therefore, in most cases of SHM applications, the threshold limit determination is carried out by considering the probabilistic properties of samples or outputs (e.g. damage indices) associated with the normal or undamaged condition. For this purpose, it is necessary to assume a probability distribution model for such samples or outputs and calculate a statistical quantity (i.e. a percentile of the distribution of interest), which is incorporated as a threshold value [146]. The simplest way is to consider the Gaussian or normal distribution and estimate a threshold limit based on a standard confidence interval (CI). Despite the simplicity and computational efficiency of this approach, Sarmadi and Karamodin [146] demonstrated that it is not able to provide a correct and reliable threshold when the samples or outputs regarding the undamaged state are non-Gaussian or heavy-tailed. To address this problem, one can utilize extreme value (EV) statistics and obtain a threshold value by fitting a proper EV distribution [161–163]. However, the selection of an appropriate EV distribution among three potential models (i.e. Gumbel, Fréchet, and Gumbel) is not trivial.

4.1 Feature Extraction by ARMA Model

Time series analysis is a powerful statistical method for modeling vibration time-domain signals (e.g. acceleration time histories) and extracting meaningful information that can be interpreted as the DSFs. The type and nature of vibration signals are important fac-

tors for choosing an appropriate time series model. From a statistical viewpoint, time series is a sequence of values at a time interval that is observable as stationary or non-stationary, deterministic or random, linear or nonlinear, etc. When time-series data is linear and stationary, a suitable choice for time series modeling is to use time-invariant representations including AR, ARX, ARMA, and ARMAX [114].

Depending upon the source of excitation, the process of time series modeling is generally decomposed into input-output and output-only problems. For the input-output problem, it is necessary to have both the excitation (input) and response (output) signals and choose a time series model between ARX and ARMAX. When the input data are unknown such as the ambient excitations, the process of time series modeling is an output-only problem, in which case the only vibration responses of the structure are available. Under such circumstances, one can apply AR and ARMA for modeling the structural responses. An important note is that the vibration time-domain signals resulting from the ambient excitations conform to the ARMA model [164]. Therefore, it is important to use this representation for modeling the structural responses caused by ambient vibration [118]. Supposing that $y(t)$ is a vibration signal (structural response) at time t, the ARMA model is expressed as:

$$y(t) = \sum_{i=1}^{na} \varphi_i y(t-i) + \sum_{j=1}^{nc} \psi_j e(t-j) + e(t) \tag{4.1}$$

where na and nc denote the orders of the AR and MA terms of the ARMA model; $\Phi = [\varphi_1, ..., \varphi_{na}]$, $\Psi = [\psi_1, ..., \psi_{nc}]$ are the vectors of the AR and MA coefficients, respectively. In Eq. (4.1), $e(t)$ is the residual of the model at time t, which can be written as follows:

$$e(t) = y(t) - \hat{y}(t) = y(t) - \left(\sum_{i=1}^{na} \varphi_i y(t-i) + \sum_{j=1}^{nc} \psi_j e(t-j) \right) \tag{4.2}$$

This value corresponds to the difference between the actual vibration signal $y(t)$ and the predicted time series $\hat{y}(t)$ obtained from the ARMA model. Determination of sufficient orders of time series representations is a crucial part of time series modeling. This is because a selection of appropriate orders guarantees the model accuracy and adequacy. In other words, a sufficient order is one that enables the time series model to generate uncorrelated residuals; otherwise, the order should be improved [141]. Considering the equality of AR and MA orders ($na = nc$), it is possible to determine them by checking the uncorrelatedness of the ARMA model residuals through the Ljung-Box test. This is a statistical hypothesis test that assesses the correlation between the residual sequences of a time series model [114]. Accordingly, if the p-value of the test is greater than a significance level, one can realize that the residual sequences are uncorrelated. As a result, the iterative order determination technique proposed by Entezami and Shariatmadar [141] is exploited to choose the sufficient orders of the ARMA model. Although this technique was proposed to determine the order of the AR model, its great merit is that one can utilize it for other kinds of time series models.

On the other hand, the process of feature extraction via time series modeling is decomposed into the coefficient-based and residual-based approaches [141]. For the ARMA model, the coefficient-based approach is intended to extract the AR coeffi-

cients, which are directly related to the structural properties. In this regard, it is necessary to determine the orders of the ARMA model from the vibration signals of the normal condition and then estimate the AR coefficients of the normal and damaged states by one of the computational techniques. For the use of the model residuals as the DSFs, one initially requires obtaining the orders and coefficients of the ARMA representation from the only normal condition and then extracting the model residuals. In the damaged state, the model information (the orders and coefficients) gained by the normal condition are utilized in an effort to extract the residuals of the ARMA model. The central idea behind the residual-based approach is that the model obtained from the normal state cannot give a reliable goodness-of-fit for time series modeling in the damaged state, which leads to increases in the model residuals [141]. Despite the high applicability of the coefficient-based and residual-based approaches to the feature extraction, the latter does not require any order determination and parameter estimation in the damaged state. Therefore, it seems that the use of the model residuals is more advantageous to the process of feature extraction.

4.2   Robust Multidimensional Scaling

The RMDS is a technique for the reduction of the dimension of sampling data and analysis of dissimilarity on a set of samples by considering outliers and uncertainties in data. In fact, this technique is an improvement of the MDS [165], which is sensitive to outliers and uncertainties [166, 167]. The RMDS aims to establish a dissimilarity model that explicitly accounts for outliers and find an embedding matrix by solving the proposed dissimilarity model in an iterative manner [166]. Consider a multivariate dataset of n vectors of m-dimensional samples $\mathbf{X} = [\mathbf{x_1}, \mathbf{x_2}, ..., \mathbf{x_n}] \in \mathbb{R}^{n \times m}$. Using the conventional Euclidean-squared distance (ESD), the dissimilarity between the vectors $\mathbf{x}h$ and $\mathbf{x}r$ is given by:

$$\delta_{h,r}(\mathbf{X}) = (\mathbf{x}_h - \mathbf{x}_r)(\mathbf{x}_h - \mathbf{x}_r)^T \tag{4.3}$$

where $h, r = 1, 2, ..., n$. The dissimilarity should satisfy $\delta_{h,r}(\mathbf{X}) \geq 0$, $\delta_{h,r}(\mathbf{X}) = \delta_{r,s}(\mathbf{X})$, and $\delta_{h,h}(\mathbf{X}) = \delta_{r,r}(\mathbf{X}) = 0$. By calculating all dissimilarities, one can obtain the distance matrix $\mathbf{D} \in \mathbb{R}^{n \times n}$, which is used in the RMDS algorithm. Given $\mathbf{D}$, this algorithm seeks an embedding of n vectors in a v-dimensional space $(n > v)$, which leads to the embedding or configuration matrix $\mathbf{U} = [\mathbf{u_1}, \mathbf{u_2}, ..., \mathbf{u_n}] \in \mathbb{R}^{n \times v}$ so that the pairwise distance $d_{h,r}(\mathbf{U}) = \|\mathbf{u}_h - \mathbf{u}_r\|_2$ approximates $\delta_{h,r}(\mathbf{X})$. Note that $\| \cdot \|_2$ refers to the Euclidean norm. In order to take into account outliers and find $\mathbf{U}$, the RMDS algorithm presents a dissimilarity model as follows:

$$\delta_{h,r}(\mathbf{X}) = d_{h,r}\mathbf{U} + o_{h,r} + \varepsilon_{h,r} \tag{4.4}$$

where $o_{h,r}$ denotes an outlier variable of $\delta_{h,r}(\mathbf{X})$, and $\varepsilon_{h,r}$ is an independent random value. For all outlier variables, one can collect them and construct the outlier matrix $\mathbf{O} \in \mathbb{R}^{n \times n}$. Hence, the estimate of $\mathbf{O}$ and $\mathbf{U}$ in the RMDS algorithm is performed by minimizing the following objective function:

$$f(\mathbf{O}, \mathbf{U}) = \sum_{h<r}(\delta_{h,r}(\mathbf{X}) - d_{h,r}(\mathbf{U}) - o_{h,r})^2 + \lambda \sum_{h<r} \|o_{h,r}\|_0 \tag{4.5}$$

where $\lambda > 0$ is a regularization value that controls the sparsity of $\mathbf{O}$ and corresponds to the l_0-norm $(\|\cdot\|_0)$ of the outlier matrix. The minimization of Eq. (4.5) in the RMDS algorithm is based on an iterative solver using a majorization-minimization (MM) approach [166]. For this purpose, one needs to expand $f(\mathbf{O}, \mathbf{U})$, which yields:

$$f(\mathbf{O}, \mathbf{U}) = \frac{1}{2}\|\mathbf{D} - \mathbf{O}\|_F^2 - 2\sum_{h<r}(\delta_{h,r}(\mathbf{X}) - o_{h,r})d_{h,r}(\mathbf{U}) + Tr(\mathbf{U}\mathbf{L}\mathbf{U}^T) + \frac{\lambda}{2}\|\mathbf{O}\|_1 \quad (4.6)$$

in which

$$\|\mathbf{O}\|_1 = \sum_{h<r}|o_{h,r}| \quad (4.7)$$

In Eq. (4.6), $\mathbf{L}$ is a matrix with diagonal and off-diagonal entries equal to 1 and -1, respectively. Furthermore, "Tr" refers to the trace operator of a matrix. Supposing that $\mathbf{V}$ is an arbitrary matrix, one can define the matrices $\mathbf{A}_1(\mathbf{O}, \mathbf{V})$ and $\mathbf{A}_2(\mathbf{O}, \mathbf{V})$ in the following forms:

$$\mathbf{A}_1(\mathbf{O}, \mathbf{V}) = \begin{cases} \dfrac{\delta_{h,r}(\mathbf{X}) - o_{h,r}}{d_{h,r}(\mathbf{V})} & (h, r) \in \delta_{h,r}(\mathbf{X}) > o_{h,r}, d_{h,r}(V) > 0 \\ 0 & \text{otherwise} \end{cases} \quad (4.8)$$

$$\mathbf{A}_2(\mathbf{O}, \mathbf{V}) = \begin{cases} -\dfrac{\delta_{h,r}(\mathbf{X}) - o_{h,r}}{d_{h,r}(\mathbf{V})} & (h, r) \in \delta_{h,r}(\mathbf{X}) \leq o_{h,r}, d_{h,r}(V) > 0 \\ 0 & \text{otherwise} \end{cases} \quad (4.9)$$

Accordingly, their Laplacian matrices are given by:

$$\mathbf{L}_1(\mathbf{O}, \mathbf{V}) = \text{diag}(\mathbf{A}_1(\mathbf{O}, \mathbf{V})\mathbf{I}) - (\mathbf{A}_1(\mathbf{O}, \mathbf{V})) \quad (4.10)$$

$$\mathbf{L}_2(\mathbf{O}, \mathbf{V}) = \text{diag}(\mathbf{A}_2(\mathbf{O}, \mathbf{V})\mathbf{I}) - (\mathbf{A}_2(\mathbf{O}, \mathbf{V})) \quad (4.11)$$

where $\mathbf{I}$ denotes an $n \times 1$ vector of all ones. Using the above-mentioned matrices, the majorizer of $f(\mathbf{O}, \mathbf{U})$ is given by:

$$\begin{aligned} g(\mathbf{O}, \mathbf{U}; \mathbf{V}) = {}& Tr(\mathbf{U}(\mathbf{L} + \mathbf{L}_2(\mathbf{O}, \mathbf{U}))\mathbf{U}^T) + \alpha(\mathbf{O}, \mathbf{V}) \\ & -2Tr(\mathbf{U}\mathbf{L}_1(\mathbf{O}, \mathbf{V})\mathbf{V})^T + \frac{1}{2}\|\mathbf{D} - \mathbf{O}\|_F^2 + \frac{\lambda}{2}\|\mathbf{O}\|_1 \end{aligned} \quad (4.12)$$

For $\delta_{h,r}(\mathbf{X}) \leq o_{h,r}$ and $d_{h,r}(\mathbf{U}) > 0$, $\alpha(\mathbf{O}, \mathbf{V})$ is expressed as:

$$\alpha(\mathbf{O}, \mathbf{V}) = \sum_{h<r}(\delta_{h,r}(\mathbf{X}) - o_{h,r})d_{h,r}(\mathbf{V}) \quad (4.13)$$

Therefore, the MM approach provides an iterative algorithm to minimize $f(\mathbf{O}, \mathbf{U})$ and obtain the matrices $\mathbf{O}$ and $\mathbf{U}$ at $(t + 1)$ iterations in the following forms:

$$\mathbf{O}_{(t+1)} = \arg\min g(\mathbf{O}, \mathbf{U}_{(t)}; \mathbf{U}_{(t)}) \qquad (4.14)$$

$$\mathbf{U}_{(t+1)} = \arg\min g(\mathbf{O}_{(t+1)}, \mathbf{U}; \mathbf{U}_{(t)}) \qquad (4.15)$$

For Eq. (4.14), each entry of $\mathbf{O}_{(t+1)}$ corresponds to the solution of:

$$\min \left(\delta_{h,r}(\mathbf{X}) - d_{h,r}(\mathbf{U}_{(t)}) - o_{h,r} \right)^2 + \lambda |o_{h,r}| \qquad (4.16)$$

which is a scalar Lasso problem, whose solution is expressible by using the operator S_λ as follows:

$$S_\lambda(x) = \mathrm{sgn}(x)\beta(x) \qquad (4.17)$$

where "sgn" is the sign function and $\beta(x) = \max(0, |x| - \lambda/2)$. Using these expressions, the solution to Eq. (4.16) can be written as:

$$o_{h,r}^{(t+1)} = S_\lambda \left(\delta_{h,r}(\mathbf{X}) - d_{h,r}(\mathbf{U}_{(t)}) \right) \qquad (4.18)$$

Since the majorizer g is defined via the matrices $\mathbf{L}_1$ and $\mathbf{L}_2$, the update of $\mathbf{U}$ in Eq. (4.15) can be expressed as:

$$\mathbf{U}_{(t+1)} = \mathbf{U}_{(t)} \mathbf{L}_1 \left(\mathbf{O}_{(t+1)}, \mathbf{U}_{(t)} \right) \mathbf{L}^+ \qquad (4.19)$$

where "+" denotes the Moore-Penrose pseudo-inverse. It is worth remarking that the arbitrary matrix $\mathbf{V}$ in Eqs. (4.8) - (4.11) is the embedding matrix at the tth iteration; that is, $\mathbf{V} = \mathbf{U}_{(t)}$. In order to terminate the iteration in the MM approach, one needs to define a stopping condition. For this aim, the RMDS method terminates when the relative error $\|\mathbf{U}_{(t+1)} - \mathbf{U}_{(t)}\|_F / \|\mathbf{U}_{(t+1)}\|_F$ is smaller than an inconsiderable positive value.

4.3 Proposed Data-Driven Method for SHM

4.3.1 Segmentation of High-Dimensional DSFs

Assume that $\mathbf{E}$ and $\bar{\mathbf{E}} \in \mathbb{R}^{nd \times ns}$ are the residual datasets (matrices) of the ARMA models in the undamaged and damaged states, where nd and ns denote the numbers of residual samples and sensors ($nd \gg ns$), respectively. Due to the high-dimensionality of the residual matrices, it is necessary to divide them into several low-dimensional partitions with the same dimension as shown in Fig. 4.1. In this regard, the matrices $\mathbf{E}$ and $\bar{\mathbf{E}}$ can be segmented into p partitions with np samples; that is, $\mathbf{E}_1^*, ..., \mathbf{E}_p^*$ and $\bar{\mathbf{E}}_1^*, ..., \bar{\mathbf{E}}_p^*$ where $\mathbf{E}^*$ and $\bar{\mathbf{E}}^* \in \mathbb{R}^{nd \times ns}$ ($nd > np \gg ns$). Based on the descriptions in Section 4.2, the residual matrices $\mathbf{E}_1^*, ..., \mathbf{E}_p^*$ and $\bar{\mathbf{E}}_1^*, ..., \bar{\mathbf{E}}_p^*$ are equivalent to $\mathbf{X}$, in which case $np = n$ and $ns = m$.
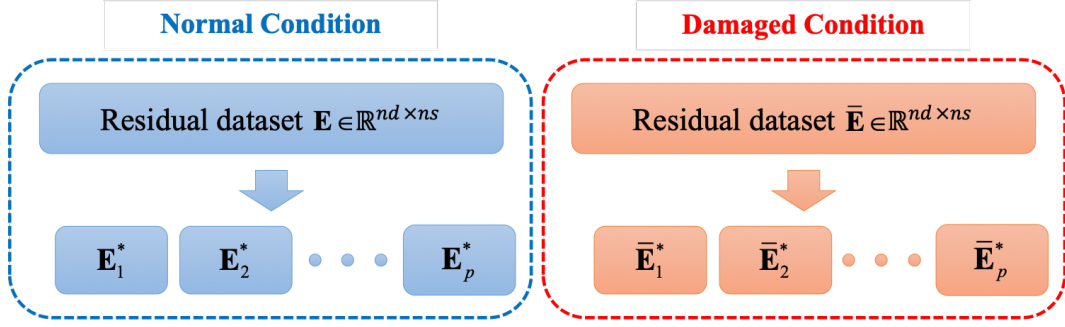
Figure 4.1: *Graphical representation of the segmentation of the residual datasets of the normal and damaged states.*

4.3.2 Determination of Embedding Norm Values as Damage Indicators

After the segmentation of the residual datasets of the normal and damaged states, one initially needs to compute the distance matrices of $\mathbf{E}_1^*, ..., \mathbf{E}_p^*$ and $\bar{\mathbf{E}}_1^*, ..., \bar{\mathbf{E}}_p^*$ by the ESD technique or Eq. (4.3). For the np vectors of the residual datasets, the distance matrices are the size of $np \times np$. In the following, the RMDS algorithm based on the iterative MM approach is applied to obtain the embedding matrices of all segments for the normal and damaged states; that is, $\mathbf{U}_1, ..., \mathbf{U}_p$ and $\bar{\mathbf{U}}_1, ..., \bar{\mathbf{U}}_p$, where $\mathbf{U}$ and $\bar{\mathbf{U}} \in \mathbb{R}^{np \times v}$. When np is relatively large, it is not trivial to use the high-dimensional large embedding matrices of all partitions for feature classification. To address this limitation, the matrix vectorization technique is used to convert the embedding matrices into vectors $\mathbf{u}_1, ..., \mathbf{u}_p$ and $\bar{\mathbf{u}}_1, ..., \bar{\mathbf{u}}_p$, each of which includes nv samples ($nv = np \times v$).

To obtain a damage indicator, an embedding norm value is defined by calculating the Euclidean norm of each embedding vector of the undamaged and damaged states. Taking the norm values of all segments (i.e. $\|\mathbf{u}_1\|_2, ..., \|\mathbf{u}_p\|_2$ and $\|\bar{\mathbf{u}}_1\|_2, ..., \|\bar{\mathbf{u}}_p\|_2$) into consideration, one can combine them into the distance vector $\mathbf{d}$ as follows:

$$\mathbf{d} = [\|\mathbf{u}_1\|_2, ..., \|\mathbf{u}_p\|_2, \|\bar{\mathbf{u}}_1\|_2, ..., \|\bar{\mathbf{u}}_p\|_2] \in \mathbb{R}^{2p} \tag{4.20}$$

where the first p embedding norm values belong to the normal condition and the remaining quantities are associated with the damaged state. In some cases, the measurement of vibration data is repeated several times in order to increase the reliability of data acquisition. Under such circumstances, there are large volumes of vibration datasets leading to the massive DSFs.

Assuming that nm refers to the number of test measurements, one can extract nm sets of the DSFs (i.e. the residual matrices $\mathbf{E}$ and $\bar{\mathbf{E}}$). Therefore, the determination of embedding norm values in the normal and damaged conditions is repeated nm times, which leads to a larger distance-vector $\mathbf{d_T} = [\mathbf{d}_1, ..., \mathbf{d}_{nm}] \in \mathbb{R}^{2p \times nm}$ including the nm vectors of $\mathbf{d}$. It is worthwhile remarking that the first $p \times nm$ embedding norm values of $\mathbf{d_T}$ belong to the normal condition and the remaining quantities are associated with the damaged state. For the problem of early damage detection, it is necessary to define a threshold limit by using the first $p \times nm$ embedding norm values in $\mathbf{d_T}$. On this basis, any deviation of the embedding norm value of the damaged state from the threshold limit is representative of the damage occurrence. For the sake of convenience, Fig. 4.2 shows the flowchart of the proposed RMDS-based method.
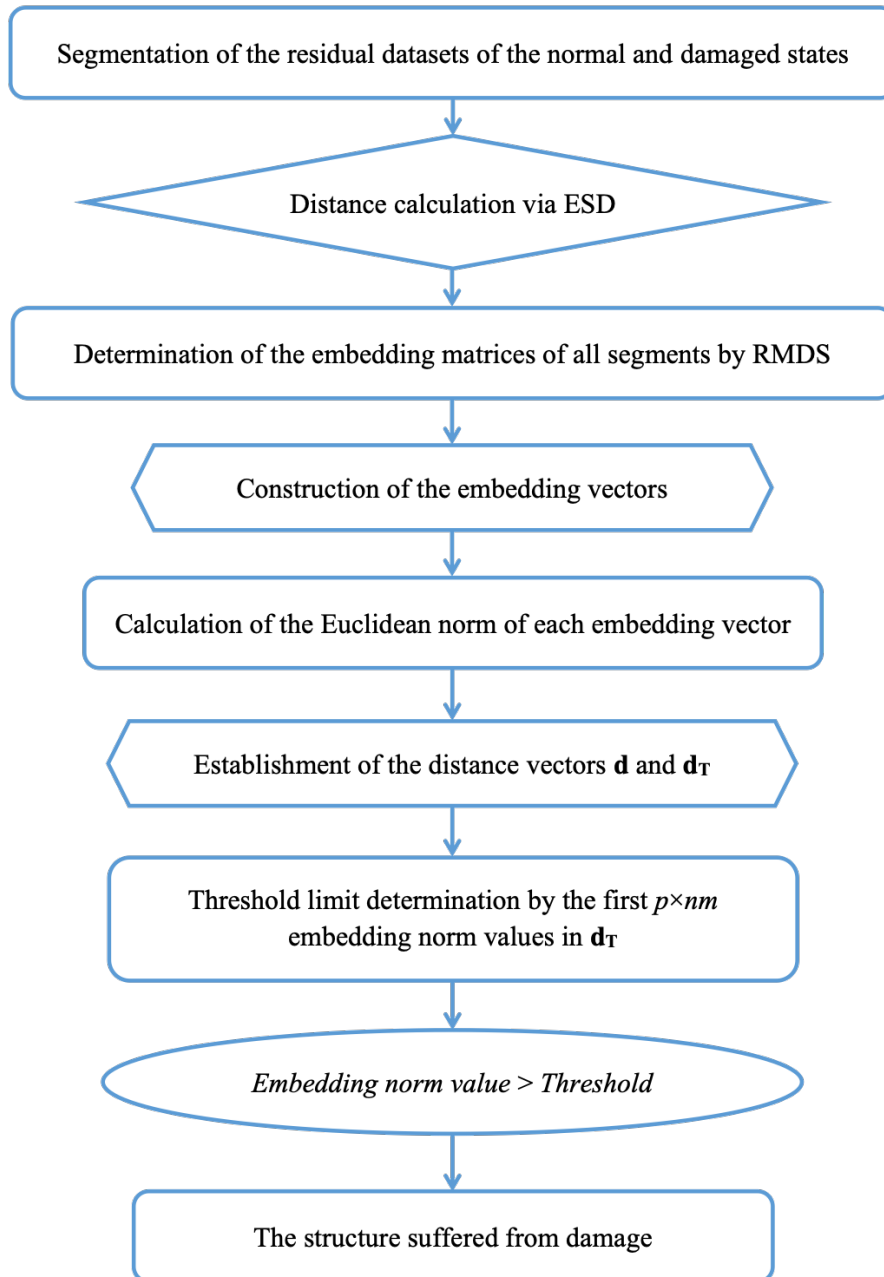
Figure 4.2: *Flowchart of the proposed RMDS-based method for SHM.*

4.4 Threshold Limit Determination

4.4.1 Extreme Value Statistics

In statistics and probability, the EV theory is a branch of order statistics that focuses on modeling the tails of distribution [168,169]. For independent and identically distributed data, the EV distributions can only take one of the three families including Gumbel (Type 1), Fréchet (Type 2), or Weibull (Type 3). Assume that $H(x)$ is a non-degenerate limit function. On this basis, the Gumbel distribution model is expressed as:

$$H_1(x) = \exp\left(-\exp\left(-\frac{x-\mu}{\sigma}\right)\right) \tag{4.21}$$

where $-\infty < x < \infty$ and $\sigma > 0$. Moreover, the Fréchet and Weibull distribution models are formulated in the following forms:

$$H_2(x) = \begin{cases} \exp\left(-\left(\frac{\sigma}{x-\mu}\right)^{\xi}\right) & x \geq \mu \\ 0 & x < \mu \end{cases} \tag{4.22}$$

$$H_3(x) = \begin{cases} 1 & x \geq \mu \\ \exp\left(-\left(\frac{\mu-x}{\sigma}\right)^{\xi}\right) & x < \mu \end{cases} \tag{4.23}$$

In Eqs. (4.21) - (4.23), μ, σ, and ξ are the parameters of the EV distributions known as the location, scale, and shape (i.e. expect for the Gumbel distribution) [169]. Given the maximum values of a dataset, it is possible to select a proper limit distribution among $H_1(x)$, $H_2(x)$, and $H_3(x)$ and fit an EV distribution model to the maximum values. Once the type of EV distribution and its unknown parameters have been obtained, the threshold limit under a significance level (α) is computed by inverting the limit function of the selected EV distribution. In the Gumbel-type EV distribution, for example, one needs to invert the following equation:

$$\exp\left(-\exp\left(-\frac{x-\mu}{\sigma}\right)\right) = 1 - \frac{\alpha}{2} \tag{4.24}$$

which leads to the upper-limit threshold value (τ_1) as follows:

$$\tau_1 = x = \mu - \sigma \ln\left(-\ln\left(1 - \frac{\alpha}{2}\right)\right) \tag{4.25}$$

The same process can be implemented for the other EV distributions to define their threshold limits in the following forms:

$$\tau_2 = x = \mu + \frac{\sigma}{\left(-\ln\left(1 - \frac{\alpha}{2}\right)\right)^{1/\xi}} \tag{4.26}$$

$$\tau_3 = x = \mu - \sigma \left(-\ln\left(1 - \frac{\alpha}{2}\right)\right)^{1/\xi} \tag{4.27}$$

4.4.2 Selection of an Appropriate EV Distribution by GEV

The process of threshold limit determination by the EV statistics depends strongly on the choice of an appropriate EV distribution among Gumbel, Fréchet, and Weibull families. To deal with this limitation, this study utilizes an effective and simple approach based on the GEV. It is a family of continuous probability distributions developed within the EV theory. The main objective of GEV is to integrate the three EV distributions into a single family of distribution as follows:

$$H(x) = \exp\left(-\left(1 + \xi_G\left(\frac{x - \mu_G}{\sigma_G}\right)\right)^{-\frac{1}{\xi_G}}\right) \tag{4.28}$$

where μ_G, σ_G, and ξ_G represent the location, scale, and shape of the GEV distribution model. The key characteristic of the GEV distribution is the ability to recognize the type of EV distribution. When $\xi_G < 0$, the GEV is the Weibull-type EV distribution. In contrast, the GEV conforms to the Fréchet-type EV distribution for $\xi_G > 0$. Finally, if ξ_G is identical to zero, one can realize that the GEV is the Gumbel-type EV distribution [168]. Therefore, it is only necessary to estimate the shape parameter of the GEV and then choose an EV distribution for the threshold limit determination. It is important to mention that the maximum likelihood estimation (MLE) is applied to estimate the unknown parameters of the EV and GEV distributions.

4.5 Summary

This chapter has presented a novel data-driven method for early damage detection under high-dimensional features and ambient vibration by robust multidimensional scaling (RMDS). The RMDS is an improvement on the traditional multidimensional scaling (MDS). Both techniques aim to create low-dimensional projections by retaining pairwise distances between data samples as much as possible. The major disadvantage of the MDS is that it may suffer from outliers and uncertainties [166]. In most real cases of SHM, the outliers and uncertainties may be noise in measurements, unknown ambient excitations, environmental variability, etc. that may seriously affect the performance of any feature classification method. On this basis, the RMDS is proposed to develop a novel data-driven SHM method. This method consists of some simple but effective computational steps including the segmentation of high-dimensional DSFs, the pairwise distance computation by the Euclidean-squared distance (ESD), the implementation of the RMDS iterative algorithm, the matrix vectorization process, and the Euclidean norm calculation. The process of feature extraction under ambient vibration is performed by fitting ARMA models to measured vibration responses and extracting their residuals as randomly high-dimensional DSFs. The major contribution of this study is to develop a novel data-driven strategy for detecting damage based on the output of the RMDS as a new method for dimensionality reduction. Dealing with the problem of using large volumes of high-dimensional DSFs for early damage detection is the main advantage of the proposed method. Concerning the challenge of the threshold limit determination based on the EV theory, this study introduces the generalized extreme value (GEV) distribution and its shape parameter to select the most appropriate EV model.

Clustering-Based Novelty Detection Method for Unsupervised Damage Detection

THE basic premise of SHM is that the occurrence of damage changes the inherent structural parameters (i.e. often stiffness) as well as the vibration responses and characteristics. Modal frequencies are popular and widely used dynamic features for structural health monitoring due to some great merits such as sensitivity to damage, simple identification via various techniques of operational modal analysis, and provision of global information for early damage detection. However, the main drawback of modal frequencies is their high sensitivity to environmental and/or operational variability conditions [170–172]. These conditions may arise from temperature fluctuations, humidity and moisture changes, wind speed and excitation amplitude variations, traffic, etc. [37]. Because the variations in structural responses caused by the environmental and/or operational variability are similar to damage, *Type I* or false alarm (i.e. the structure is undamaged but the method of damage detection mistakenly alerts the occurrence of damage) and *Type II* or false detection (i.e. the structure suffers from damage but the method of damage detection incorrectly declares the normal condition) are common errors in most of the modal-based SHM methods.

Machine learning algorithms present effective and tried-and-tested approaches to analyzing features extracted from vibration data (e.g. modal frequencies) and making decisions about the current state of the structure, thereby finding its normal or damaged status [173, 174]. These algorithms are usually divided into two main classes called supervised learning and unsupervised learning. Both algorithms are intended to learn a statistical model (classifier or detector) by training data and make a decision via testing data. The main difference between supervised and unsupervised learning is that the former needs the information (features) of both undamaged and damaged (current) states

to learn a model, while the latter requires the only information or features of the undamaged condition. In most cases of SHM applications, the current state of the structure is unknown. Under such circumstances, it is not practical and economical to impose intentional damage patterns on complex and expensive civil structures in an effort to obtain information about the damaged condition. Therefore, one can conclude that unsupervised learning is more beneficial than supervised learning for health monitoring of civil structures.

Cluster analysis is a popular unsupervised learning method that aims at dividing similar objects into subsets or clusters. Regardless of the type of vibration data, damage-sensitive features, and structural systems, some well-known clustering techniques such as k-means [175, 176], k-medoids [177, 178], fuzzy clustering [179], and Gaussian mixture model [180, 181] have been utilized to detect damage. Although the utilization of cluster analysis is simple, the environmental and/or operational variability conditions seriously affect the performances of clustering algorithms (and the other unsupervised learning methods). Therefore, this problem is still a major challenge in SHM and it may become worse if the distance metric used in the algorithm of clustering has low damage detectability.

On the other hand, the decision-making for early damage detection in most of the unsupervised learning methods requires an alarming threshold (i.e. a threshold limit) that enables them to alarm adverse changes in the structure caused by damage and correctly distinguish the damaged state from the undamaged condition. To put it another way, the estimate of a reliable threshold is critical because the final decision about the occurrence of damage depends strongly on it. In most cases, this limit is obtained by the probabilistic properties of the outputs of the model learned by the training data [146]. One of the powerful and effective ways for threshold estimation is based on the extreme value theory (EVT) [168, 169]. Under this theory, it is only necessary to select an extreme value distribution among Gumbel, Fréchet, and Weibull distribution models and use a technique for modeling that distribution. The threshold limit is estimated by using the extreme quantile of the cumulative density function of the distribution under a significance level [161]. Nonetheless, this approach suffers from two main limitations. First, it is important to apply an analytical technique to select the most appropriate extreme value distribution among Gumbel, Fréchet, and Weibull models. Second, one needs to use an alternative technique so as to verify this choice [168].

To deal with these limitations, the best solution is to consider the generalized extreme value theory and utilize generalized extreme value (GEV) and generalized Pareto (GP) distribution models [168]. The great merit of these distributions is that each of them is a single distribution for modeling extreme quantities or rare events without any requirement of applying additional techniques for choosing and verifying the distribution model. In this regard, Block maxima (BM) and peak-over-threshold (POT) are two well-known approaches to modeling the GEV and GP distributions, respectively. Despite the applicability and effectiveness of these techniques to the threshold estimation, choosing an optimal block number for the BM and determining a threshold value for the POT are their limitations. Any inappropriate choices of these parameters cause inaccurate alarming thresholds for damage detection along with increases in the false alarm and false detection errors.

5.1 Backgrounds

Cluster analysis is an unsupervised learning method based on dividing similar points with the small discrepancies or distances into a group or cluster. This concept provides an appropriate opportunity to utilize clustering techniques in SHM. Based on the general definition of the cluster analysis, one can exploit several clustering methods via the prototype-based, density-based, graph-based, and hybrid algorithms [182]. The major merit of prototype-based clustering approaches is that they are suitable for large and high-dimensional samples [183]. Therefore, the main focus of this study is to present a new application of one of the prototype-based clustering methods called the *k*-medoids clustering to the SHM problem.

5.1.1 The K-Medoids Clustering

The *k*-medoids clustering is a prototype-based partitioning method commonly used in domains that require robustness to outlier data, arbitrary distance metrics, and conditions that the mean and/or median do not have clear definitions [184]. This method is similar to the *k*-means clustering and the objective of both methods is to divide a set of observations or data points into k subsets (clusters) so that the subsets minimize the sum of distances between an observation and a center of the observation's cluster. In fact, both methods attempt to minimize the distance between points labeled to be in a cluster and a point designated as the center of that cluster by a predefined objective function. For the *k*-means clustering, the prototype of interest is the centroid of data (the average between the points) in a cluster. This method employs the Euclidean distance as the usual distance metric and assigns a data point into the cluster that has the minimum distance from its centroid. In contrast, the *k*-medoids algorithm selects data points as centers (medoids) that can be chosen by arbitrary distances. Unlike the k-means clustering, the center of data in a cluster is a prototype in the *k*-medoids clustering. For this reason, this method is more resilient to noise and outliers in sampling data compared to the *k*-means clustering [184].

Assume that $\mathbf{X} = [\mathbf{x}_1, ..., \mathbf{x}_n] \in \Re^{q \times n}$ is a matrix of n observations and q variables. The algorithm of the k-medoids clustering divides the data set $\mathbf{X}$ into k clusters, which the number of clusters (k) is known as *a priori*. This method implements the clustering process iteratively by a predefined objective function until each representative observation is actually the medoid of the cluster. The objective function of interest is expressed as:

$$J(\mathbf{c}_1, ..., \mathbf{c}_k) = \min \sum d(\mathbf{x}_i, \mathbf{c}_j) \tag{5.1}$$

where $i = 1, 2, ..., n$ and $j = 1, 2, ..., k$. Moreover, in Eq. (5.1), $\mathbf{c}_1, ..., \mathbf{c}_k$ are the cluster centers (medoids) and d denotes a dissimilarity measure, which is no need for this measure to be symmetric or even metric. For the k-medoids clustering, the medoids or centers are obtained from an iterative algorithm when the objective function J reaches its minimum. One of the algorithms is called partitioning around medoids (PAM), which proceeds in two steps including *build-step* and *swap-step*. The algorithm iterates the build-steps and swap-steps until the medoids do not change, or termination criteria are satisfied. The PAM algorithm minimizes the objective function by swapping all the non-medoid points and medoids iteratively until convergence.

5.1.2 Clustering in SHM

To detect damage by clustering techniques, it is necessary to define a strategy based on a clustering algorithm and a damage indicator. Generally, the process of clustering for SHM is carried out in the baseline (training) and monitoring (inspection) phases. During the baseline period, the damage-sensitive features (e.g. modal frequencies) of the undamaged states of the structure under different sources of environmental and/or operational variations are used to produce a training data set. The main goal of the clustering algorithm used in the damage detection framework in the baseline phase is to determine the number of clusters. For the monitoring stage, the damage-sensitive features of the current state of the structure are applied to make a testing data set. Because this state is unknown, which means that it can be normal or damaged, the use of testing data in the clustering algorithm indicates whether the structure is undamaged or damaged.

Here, it is supposed that $\mathbf{X} \in \Re^{q \times n}$ and $\mathbf{Z} \in \Re^{q \times m}$ are the training and testing matrices with the same variables and different observations. To employ the k-medoids clustering in the damage detection framework, the main requirements in the baseline phase are the number of clusters (k) and the cluster medoids $\mathbf{c}_1, ..., \mathbf{c}_k$. In most cases, the damage indicator used in the framework of interest is defined as a distance measure so as to determine the dissimilarity between a feature vector and the cluster medoids. For a given q-dimensional feature vector of the testing data $(\mathbf{z})$, the damage indicator is the smallest distance between $\mathbf{z}$ and all cluster medoids. Using the Euclidean distance as a popular and widely-used distance measure, the damage indicator DI^* is given by:

$$DI^* = \min \left(\|\mathbf{z} - \mathbf{c}_1\|_2, \|\mathbf{z} - \mathbf{c}_2\|_2, ..., \|\mathbf{z} - \mathbf{c}_k\|_2 \right) \tag{5.2}$$

For each feature vector of the testing data, the calculation of DI continues to obtain a vector of the smallest distance values of DI^* regarding all observations. In the monitoring phase, this vector is designated as $\mathbf{d_m} = [DI_1^*, ..., DI_m^*]$, where m denotes the number of observations (feature vectors) of the testing data. The decision about the occurrence of damage needs an alarming threshold. For this purpose, the feature vectors of the training data $(\mathbf{x}_1, ..., \mathbf{x}_n)$ are used in Eq. (5.2) to define a vector of the smallest distance values of DI^* in the baseline phase, which is designated as $\mathbf{d_b} = [DI_1^*, ..., DI_n^*]$. This vector is the output of the clustering-based method for estimating an alarming threshold. Any deviation of the values in $\mathbf{d_m}$ from the threshold is indicative of damage occurrence.

5.2 Proposed Clustering-Based Method

The proposed clustering-based method is based on the k-medoids algorithm. The main objective is to obtain a set of medoids using an optimal cluster number that enables the proposed method to deal with the effects of environmental and/or operational variability. This method also presents a new damage indicator on the basis of an $L_{p,r}$-distance metric to increase damage detectability so that p and r are scalar values implying the powers of the $L_{p,r}$-distance.

5.2.1 $\mathbf{L_{p,r}}$-Distance Measure

In most cases, the L_2-norm or Euclidean distance is a popular and widely used measure for defining an indicator for damage detection. The $L_{p,r}$-distance measure is a general form of the Euclidean distance. This is a kind of power distance measure that uses a formula mathematically equivalent to the power (p, r)-distance [185]. High damage detectability should be the main characteristic of an appropriate damage indicator. If the current state of the structure suffered from damage, the damage indicator with high detectability is able to effectively indicate this situation. Given the two arbitrary vectors $\mathbf{x}$ and $\mathbf{z}$, the $L_{p,r}$-distance measure is defined as follows [186]:

$$L_{p,r} = \left(\sum |\mathbf{x} - \mathbf{z}|^p \right)^{\frac{1}{r}} \tag{5.3}$$

Depending on different values of p and r, it is feasible to express several distance metrics. For $p = r \geq 1$, the $L_{p,r}$-distance measure can be called the Euclidean, Manhattan, and Chebyshev metrics when the powers p and r are identically set as 2, 1, and ∞, respectively. In mathematics, the Chebyshev distance or maximum metric is a measure for calculating dissimilarity between two vectors, where the distance between them is the greatest of their differences along any coordinate dimension [187]. In the case of $p = 2$ and $r = 1$, the $L_{p,r}$-distance measure is equivalent to the squared Euclidean distance. For $0 < p = r < 1$, furthermore, this measure is called the fractional L_p-distance [186]. Based on the definition of the $L_{p,r}$-distance, one can define a new damage indicator by using the feature vector of the testing data and the cluster medoids in the following form:

$$DI = \min \left(L_{p,r}(\mathbf{z} - \mathbf{c}_1), L_{p,r}(\mathbf{z} - \mathbf{c}_2), ..., L_{p,r}(\mathbf{z} - \mathbf{c}_k) \right) \tag{5.4}$$

where

$$L_{p,r}(\mathbf{z}, \mathbf{c}_j) = \left(\sum |\mathbf{z} - \mathbf{c}_j|^p \right)^{\frac{1}{r}} \tag{5.5}$$

where $j = 1, 2, ..., k$. Having considered all feature vectors of the testing matrix, it is possible to determine the vector $\mathbf{d_m} = [DI_1, ..., DI_m]$. The same procedure is performed to obtain the vector $\mathbf{d_b} = [DI_1, ..., DI_n]$ by using the feature vectors of the training data. In other words, each of the vectors $\mathbf{x}_1, ..., \mathbf{x}_n$ is incorporated into Eq. (5.4) instead of $\mathbf{z}$. Finally, the vector $\mathbf{d_b}$ is applied to estimate an alarming threshold for damage detection.

5.2.2 Selection of An Appropriate Cluster Number for SHM

The selection of a proper and optimal cluster number is an important subject in the prototype-based clustering algorithms such as the *k*-means, fuzzy *c*-means, and *k*-medoids. Because the final results of clustering depend on the number of clusters, it is essential to specify it in advance. Generally, the use of a few clusters may increase the errors in results, while relatively large clusters enable the clustering algorithm to decrease the errors. For SHM applications, the number of clusters is determined by using the training data concerning the normal condition of the structure in the baseline

phase. The common approach to choosing the cluster number for prototype-based clustering algorithms is to employ the Silhouette value technique [184]. However, it will be indicated that this technique is not resilient to SHM due to the presence of outliers, noise, or environmental and/or operational variability.

On this basis, it will be proved in this study that the poor performance of the k-medoids clustering in SHM due to high rates of Type I and Type II errors, as well as low damage detectability, arises from using an improper and relatively small cluster number. Because the effects of environmental and/or operational variations on the clustering results lead to false alarms and false detection errors, the choice of an appropriate cluster number with the emphasis on dealing with these effects highly enhances the performance of the clustering-based SHM method.

The central idea behind the proposed approach to selecting an appropriate cluster number is to find a number among a relatively wide range of sample clusters K_{max}, which is a large scalar value (e.g. 1000). The main criterion for this selection is based on evaluating the variances of different DI amounts of the vector $\mathbf{d_b}$ and choosing a cluster number with the smallest variance value. This approach aims to select a proper value of k to decrease or remove the variations in DI quantities resulting from the environmental variability. To obtain this amount, the k-medoids clustering is initially implemented by considering various cluster numbers. Under such circumstances, one can obtain different sets of $\mathbf{d_b}$ in the baseline phase. Subsequently, the variances of all distance vectors are calculated to choose an appropriate cluster number, which possesses the smallest variance value. For the sake of simplicity, Fig. 5.1 depicts the flowchart of the proposed cluster selection approach.

5.3 Proposed Threshold Estimation Method

5.3.1 Extreme Value Theory

In statistics, the EVT is an approach to modeling the tails of a distribution by considering extreme quantities of sampling data or rare events [168]. The great advantage of this approach is to only focus on a few assumptions about the distribution of data rather than the modeling of whole data distribution. Furthermore, the EVT presents a robust method for the threshold limit determination [146]. Considering a large number of random data points, one can utilize three extreme value distributions including Gumbel, Fréchet, and Weibull [168, 169]. To determine a threshold value, it is necessary to select one of the above-mentioned distributions and then estimate the unknown parameters of the selected distribution. Finally, the alarming threshold is obtained from the extreme quantile of that distribution under a significance level. Due to the limitations of this approach, which have been explained earlier, it is possible to use the GEV or GP distribution models [168]. The main difference between these distributions originates from the methodology of modeling extreme values. More precisely, the extreme value modeling via the GEV distribution is based on the BM method [146], while the same modeling procedure by the GP distribution is carried out via the POT method [162]. The BM method relies upon dividing a set of data samples into non-overlapping blocks with equal size, extracting the maximum amount of each block, and fitting the GEV distribution model to the set of maximum quantities extracted from all blocks. In contrast, the POT method is based on defining a threshold, choosing all extreme values
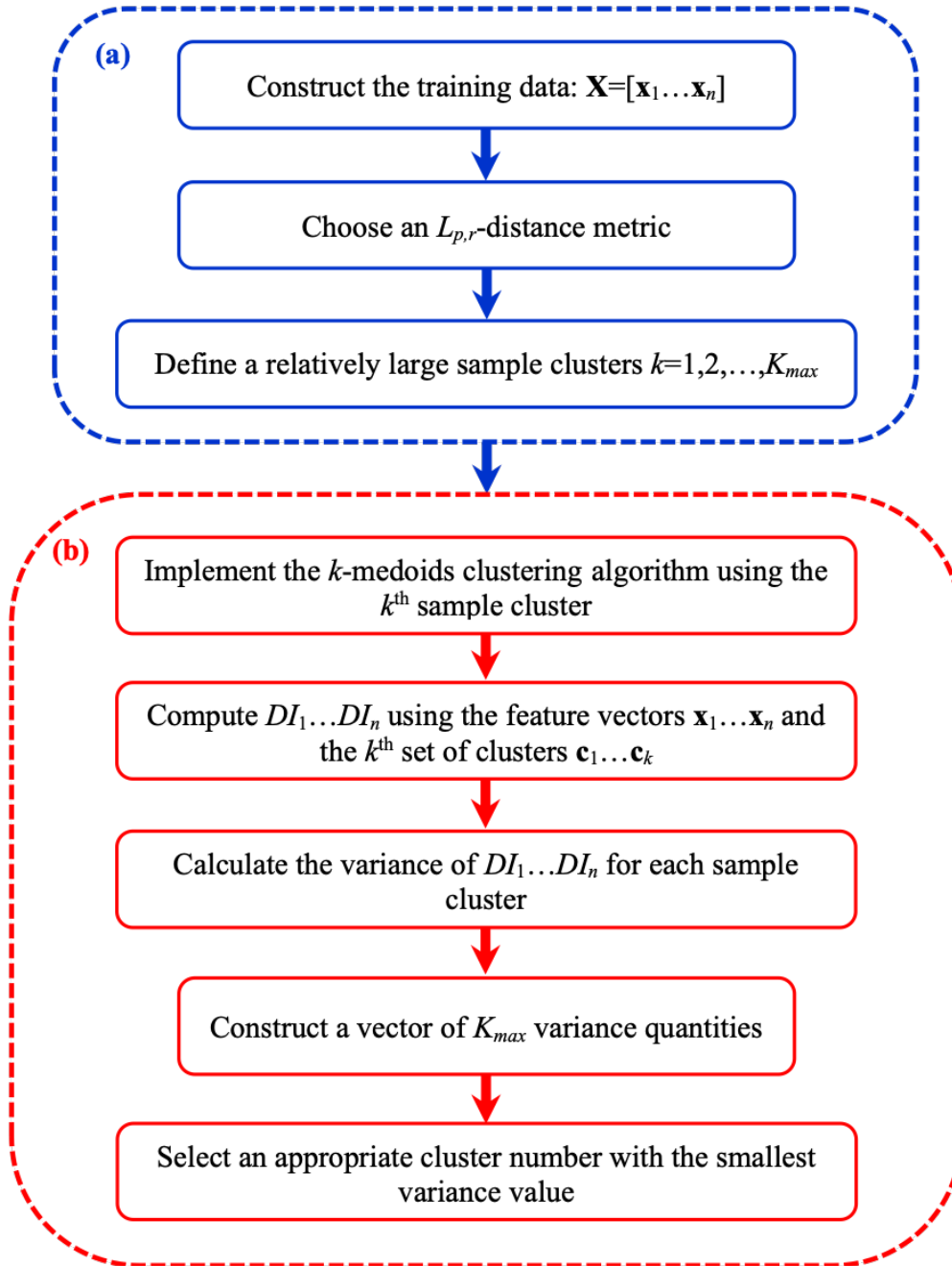
Figure 5.1: *The flowchart of the proposed approach to select an appropriate cluster number for dealing with the environmental variability: (a) the preliminary steps, (b) the iterative steps.*

(exceedances) above the threshold of interest, and fitting the GP distribution model to the exceedances. It should be clarified that the threshold used in the POT method and the threshold limit regarding the decision-making and damage detection are two distinct subjects. For both the BM and POT techniques, the maximum likelihood estimation (MLE) is usually applied to estimate the unknown parameters of the GEV and GP distributions including the shape, scale, and location [168, 169].

5.3.2 Proposed GOF Method

The strategy for modeling the tails or extremes of a distribution by the proposed GOF (goodness-of-fit) method differs from the conventional BM and POT techniques. The great advantage of this method against the mentioned classical approaches is that it allows modeling an extreme value distribution without choosing any block number or determining any threshold level. It is needed to mention that the GEV distribution model is considered to estimate an alarming threshold via the proposed GOF method. The fundamental principle of the proposed GOF method is to arrange data samples in descending order and find adequate maximum quantities from the first arranged samples via a GOF measure. In statistics, this measure is a statistical test for assessing the accuracy and adequacy of a fitted model. To put it another way, this test is intended to evaluate the acceptance or rejection of a theory or an idea. As a result, in the theory of interest, the test conforms to a null hypothesis ($\mathbb{H}_0$) in the case of acceptance, and it is an alternative hypothesis ($\mathbb{H}_1$) in the case of rejection. Generally, a GOF test relies on a statistic (Q) that is a measure of the comparison between theoretical and empirical quantities. In most cases, the null hypothesis is rejected when the statistic Q is very large [188].

For the EVT, there are several GOF tests by considering their properties and ideas based on probability plots, an empirical distribution function, a log-likelihood function, Akaike or Bayesian information criteria, and Shapiro-Wilk's approach [188]. Recently, Pérez-Rodríguez et al. [189] proposed a new GOF test for the extreme value distribution based on the Kullback-Leibler information. Suppose that $y_1, ..., y_n$ are n random data samples, which are equivalent to $DI_1, ..., DI_n$ of the vector $\mathbf{d_b}$ regarding the normal condition. The Kullback-Leibler information between the empirical and estimated probability distribution functions, called $G(y)$ and $\hat{G}(y)$, is given by:

$$
KL(G, \hat{G}) = \int_{-\infty}^{+\infty} G(y) \ln \frac{G(y)}{\hat{G}(y)} \, dy =
$$
$$
\int_{-\infty}^{+\infty} G(y) \ln G(y) \, dy - \int_{-\infty}^{+\infty} G(y) \ln \hat{G}(y) \, dy
\tag{5.6}
$$

To obtain $KL(G, \hat{G})$, the first term of the right-hand side of Eq. (5.6) is estimated by the Vasicek estimator in the following form:

$$
\int_{-\infty}^{+\infty} G(y) \ln G(y) \, dy = \frac{1}{n} \sum_{i=1}^{n} \ln \left(\frac{n}{2h} (\ln(y_{i+h}) - \ln(y_{i-h})) \right)
\tag{5.7}
$$

where $h < n/2$, $y_{i-h} = y_1$ and $y_{i+h} = y_n$ if $i - h < 1$ and $i + h > n$. Regarding the variable h, it should be clarified that it is possible to choose any positive integer smaller than $n/2$. In this regard, the smallest (the lower-bound) and largest (the upper-bound) choices of h correspond to 1 and $\left(\frac{n}{2} - 1 \right)$. In this study, the upper bound of h is considered to calculate the first term of the statistic of the Kullback-Leibler information. Another important note about the variable h is that it should be a positive integer. For a non-integer, therefore, one should round it to the lowest value. On the other hand, the second term of the right-hand side of Eq. (5.6) is estimated by:

$$\int_{-\infty}^{+\infty} G(y) \ln \hat{G}(y) \, dy = \frac{1}{n} \sum_{i=1}^{n} \ln G\left(\ln(y_i), \mu_y, \sigma_y\right) \tag{5.8}$$

where μ_y and σ_y are the mean and standard deviation of $y_1, ..., y_n$. Eventually, the statistic of the Kullback-Leibler information $(Q_K L)$ is rewritten by using the data samples $y_1, ..., y_n$ and the amounts of n and h as follows:

$$Q_{KL} = -\frac{1}{n} \sum_{i=1}^{n} \ln\left(\frac{n}{2h}(y_{i+h} - y_{i-h})\right) - \frac{1}{n} \sum_{i=1}^{n} y_i + \frac{1}{n} \sum_{i=1}^{n} \exp(y_i) \tag{5.9}$$

The null hypothesis $(\mathbb{H}_0)$ is rejected for large values of Q_{KL}. Using the concept of the Kullback-Leibler information, the proposed GOF method arranges the samples $y_1, ..., y_n$ in descending order so that the arranged data begins with y_{max} and ends with y_{min}. Subsequently, an iterative algorithm is developed to obtain the number of adequate maximum quantities (the extreme values) for modeling by the GEV distribution. To determine this number, the iterative algorithm in the proposed GOF method measures different values of Q_{KL} from sample maximum numbers ($i = 1, 2, ..., S$, where i is the number of iterations); that is, $Q_{KL}^1, Q_{KL}^2, ..., Q_{KL}^S$. A number (s) with the smallest Q_{KL} quantity presents the adequate maximum or extreme samples designated as $\hat{y}_1, ..., \hat{y}_s$, where $\hat{y}_1 = y_{max}$ and $\hat{y}_s > \hat{y}_{s+1}$. Eventually, the process of threshold estimation is carried out by using the mentioned maximum samples and modeling them via the GEV distribution in the following form [168]:

$$F(\hat{y}) = \exp\left\{ - \left[1 + \beta\left(\frac{\hat{y} - \mu}{\sigma}\right)\right]^{-\frac{1}{\beta}} \right\} \tag{5.10}$$

where F is a non-degenerate distribution function. Furthermore, β, σ, and μ are the unknown parameters of the GEV distribution known as the shape, scale, and location, respectively. The threshold value is then determined by inverting Eq. (5.10) and estimating the extreme quantile of the GEV distribution. On this basis, the alarming threshold under a significance level (α) is expressed as:

$$\tau_\alpha = \begin{cases} \mu - \dfrac{\sigma}{\beta}\left[1 - \{-\log(1 - \alpha)\}^{-\beta}\right] & \beta \neq 0 \\ \mu - \sigma \log\{-\log(1 - \alpha)\} & \beta = 0 \end{cases} \tag{5.11}$$

By using the threshold τ_α, it is expected that no DI values of the vector $\mathbf{d_b}$ violate from τ_α. On the other hand, any deviation of the DI quantity of the vector $\mathbf{d_m}$ from the threshold limit is indicative of damage occurrence. For simplicity, Fig. 5.2 presents the flowchart of the threshold estimation by the proposed GOF method.

5.4 Summary

Due to the importance of structural health monitoring under varying environmental conditions, this chapter has proposed a new machine learning method in an unsupervised learning manner by using the *k*-medoids clustering algorithm. The proposed clustering-based method aims to remove the deceptive effects of environmental variability and
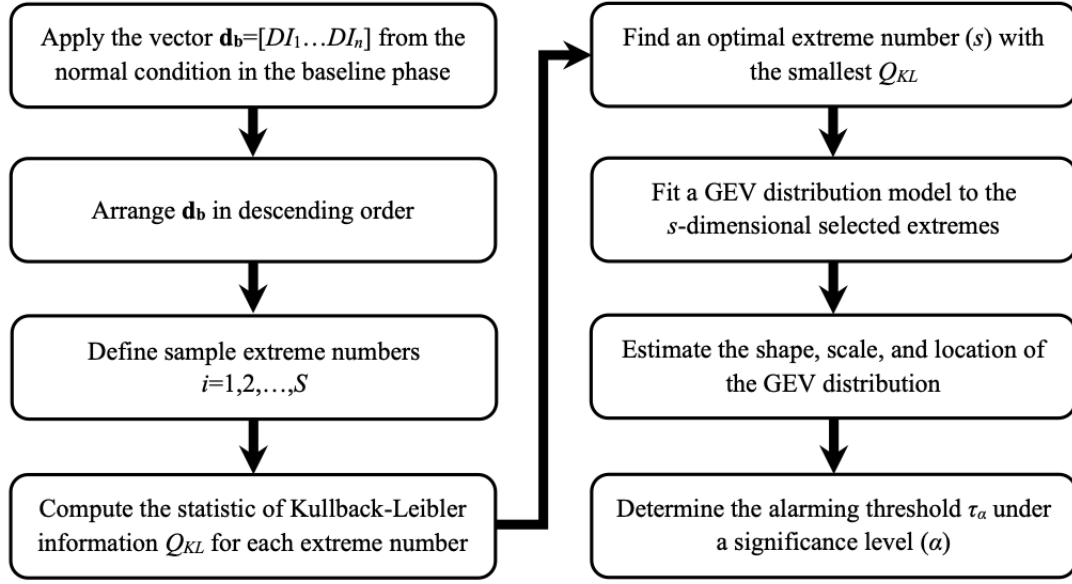
Figure 5.2: *The flowchart of the threshold estimation by the proposed GOF method .*

increase the detectability of damage. For these purposes, an $L_{p,r}$-distance measure is proposed to define a new damage indicator that can provide accurate results of damage detection with high damage detectability. In the proposed clustering-based method, the unfavorable effects of the environmental variability are removed by choosing an adequate cluster number among a wide range of sample clusters based on analyzing the variances regarding the outputs of the damage indicator obtained from the normal condition. For the first time, this study proposes a novel approach to model the GEV distribution and address the drawbacks of the BM and POT techniques for threshold estimation. The central idea behind the proposed approach is to utilize a goodness-of-fit (GOF) test based on Kullback-Leibler information for choosing adequate extreme values without selecting any block number or determining any threshold amount. Proposing a new clustering-based method using the *k*-medoids algorithm and an innovative cluster selection approach, a new damage indicator by the $L_{p,r}$-distance measure, a novel method for modeling the GEV distribution and threshold estimation are the main contributions of this chapter. The great advantages of these approaches include dealing with the problem of environmental variability, increasing damage detectability, determining a reliable threshold limit, and facilitating the process of threshold estimation by GOF without obtaining some requirements of the conventional techniques such as the number of blocks for Block maxima (BM) and a threshold value for peak-over-threshold (POT).

Applications and Results

A number of examples including numerical models, experimental benchmark structures, and real structures are examined in the present chapter so as to verify the accuracy and performance of the proposed techniques for SHM purposes. The numerical examples are a Reinforced Concrete Beam and an Offshore Jacket Structure. In addition, the experimental models involve the Three-Story Laboratory Structure, the IASC-ASCE Structure, and an Offshore Jacket Platform. Finally, full-scale examples are included the Cable-Stayed Bridge and the Z24 Bridge.

6.1 Verification of Iterative Time Series-Based Method

In this section, two examples are used to validate the effectiveness and reliability of the proposed iterative feature extraction technique described in Chapter 3. The first one is a numerical model of the reinforced concrete beam and the second one is a three-story laboratory structure, which belongs to the Engineering Institute Los Alamos National Laboratory.

6.1.1 Application to the Numerical Reinforced Concrete Beam

In order to verify the accuracy and capability of the proposed methods, a numerical model of the reinforced concrete beam is built as shown in Fig. 6.1. This model is constructed by Finite Element Method from Bernoulli-Euler beam theory [190] with the aid of an in-house finite element code implemented in MATLAB. On the basis of this theory, each element of the beam has two nodes with four degrees of freedom (DOFs), in which case the beam is discretized by 11 elements, 12 nodes, and 22 DOFs. Assume that similar damping mechanisms are distributed throughout the beam; hence,

the classical damping is an appropriate idealization. Furthermore, Rayleigh damping model is utilized to construct the damage matrix using 5% damping ratio for all modes.
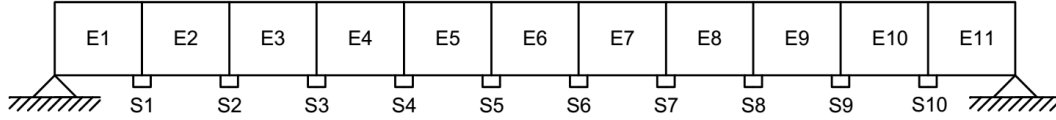
Figure 6.1: *The numerical model of the concrete beam.*

The geometry of the beam element is length 300 mm, height 250 mm and width 250 mm in the cross section. The material properties of the beam are composed of the modulus of elasticity 22.3 GPa, material density 2400 Kg/m^3, and Poisson coefficient of 0.2. There are ten sensor mounted at the bottom of the beam (S1-S10). These sensors acquire the acceleration time-domain data at 25 sec with 0.003125 sec sample interval. In this regard, the data points at each sensor are 8000 samples.

To implement the global health monitoring, a single damage as a flexural crack is simulated by reducing the concrete flexural rigidity at the middle-span of beam. Based on this damage pattern, several incremental damage scenarios are defined at the damage location. This pattern is a realistic simulation of cracks in the reinforced concrete beams, which is introduced as a common way to use in the numerical applications [191]. Furthermore, in order to consider the effects of environmental and operational variability, four structural changes are applied to the simulated beam by increasing the mass of some elements of the beam. Table 6.1 represents all undamaged and damaged cases in the numerical beam.

Table 6.1: *The structural state conditions in the numerical model of beam.*

State	Condition	Location	Structural Changes	Index(%)
1	Undamaged	—	Baseline	—
2	Undamaged	E2		15
3	Undamaged	E5	The increase in the	30
4	Undamaged	E9	material density (ρ_c)	20
5	Undamaged	E2		30
		E9		40
6	Damaged	E6		−5
7	Damaged	E6	The reduction of concrete	−15
8	Damaged	E6	flexural rigidity (EI_c)	−20
9	Damaged	E6		−30
10	Damaged	E6		−40

It is worth mentioning that the state 1 refers to the baseline condition of structure, where there are neither damage patterns nor environmental and operational variability. To simulate a dynamic test and acquire acceleration time history at each sensor location, the dynamic analysis in the time domain is implemented by Newmark method [192]. Furthermore, Gaussian white noise signals are applied to the beam to excite the beam and simulate ambient vibration. In this case, Gaussian white noise signals with the different energy levels are subjected to the translation DOFs. As a sample, Figs. 6.2 and 6.3 illustrate the signals of Gaussian white noise and the acceleration responses at

the sensor 5 in the states 1 and 8.

(a)
(b)
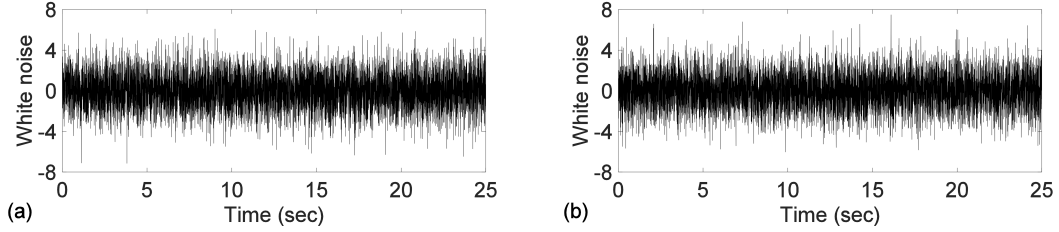
Figure 6.2: *The excitation forces as the white noise signals at the sensor 5: (a) state 1, (b) state 8.*

(a)
(b)
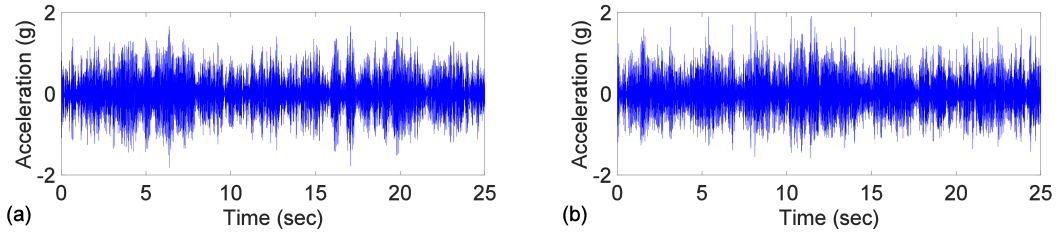
Figure 6.3: *The acceleration time histories at the sensor 5: (a) state 1, (b) state 8.*

It is significant to remark that each state in Table 6.1 includes five measurements in the sense that the time-domain dynamic analysis of the beam is carried out five times at each state leading to a 3D-dimensional measurement matrix with 8000 data points of the acceleration time histories at 10 sensors in 50 measurements.

6.1.1.1 Time Series Modelling

After the simulation of the acceleration time histories by the numerical Newmark method, the best time series model compatible with these data is identified to extract its parameters as the DSFs. As remarked previously, autocorrelation and partial autocorrelation functions are two useful graphical tools for identifying the model according to Box-Jenkins methodology. Figs. 6.4 and 6.5 illustrate the plots of these functions associated with the acceleration time histories at the location of sensor 5 in the states 1 and 8, respectively. In these figures, the x axis illustrates time-unit lags (microsecond) at which the autocorrelation is computed, and the y axis indicates the value of correlation. It is noticeable that the two horizontal lines in these figures are the confidence intervals.

As can be seen from these figures, the plots of the partial autocorrelation function in both states approximately become zero after 30th lag (microsecond), whereas the graphs of the autocorrelation function have exponentially decreasing forms without any trend in being zero. Based on Box-Jenkins methodology, these evidences confirm that AR model is the most appropriate time series model for fitting the acceleration time histories. Although the present results have been achieved for the only two states of the beam at the one sensor location, it is worth remarking that the AR model is also valid for the other states and sensor locations.

51
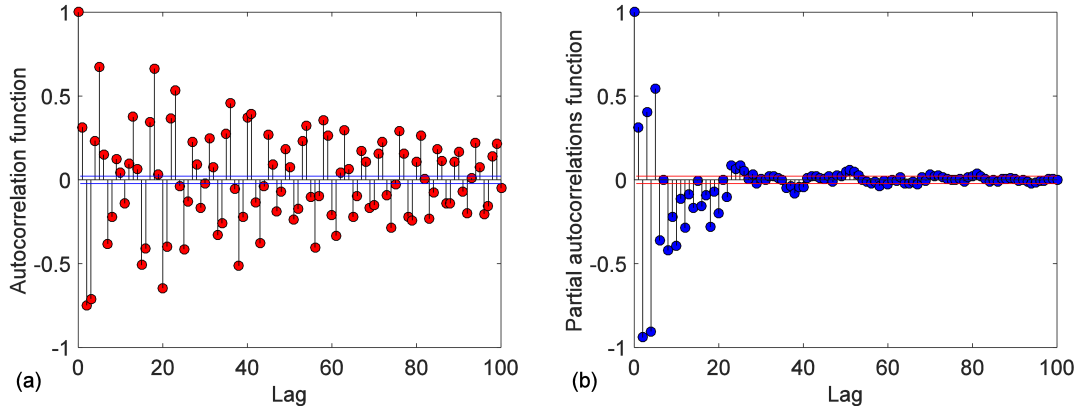
Figure 6.4: *The process of identifying the time series model by Box-Jenkins methodology at the sensor 5 in the state 1: (a) autocorrelation, (b) partial autocorrelation.*
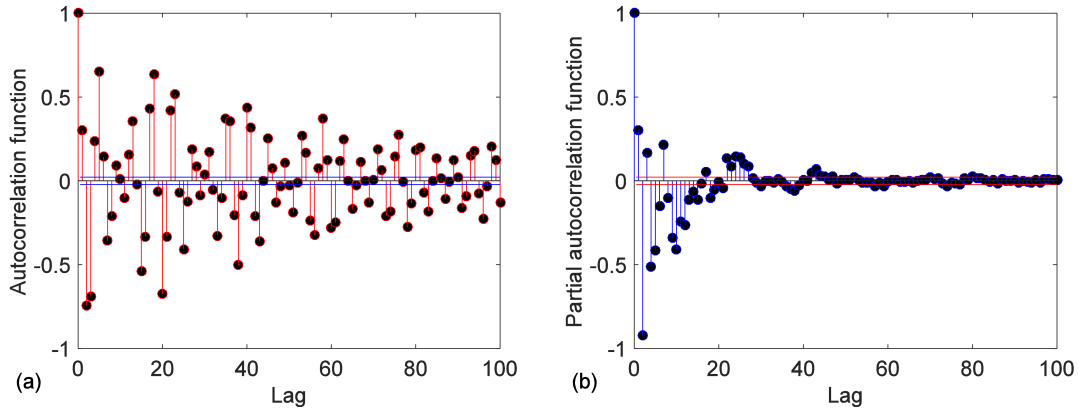
Figure 6.5: *The process of identifying the time series model by Box-Jenkins methodology at the sensor 5 in the state 8: (a) autocorrelation, (b) partial autocorrelation.*

6.1.1.2 The Iterative Feature Extraction Technique

On the basis of the proposed iterative feature extraction technique, the maximum order of AR model should be determined to define a limit of iteration. To achieve this goal, the p-value of Ljung-Box test is applied to analyze the correlation of the extracted AR residuals. The maximum order of AR model at each sensor location is one that the p-value of the AR residuals should be larger than 0.05. Note that Ljung-Box test is a statistics or numerical tool that is mostly used to examine the adequacy of model. The time series model with the p-values less than 0.05 should be modified since this criterion is indicative of the insufficiency of model. Table 3 shows the p-values and maximum orders of the AR model at each sensor based on the first iterative algorithm of the proposed feature extraction technique as shown in Fig. 3.2. Notice that the maximum order at each sensor implies the number of iterations to produce an adequate AR model.

As seen in Table 6.2, the p-values of the AR residuals at all sensors are larger than 0.05, which means that the AR models with their maximum orders are adequate and

Table 6.2: *The maximum orders and the p-values of AR residuals.*

Sensor no.	Maximum order	p-value
1	59	0.0983
2	59	0.0821
3	53	0.0736
4	53	0.1016
5	49	0.1729
6	48	0.1266
7	53	0.3787
8	53	0.1241
9	59	0.0737
10	59	0.1431

correct. In other words, all of them make the uncorrelated residuals that is the main and underlying criterion for the adequacy and accuracy of time series models. As a sample, Fig. 6.6 displays the number of iterations in the state 1 at the sensors 6 and 10.
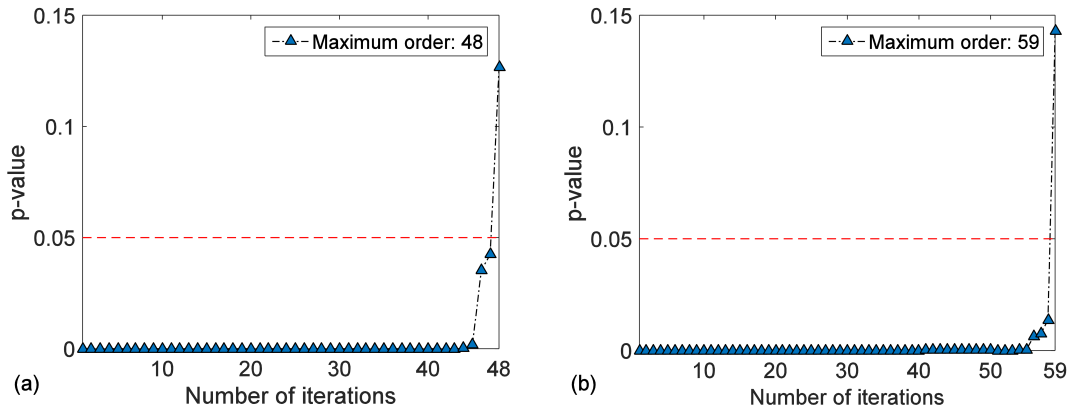
Figure 6.6: *The number of iterations in the state 1: (a) sensor 6, (b) sensor 10.*

Once the maximum orders of the AR models are calculated, the parameters of models are extracted as the DSFs through choosing a minimum arbitrary order. With regard to the partial autocorrelation functions, the number 5 is chosen as the minimum order and the process of extracting the parameters of AR model at each sensor location is implemented through the iterative algorithm depicted in Fig. 3.2. In this regard, the iterative algorithm needs 15 iterations or 15 optimal orders for the AR models. Thus, 15 parameters of the model at all sensor locations are determined by Yule-Walker methods [114].

It is evident that this order is very smaller than the maximum orders obtained by the first iterative algorithm because it can deal with underfitting or overfitting in the time series modeling. These problems pertain to the adequacy of times series models. When the number of orders of a time series model exceeds a reliable and sufficient number, the model becomes overfitting. On the contrary, if the model contains fewer orders than the sufficient one, the underfitting issue occurs in the model. Based on the obtained results, one can realize that the model with the maximum order may be overfitting since it is possible to choose smaller order than the maximum order, in which the model is able

to produce the uncorrelated residuals. On the other hand, the minimum order results in an underfitting model. To indicate the correlation of residuals, the autocorrelation function of the residuals of AR(15) at the sensors 3 and 8 in the state 1 are shown in Fig. 6.7.
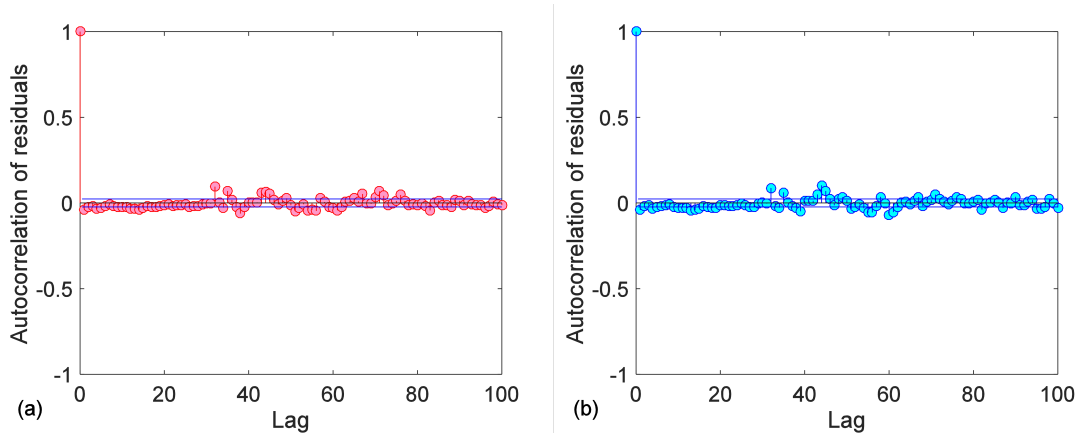
Figure 6.7: *The autocorrelation function of the residuals of AR(15) in the baseline condition (state 1): (a) sensor 3, (b) sensor 8.*

The observations in Fig. 6.7 demonstrate that there are no correlation patterns in the residuals of AR(15); thus, it can be argued that the model residuals are uncorrelated based on the confidence intervals. This result is also valid for the residuals at the other sensors.

6.1.1.3 The Global Health Monitoring by the Machine Learning Algorithms

Here, the results of global health monitoring or the first level of damage detection process in the context of SHM are discussed using the parameters of AR(15). Before the analysis of damage identification results, it is necessary to specify the training and test data. For the training data, the AR parameters of all sensors in the states 1-5 in all measurements (5 tests) are selected since these states are undamaged. In contrast, the test data set consists of the AR parameters belonging to the only fifth measurement at all sensors in the states 1-10.

In the following, the training and test data sets are used in the machine learning algorithms to assess the global state of the beam. Fig. 6.8 (a)-(d) shows the results of global structural health monitoring in the simulated beam based on MSD, FA, PCA, and AANN methods, respectively.

As Fig. 6.8 (a)-(d) reveals, there are considerable deviations in the states 6-10 so that all of them exceed the threshold levels. This is a reasonable result since these states have been defined as the damaged conditions in the simulated beam. On the contrary, all of the undamaged cases (i.e. the states 1-5) are under the threshold levels. Notice that in this figure, the horizontal line is the threshold level in each method. On this basis, any deviation from this line is an indication of the damage occurrence in the beam. Table 6.3, shows the threshold quantities obtained from the machine learning methods.

In Fig. 6.8 (a), the values of damage index values in the undamaged conditions
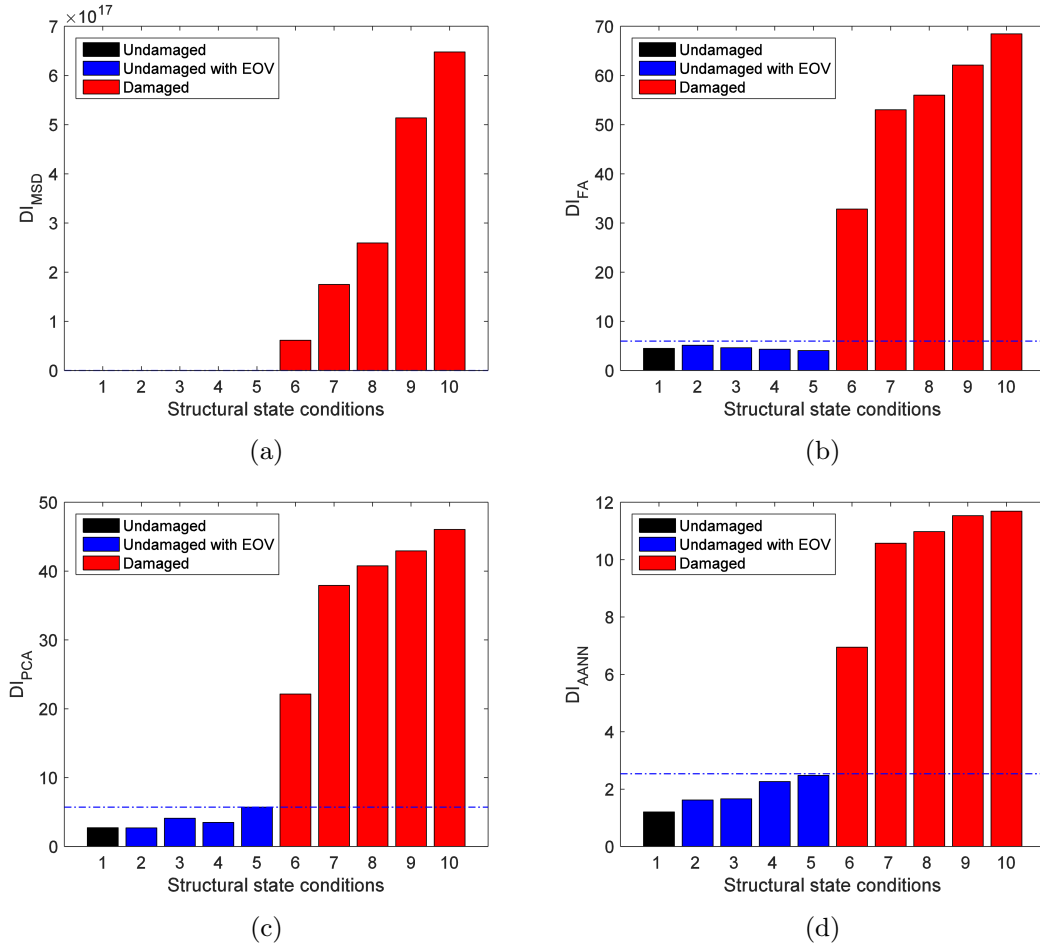
Figure 6.8: *The global health monitoring in the simulated beam by the machine learning methods: (a) MSD, (b) FA, (c) PCA, and (d) AANN.*

Table 6.3: *The threshold values for the machine learning methods.*

Methods	MSD	FA	PCA	AANN
Threshold values	23.042	5.992	5.714	2.849

are much smaller than the corresponding values in the damaged conditions leading to the MSD values in the undamaged conditions become invisible. Moreover, Thomson's method has been applied to compute the factor score matrix $\mathbf{F}$ in the factor analysis method and the number of factors is two. In AANN, the number of nodes in the bottleneck, mapping, and de-mapping layers are equal to one.

Another result in this section is related to estimating the level of damage severity based on the proposed methods. As Table 6.1 indicates, the severity of damage increases from the state 6 to the state 10, in which the first damage scenario (state 6) possesses the lowest level of damage, whereas the state 10 indicates the highest one. With these explanations, it can be observed that all the machine learning methods give the accurate estimation results. In Fig. 6.8 (a)-(d), it can be suggested that the level of damage increases with increasing the damage severity; however, the results of MSD are much better than the other methods.

6.1.2   Application to the Three-Story Laboratory Structure

For further verifications of the performance and ability of the proposed methods, an experimental study is implemented with the aid of the experimental data of a laboratory benchmark model. This structure as shown in Fig. 6.9 is a three-story laboratory frame constructed at the Engineering Institute Los Alamos National Laboratory [193]. The frame schematic and sensor locations are shown in Fig 6.10. A random vibration load was applied by means of an electrodynamics shaker to the base floor along the centerline of the frame. The structure was instrumented with four accelerometers mounted at the centerline of each floor on the opposite side from the excitation source to measure the acceleration time-domain response. The shaker and frame were mounted together on an aluminum baseplate and the entire system rested on rigid foam. The sensor signals were sampled at 320 Hz for 25.6 sec in duration, which are discretized into 8192 data samples at 3.125 microsecond intervals. A comprehensive documentation associated with this model is available in [194].
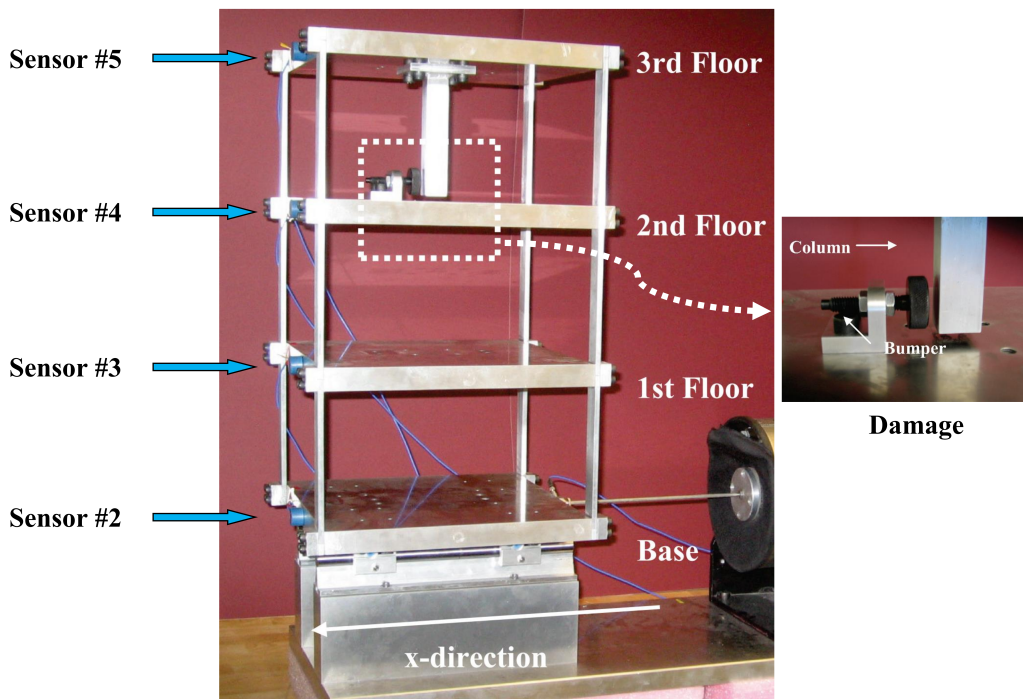
Figure 6.9: *The three-story laboratory benchmark frame [194].*

To induce nonlinear damage, a center column was suspended from the third floor. This column was contacted a bumper mounted on the second floor, which the position of the bumper can be adjusted to define diverse structural damage. The source of the damage is a simulation of breathing cracks to produce nonlinear behavior through opening and closing under excitation forces. The acceleration time-domain responses at all floors and base were measured under 17 structural state conditions as shown in Table 6.4.
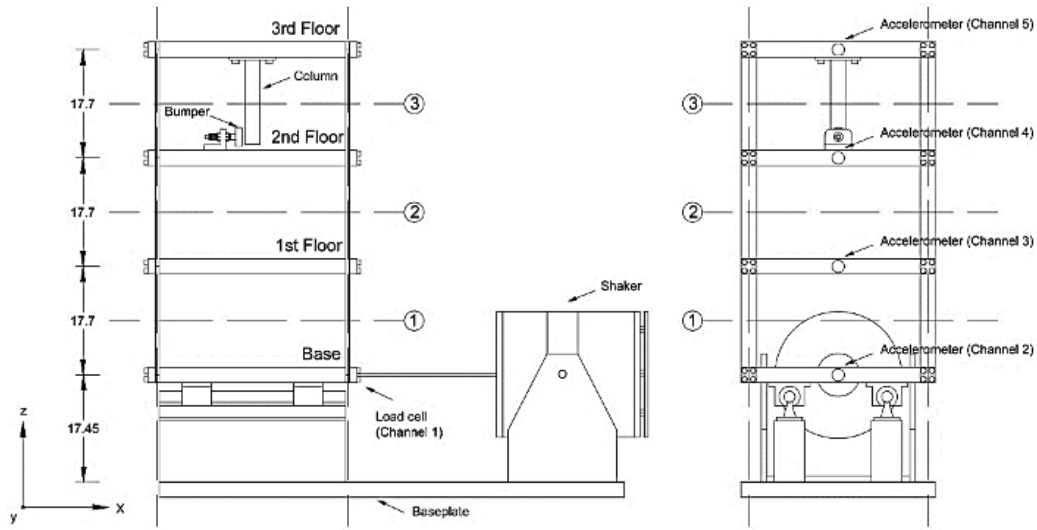
Figure 6.10: *The frame schematic and sensor locations [194].*

Table 6.4: *The structural state conditions in the laboratory frame [194].*

State	Condition	Description
1	Undamaged	Baseline
2	Undamaged	Added mass of 1.2 kg at the base
3	Undamaged	Added mass of 1.2 kg at the 1st floor
4	Undamaged	87.5% stiffness reduction in one column of the 1st inter-story
5	Undamaged	87.5% stiffness reduction in two columns of the 1st inter-story
6	Undamaged	87.5% stiffness reduction in one column of the 2nd inter-story
7	Undamaged	87.5% stiffness reduction in two columns of the 2nd inter-story
8	Undamaged	87.5% stiffness reduction in one column of the 3rd inter-story
9	Undamaged	87.5% stiffness reduction in two columns of the 3rd inter-story
10	Damaged	Distance between bumper and column tip 0.20 mm
11	Damaged	Distance between bumper and column tip 0.15 mm
12	Damaged	Distance between bumper and column tip 0.13 mm
13	Damaged	Distance between bumper and column tip 0.10 mm
14	Damaged	Distance between bumper and column tip 0.05 mm
15	Damaged	Bumper 0.20 mm from column tip, 1.2 kg added at the base
16	Damaged	Bumper 0.20 mm from column tip, 1.2 kg added at the 1st floor
17	Damaged	Bumper 0.10 mm from column tip, 1.2 kg added at the 1st floor

The structural state conditions in the laboratory frame were categorized into the four main groups including the baseline condition (state 1), the operational and environmental conditions (states 2-9), the damaged conditions (states 10-14), and the damaged conditions along with the environmental and operational variability (states 15-17). In the baseline condition, there are no changes (damage nor non-damage) in the laboratory frame, which make it as an ideal condition in the SHM community. The environmental and operational variability are linear changes in the structures resulting from either environmental conditions such as temperature, wind loading, and moisture or operational conditions including live loads, operation speed and changing the source of excitations [123].

6.1.2.1 Time Series Modeling and Feature Extraction

For extracting the DSFs, the type of time series model should be identified on the basis of Box-Jenkins methodology. Similar to the previous section, the plots of autocorrelation and partial autocorrelation functions are utilized to identify the most appropriate model for the acceleration time histories. Figs. 6.11 and 6.12 show the results of the model identification at the channel 5 in the states 1 and 14, respectively.
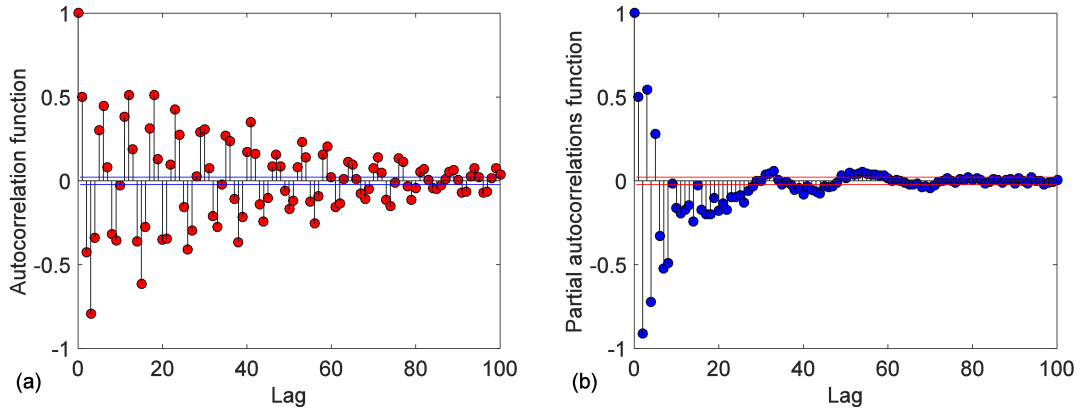
Figure 6.11: *The process of identifying the time series model by Box-Jenkins methodology at the channel 5 in the state 1: (a) autocorrelation function, (b) partial autocorrelation function.*
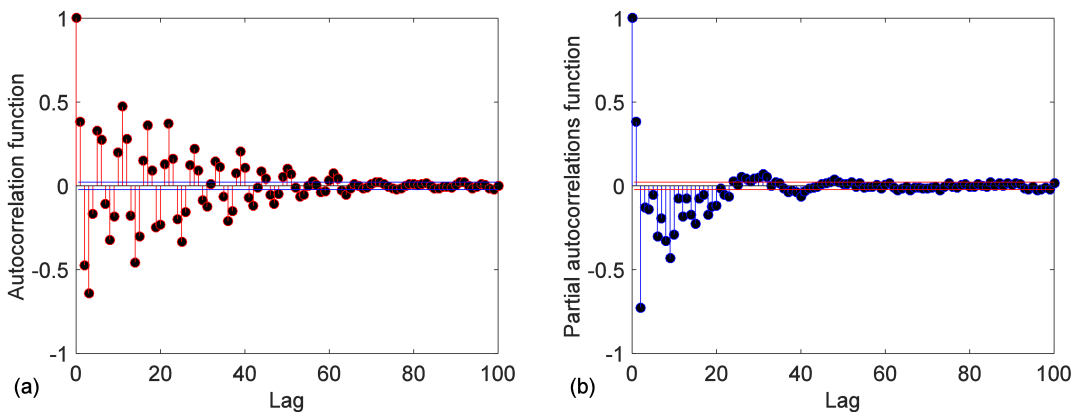
Figure 6.12: *The process of identifying the time series model by Box-Jenkins methodology at the channel 5 in the state 14: (a) autocorrelation function, (b) partial autocorrelation function.*

As can be observed from these figures, the plots of autocorrelation function in both states have exponentially decreasing forms, which do not tend to become zero, while the plots of partial autocorrelation function gradually decay after 35th lag (microsecond). From such observations, it can be concluded that AR model is the best time series model for fitting the acceleration time histories.

In order to choose an optimal model order and then extract the parameters of AR model, the maximum number of orders at each channel should be determined. Based on the first algorithm of iterative feature extraction technique, the maximum orders are

identical to the number of iterations such that the p-values of AR residuals in these orders become larger than 0.05. Table 6.5 represents the maximum orders and the p-values in Ljung-Box test in the baseline condition.

Table 6.5: *The maximum orders and the p-values of AR residuals in the baseline condition.*

Channel no.	2nd	3rd	4th	5th
Threshold values	60	54	46	56
p-values	0.534	0.306	0.072	0.190

All of the p-values represented in Table 6.5 are larger than 0.05 since the residuals of AR model with the maximum orders are uncorrelated, even though using these orders may cause overfitting problem in the time series modelling. Actually, the main reason to select an optimal order between the minimum and maximum orders is to avoid in achieving an underfitting or an overfitting model. In the same manner to the numerical verification, the minimum order is 5.

Fig. 6.13 shows the autocorrelation of the residuals of AR model gained by the minimum order at the channel 5 in the states 1 and 14.

(a) (b)
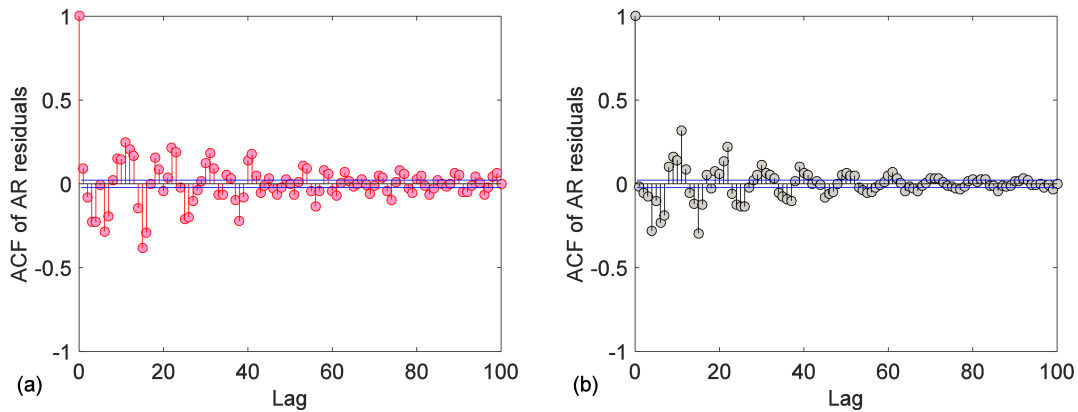
Figure 6.13: *The residual analysis by the ACF of the AR residuals using the minimum order at the channel 5: (a) state 1, (b) state 14.*

It is seen from Fig. 6.13 that there are substantial correlation patterns in the plots of autocorrelation function of the residuals in the sense that the AR(5) is not sufficient and its residuals are correlated. Based on the second iterative algorithm of the proposed feature extraction technique, the residuals of AR(5) is chosen as the new data for modelling rather than using the raw acceleration vibration data. Fig. 6.14 illustrates the parameters of the optimal AR model that has 25 parameters. This means that the optimal AR order between the minimum and maximum orders is 25. In addition, Yule-Walker method [114] is employed to determine the parameters of AR(25).

To realize the adequacy and accuracy of AR(25), Fig. 6.15 shows the autocorrelation function of the model residuals at the channel 5 in the structural conditions 1 and 14. From this figure, it can be observed that the patterns of autocorrelation function for the residuals of AR(25) are roughly within the correlation bounds, which mean that this model is adequate and its residuals are uncorrelated.
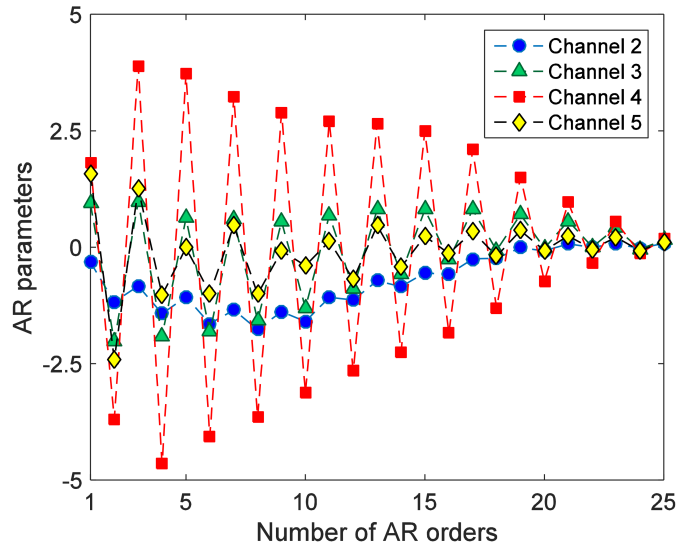
Figure 6.14: *The parameters of AR(25) in the laboratory frame at all channels in the state 1.*

(a)   (b)
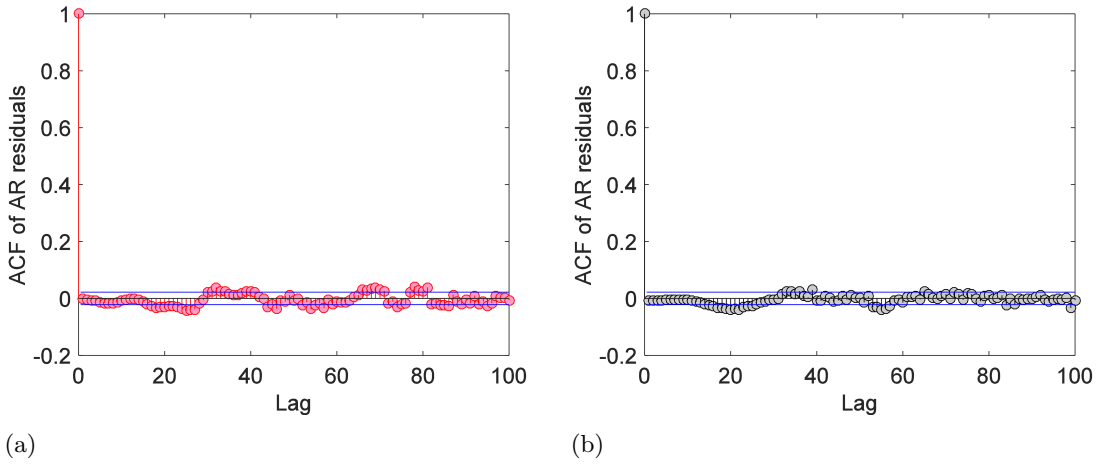
Figure 6.15: *The residual analysis by the autocorrelation function for the residuals of AR(25) at the channel 5: (a) state 1, (b) state 14.*

6.1.2.2   The Structural Health Monitoring in the Laboratory Frame

In this section, it is attempted to discern whether the proposed methods including the iterative feature extraction technique and machine learning methods are able to recognize and classify the undamaged and damaged conditions in the laboratory frame. Therefore, the parameters of optimal AR(25) are applied to the machine learning methods to calculate the quantity of damage indices in order for assessing the global state of the laboratory frame.

The training data set is a matrix with 90 rows and 100 columns, where the rows represent the total number of measurements and undamaged conditions and the columns are the total parameters of optimal AR(25) at four channels. It should be pointed out that each state of the laboratory frame has 10 measurements; that is, the dynamic tests

on the frame were implemented 10 times at each state. In contrast, the matrix of test data consists of 17 rows and 100 columns, at which the rows denote the total number of structural states in one measurement. In order to define the threshold level for each machine learning method, the training data set is employed as stated in Subsection 3.3.2. Table 6.6 represents the threshold values in the laboratory frame for the machine learning methods.

Table 6.6: *The threshold values for the machine learning methods in the laboratory frame.*

Methods	MSD	FA	PCA	AANN
Threshold values	79.0123	8.1261	4.3495	2.0951

After computing the threshold values, the test data set is used to compute the quantity of damage indices quantities for specifying the global condition of the frame. To learn a model in the factor analysis method, the number of factors (f) is 2 and Thomson's method is applied to determine the factor score matrix $\mathbf{F}$. Moreover, the neural network trained in the AANN method consists of 2, 4, and 4 nodes in the bottleneck, the mapping and the de-mapping layers.

Fig. 6.16 (a)-(d) illustrates the results of global health monitoring for MSD, FA, PCA, and AANN methods, respectively. It is observed from this figure that the damaged conditions (states 10-17) exceed the threshold levels, whereas all of the undamaged conditions are approximately under the threshold values, which mean reasonable results about the condition of frame in these conditions. In other words, the states 2-9 have been classified as the undamaged conditions despite the existence of operational and environmental variability. These observations demonstrate that the proposed methods influentially enable us to detect the global state of the structures by overcoming the operational and environmental conditions.

Another important result is to estimate the level of damage severity by the proposed methods. In Fig. 6.16 (a)-(d), it can be seen that the values of damage indices in the damaged conditions increase with increasing the damage level from the state 10 (the lowest level of damage severity) to the state 14 (the highest level of damage extent). In addition, this observation can be achieved in the damaged conditions with the operational and environmental variability, where the level of damage severity rises from the conditions 15 and 16 (the lowest level of damage severity) to the state 17.

6.1.3 Conclusion

A numerical model of the reinforced concrete beam in Sunsection 6.1.1 and a benchmark model of the laboratory frame in Subsection 6.1.2 were employed to prove the accuracy and performance of the proposed iterative feature extraction technique described in Chapter 3. The method based on time series modeling and some powerful machine learning methods for evaluating the global state of the structures under varying the operational and environmental conditions. The main objectives of the proposed iterative feature extraction technique were to identify the best time series model for the raw vibration time-domain data according to Box-Jenkins methodology and choose an optimal order for the identified model to produce uncorrelated residuals. The machine learning methods were MSD, FA, PCA, and AANN. Based on these methods, a simple approach was proposed to determine the threshold values.
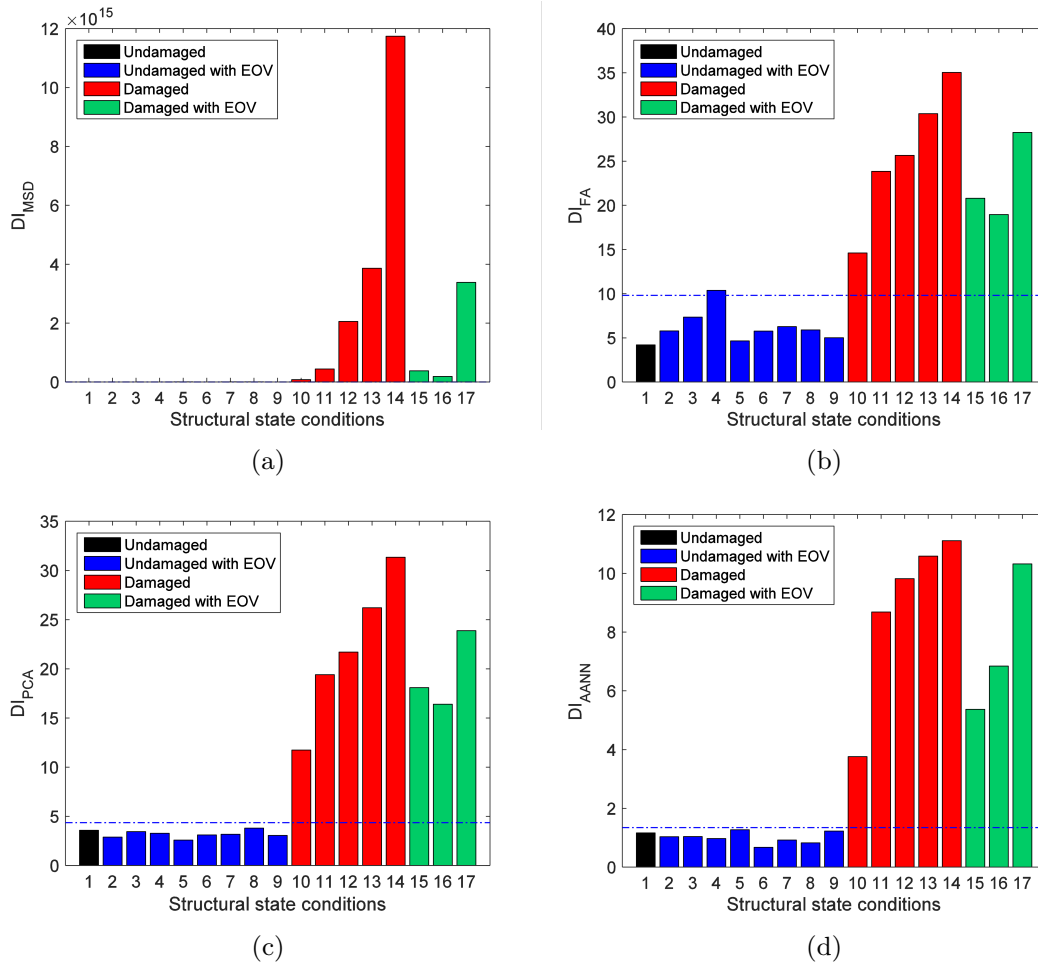
Figure 6.16: *The global health monitoring in the laboratory frame by the machine learning methods: (a) MSD, (b) FA, (c) PCA, and (d) AANN.*

In both cases, the proposed methods showed the excellent results in extracting the reliable DSFs and recognizing the global condition of the structures. It was demonstrated that using the Box-Jenkins methodology enables us to identify the most consistent time series model with the vibration responses. Furthermore, the residual analysis of optimal AR models confirmed that the proposed iterative feature extraction technique is able to fit an accurate and adequate time series model with uncorrelated residuals. The observations of machine learning methods confirmed that these methods are capable of detecting any probable damage, even in the presence of the operational and environmental variability. Moreover, they can appropriately estimate the level of damage in the structures.

6.2 Verification of Robust Multidimensional Scaling-Based Method

Three different applications are provided in this section to demonstrate the effectiveness and capability of the robust multidimensional scaling (RMDS) method and generalized extreme value (GEV) distribution for determining appropriate threshold which is discussed in Chapter 4, for damage detection under high-dimensional features and am-

bient vibration. The examples are: 1) a model-scale four-story steel structure related to the second phase of the IACE-ASCE SHM problem [195], 2) a full-scale cable-stayed bridge, which belongs to Structural Monitoring and Control (SMC) at the Harbin Institute of Technology in China [196], and 3) a numerical offshore jacket structure.

6.2.1 Application to the IASC-ASCE Structure

The four-story structure of the IASC-ASCE problem consisted of 2-bay-by-2-bay steel frames with 2.5×2.5 m in plan and 3.6 m in tall as shown in Fig. 6.17(a). The members were hot-rolled grade 300 W steel with the nominal yield stress 300 MPa. The columns and floor beams were constructed by $B100 \times 9$ and $S75 \times 11$ sections, respectively. In each bay, the bracing system included two 12.7 mm diameter threaded steel rods placed in parallel along the diagonal. To make a reasonably realistic mass distribution, there was one-floor slab per bay per floor so that four 1000 kg slabs were placed at each of the first, second, and third levels and four 750 kg slabs on the fourth floor. On each floor, two of the masses were placed off-center to increase the degree of coupling between the translational motions of the structure. Fig. 6.17(b) depicts the plan of the IASC-ASCE structure.
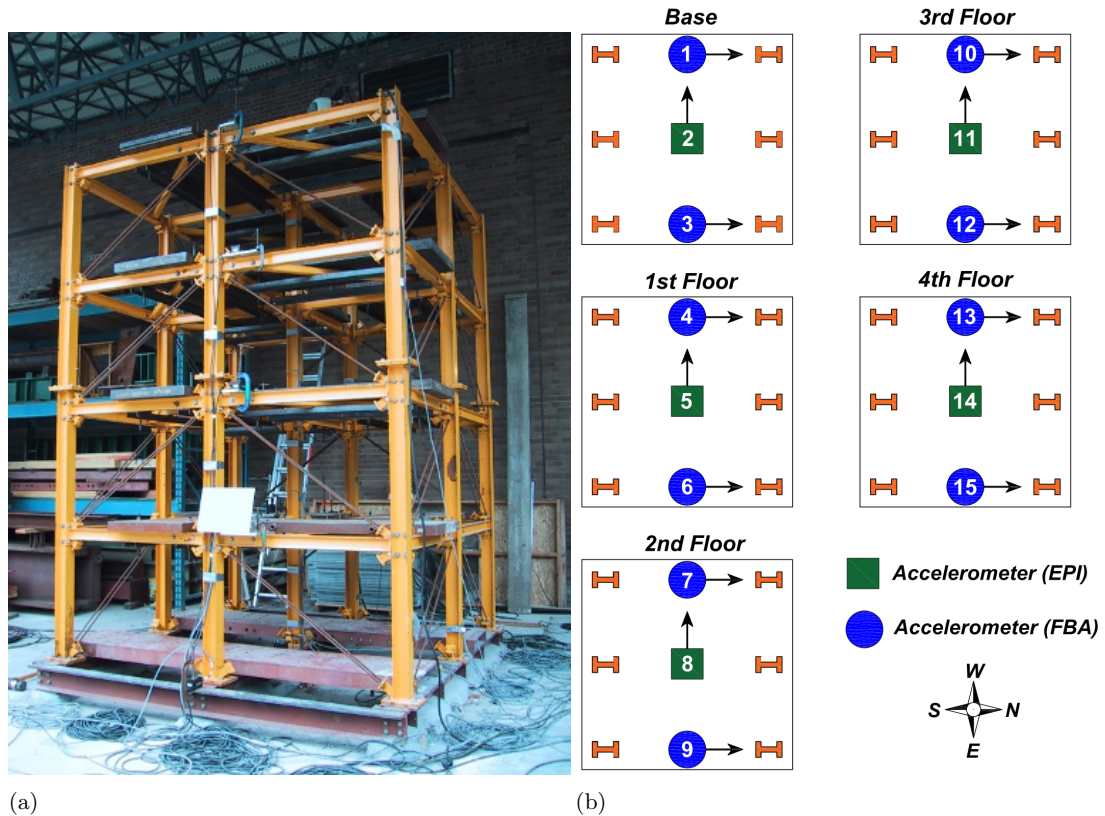
Figure 6.17: *(a) The IASC-ASCE structure, (b) The sensor numbers and locations [197].*

The structure was subjected to ambient vibrations including excitations present from the environment due to the wind, pedestrians, and traffic. The vibration signals were acquired by 15 accelerometers with 5 Volts/g sensitivity distributed on the four stories

and the base of the structure as shown in Fig. 6.17(b). The FBA accelerometers were located on the east and west frames to measure the acceleration time histories in the north-south direction (along the strong axis). The EPI accelerometers were installed near the center column of the structure to measure acceleration responses in the east-west direction (along the weak axis). It needs to mention that the vibration responses of Sensors 1-3 mounted on the base do not provide relevant information about the dynamic behavior of the structure. For this reason, one can neglect to use them in the process of feature extraction. The damage scenarios of the IASC-ASCE structure were simulated by removing some braces from the east, southeast, and north sides (the first pattern) and loosening bolts at the beam-column connections (the second pattern). This study considers the first damage pattern to evaluate the performance of the proposed methods for early damage detection. Table 6.7 lists the five damaged cases resulting from the elimination of the bracing systems from the east and southeast sides.

Table 6.7: *The undamaged and damaged conditions of the IASC-ASCE structure.*

Case no.	Structural Condition	Description
1	Undamaged	Full braced structural system
2	Damaged	Removing the braces of all floors from the east side
3	Damaged	Removing the braces of all floors from the south-east corner
4	Damaged	Removing the braces of the first and fourth floors from the south-east corner
5	Damaged	Removing the braces of the first floor from the south-east corner

Before performing the process of feature extraction, it is necessary to implement some signal pre-processing techniques such as data detrending (i.e. removing linear trends from time series) and standardizing (i.e. normalizing time series by its mean and standard deviation). After that, the initial step of response modeling via the ARMA representation is to determine the model orders (na and nc). Using the iterative order determination technique for the ARMA model [141], Table 6.8 presents the amounts of na and nc as well as the p-values of the Ljung-Box test under the 5% significance level. All p-values in Table 6.8 are larger than the amount of significant level (0.05), in which case one can infer that the residuals of ARMA models for the undamaged condition are uncorrelated. As a sample, Fig. 6.18 indicates the evolution of the p-values associated with the residuals of Sensor 15. It is clear that the p-value at the 54th iteration is greater than 0.05; hence, the appropriate amount for na and nc is 54.

Using the orders gained by the iterative algorithm, the coefficients of ARMA models of the normal condition are estimated by the prediction-error technique [114]. In the following, the uncorrelated residuals at all sensors of the first case are extracted as the randomly DSFs, which make the residual dataset (matrix) of the normal condition $\mathbf{E} \in \mathbb{R}^{60000 \times 12}$ (i.e. $nd = 60000$ and $ns = 12$). Based on the residual-based feature extraction, the ARMA models (i.e. the orders and coefficients) obtained from the first case are used to extract the residuals of the damaged cases. For each case, one can make a matrix of residual samples as $\bar{\mathbf{E}} \in \mathbb{R}^{60000 \times 12}$. To demonstrate the sensitivity of the ARMA model residuals to damage, Fig. 6.19 shows the comparison between the residual samples of the normal condition and each damaged case at Sensor 15. Based on Fig. 6.17(b) and the descriptions in Table 6.7, one can understand that the location of Sensor 15 is near to the damaged area of the structure for Cases 2-4 (i.e. at the east

Table 6.8: *The orders of ARMA models and the p-values of the Ljung-Box test for the first case.*

Sensor no.	Order no.		p-value
	na	*nc*	
4	45	45	0.1422
5	42	42	0.7971
6	40	40	0.1775
7	61	61	0.1280
8	43	43	0.8807
9	39	39	0.0819
10	64	64	0.1652
11	48	48	0.2876
12	40	40	0.0853
13	47	47	0.2793
14	46	46	0.5056
15	54	54	0.0754
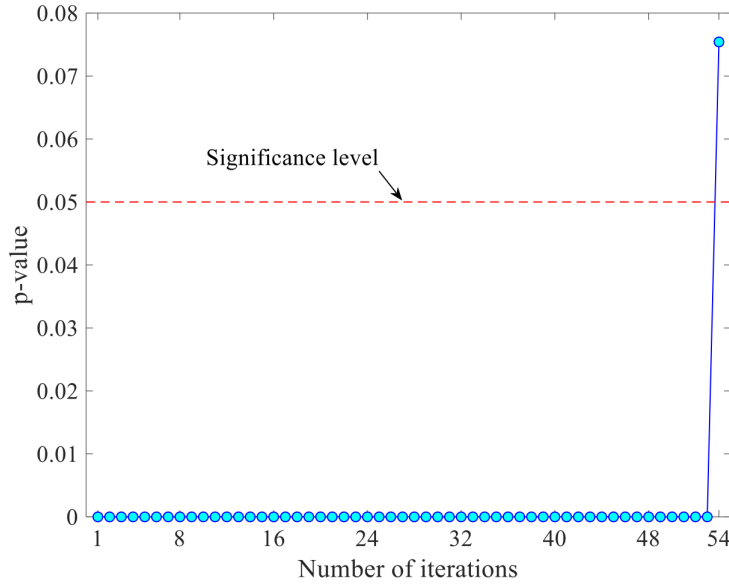
Figure 6.18: *The evolution of p-values of the ARMA residuals at Sensor 15.*

side of the fourth floor) except for Case 5. As can be seen in Fig. 6.19(a)-(c), there are clear increases in the ARMA residuals regarding Cases 2-4 compared to Case 1. On the contrary, since the location of Sensor 15 is not the damaged area of Case 5, no increase in the residuals is observable in Fig. 6.19(d) between Cases 1 and 5. Therefore, the observations in Fig. 6.19 prove the sensitivity of ARMA residuals to damage.

Based on the proposed RMDS-based method, the first step is to divide the residual matrices $\mathbf{E}$ and $\bar{\mathbf{E}}$ of the normal and damaged conditions into several partitions with the same dimension. In this regard, the number of the partition (p) is set as 60, in which case the number of data points (np) of each partition becomes 1000. Hence, the matrices $\mathbf{E}$ and $\bar{\mathbf{E}}$ are decomposed into 60 smaller matrices $(\mathbf{E}_1^*, ..., \mathbf{E}_{60}^*$ and $\bar{\mathbf{E}}_1^*, ..., \bar{\mathbf{E}}_{60}^*)$ consisting of 1000 rows and 12 columns. Subsequently, the distance matrices $(\mathbf{D}_1^*, ..., \mathbf{D}_{60}^*$ and $\bar{\mathbf{D}}_1^*, ..., \bar{\mathbf{D}}_{60}^*)$ (of the sizes of 1000×1000) are computed by using the ESD tech-
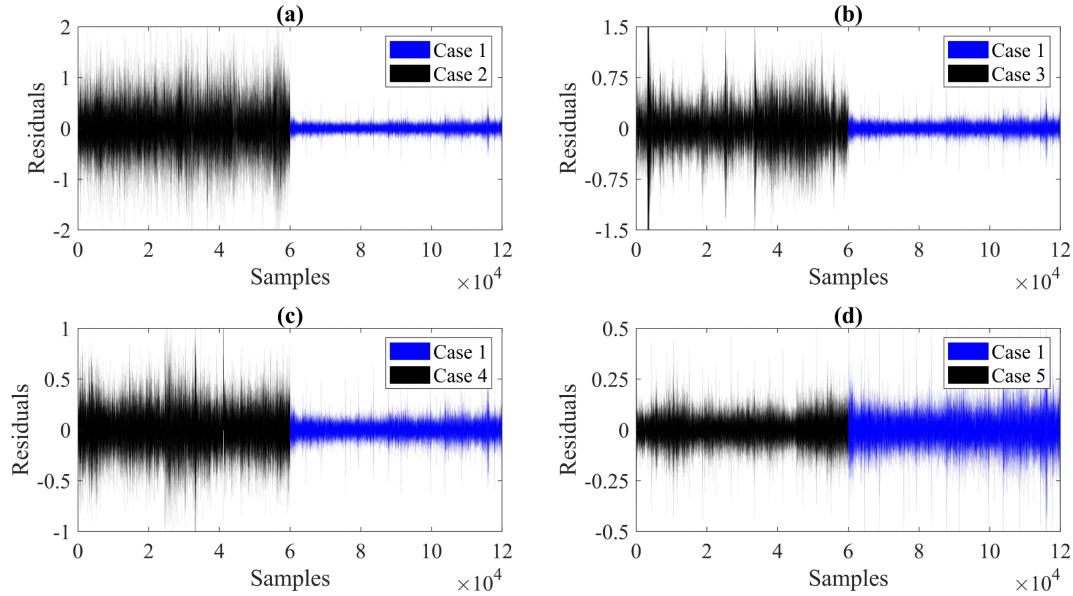
Figure 6.19: *Comparison of the ARMA residuals between the normal and damaged cases at Sensor 15: (a) Case 1 vs. Case 2, (b) Case 1 vs. Case 3, (c) Case 1 vs. Case 4, (d) Case 1 vs. Case 5.*

nique. The RMDS method based on the MM approach is applied to obtain the embedding matrices ($\mathbf{U}_1, ..., \mathbf{U}_{60}$ and $\bar{\mathbf{U}}_1, ..., \bar{\mathbf{U}}_{60}^*$) with the sizes of 1000×2. The matrix vectorization technique is then utilized to make the vectors $\mathbf{u}_1, ..., \mathbf{u}_{60}$ and $\bar{\mathbf{u}}_1, ..., \bar{\mathbf{u}}_{60}$, each of which has 2000 embedding samples. Using the Euclidean norm, the vector $\mathbf{d}$ is determined to use in the process of early damage detection. Since the vibration data of the IASC-ASCE problem in the undamaged and damaged cases were acquired once, there is a set of vibration datasets and residual matrices $\mathbf{E}$ and $\bar{\mathbf{E}}$. In other words, the number of test measurements (nm) is equal to one, in which case $\mathbf{d_T} = \mathbf{d}$.

For early damage detection, one initially needs to define an accurate and appropriate threshold limit via the EV statistics and the first 60 embedding norm values of $\mathbf{d}$ regarding the undamaged state. First, the GEV theory is applied to choose one of the Gumbel, Fréchet, and Weibull distributions. Based on the MLE technique under the 5% significance level, the shape of GEV is equal to 0.1859. Hence, one can realize that the Fréchet-type EV distribution is suitable for modeling the first 60 embedding norm values of $\mathbf{d}$ for the threshold limit determination. The shape, scale, and location of the Fréchet distribution correspond to 5.3787, 6.3256, and 1.9304, respectively, which lead to the threshold limit $\tau_2 = 16.5615$. Having considered all embedding norm quantities of $\mathbf{d}$ and the threshold value of interest, Fig. 6.20 indicates the results of damage detection of the IASC-ASCE structure in Cases 2-5. As can be observed, the first 60 embedding norm values associated with the normal condition of the structure are smaller than the threshold limit without any false alarms or Type I errors. In contrast, the remaining 60 embedding norm values in Fig. 6.20(a)-(c) are larger than the threshold limit implying the occurrence of damage in Cases 2-4. The same conclusion is observable for Case 5 in Fig. 6.20(d), where the only three points are under the threshold limit leading to the 5% Type II error. Therefore, one can conclude that the

proposed RMDS-based method in conjunction with the residuals of the ARMA model and the EV theory is sufficiently able to detect damage with different severities and distinguish the damaged state from the normal condition under ambient vibration.

Figure 6.20: *Early damage detection of the IASC-ASCE structure by the proposed RMDS-based method and the EV statistics: (a) Case 2, (b) Case 3, (c) Case 4, (d) Case 5.*

To demonstrate the effect of the threshold limit on the early damage detection, a comparative study is conducted by using the standard confidence interval (CI) under the normality assumption of the embedding norm values of the undamaged conditions. Using a 5% significance level leading to the 95% CI, the threshold amount is equal to 9.4983. Accordingly, the results of damage detection by the standard CI are illustrated in Fig. 6.21. It is clear that all embedding norm values of Cases 2-5 exceed the threshold value without any Type II error. However, there are numerous false alarms in the embedding norm values of Case 1 (Type I=35%).

For more details, Fig. 6.22 shows the normal probability plot of the first 60 embedding norm values as well as the comparison between the EV theory and standard CI in terms of the rate of false alarm. As Fig. 6.22(a) indicates, there are clear deviations from the straight line in the sense that the probability distribution of the first 60 embedding norm values of $\mathbf{d}$, which are applied to determine the threshold limit, is non-normal. For this reason, the use of standard CI based on the normality assumption is not sufficiently effective in estimating the accurate threshold limit. Furthermore, Fig. 6.22(b) reveals the superiority of the EV theory over the standard CI in terms of defining an accurate threshold value without any false alarm (Type I error). As can be observed, all norm values regarding the normal condition fall below the threshold
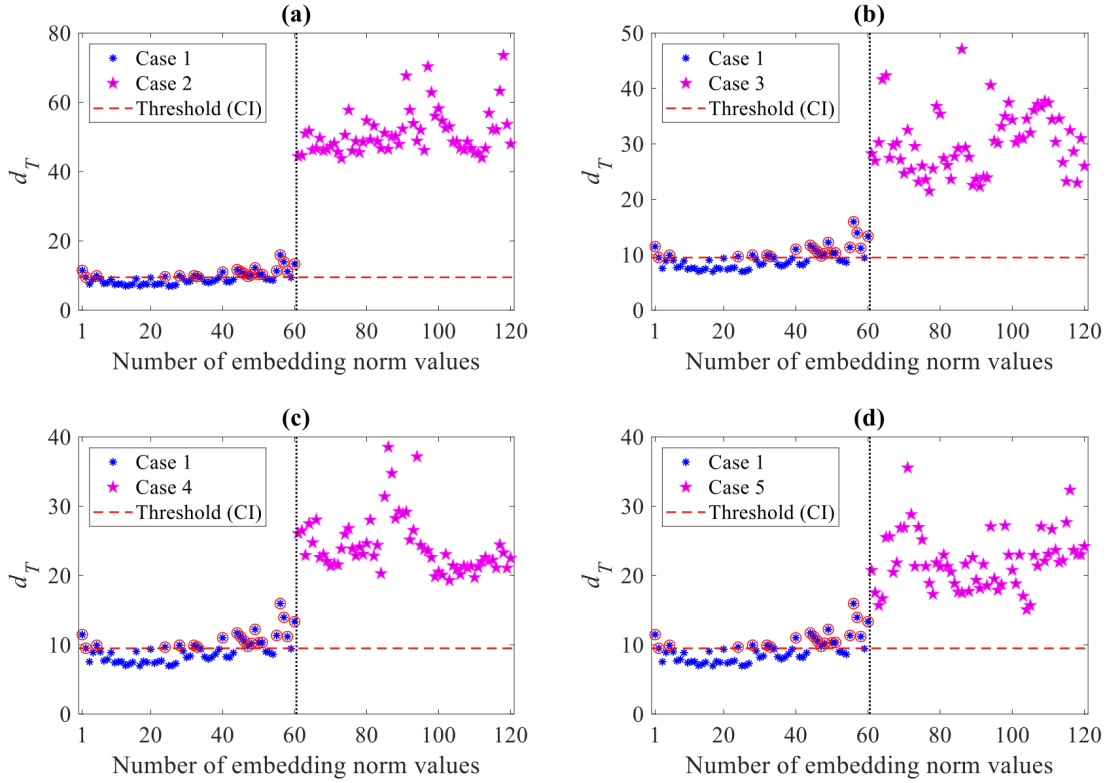
Figure 6.21: *Early damage detection of the IASC-ASCE structure by the proposed RMDS-based method and the standard CI: (a) Case 2, (b) Case 3, (c) Case 4, (d) Case 5.*
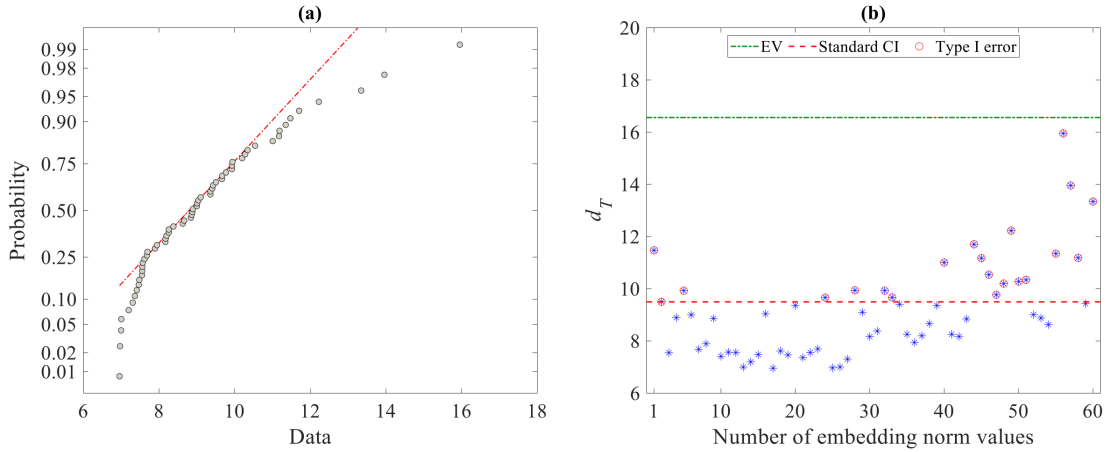
Figure 6.22: *(a) The normal probability plot of the first 60 embedding norm values of $\boldsymbol{d}$, (b) Comparison between the EV theory and standard CI for the threshold limit determination.*

obtained from the EV theory implying no Type I error, whereas one can observe that several norm values exceed the threshold gained by the standard CI.

As the other comparative study, it is attempted to compare the proposed RMDS-based method with the well-known Mahalanobis distance (MD) technique, which is widely used in SHM applications. This statistical distance measures the dissimilar-
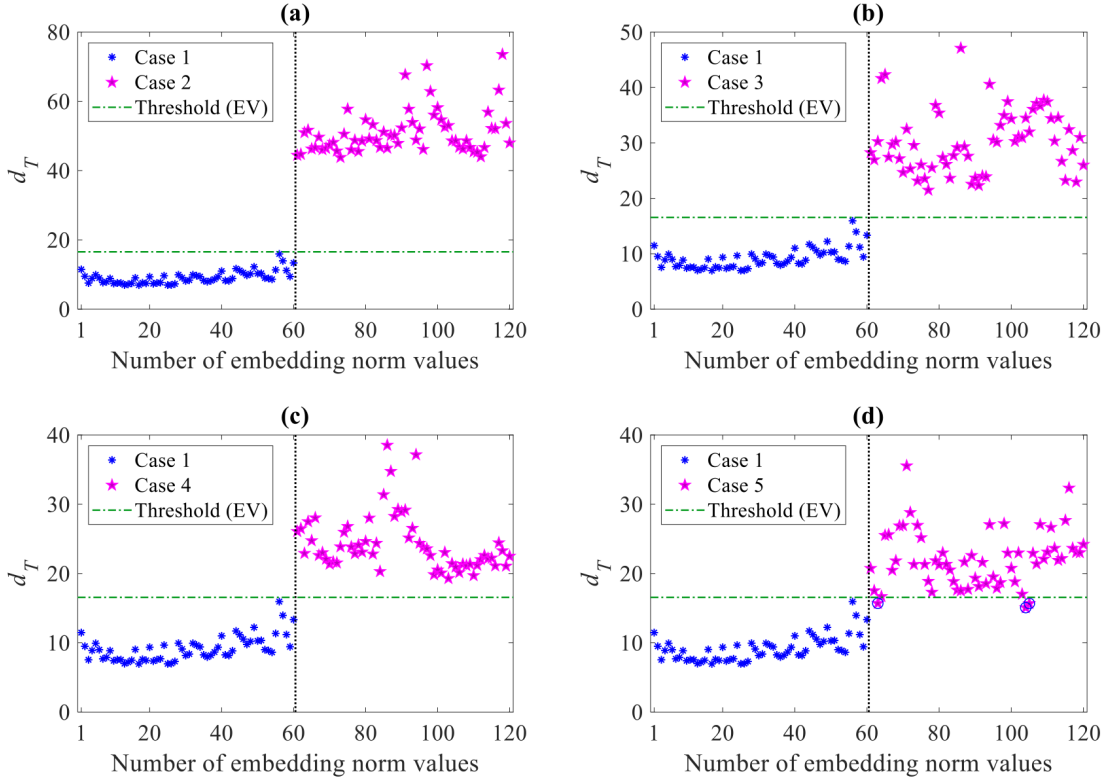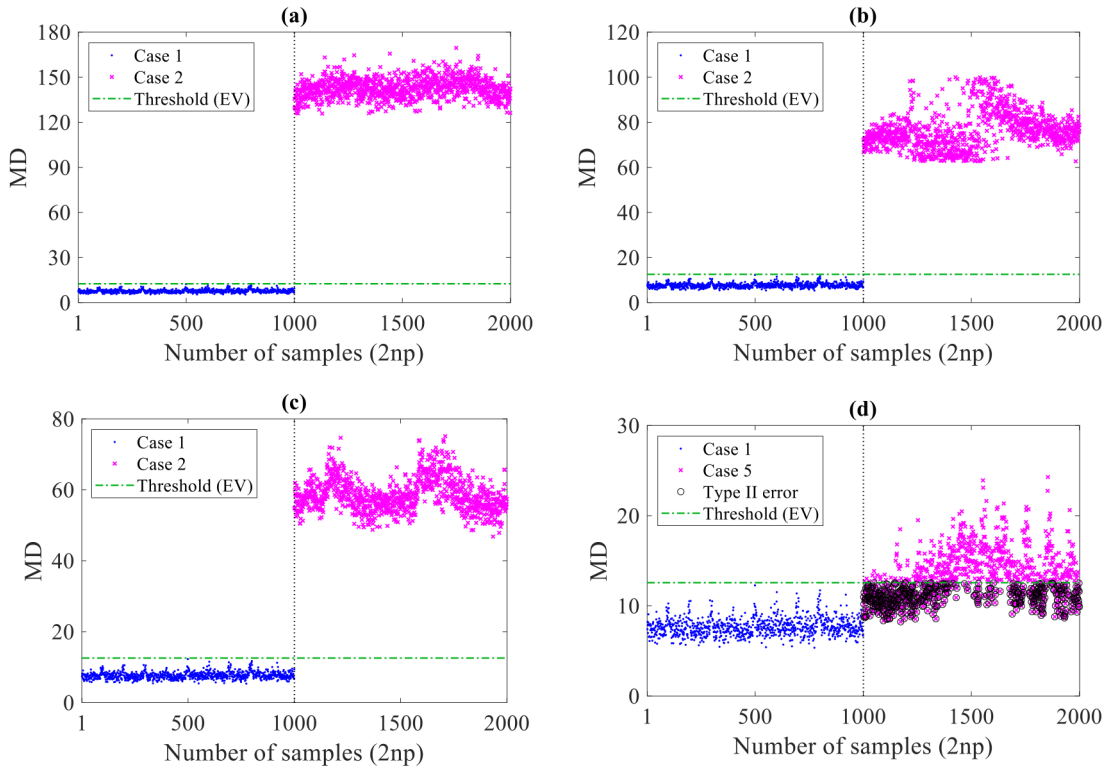
Figure 6.23: *Early damage detection of the IASC-ASCE structure by the conventional MD method and the EV statistics: (a) Case 2, (b) Case 3, (c) Case 4, (d) Case 5.*

ity between two multivariate datasets based on the correlation of data samples. For a reasonable comparison, the Euclidean norms of the residual matrices ($\mathbf{E}_1^*, ..., \mathbf{E}_{60}^*$ and $\bar{\mathbf{E}}_1^*, ..., \bar{\mathbf{E}}_{60}^*$) at all sensors are calculated to create the multivariate feature dataset of the size of 1000×60 for each of Cases 1-5. On this basis, there are 1000 MD values for each case. The EV theory is then applied to estimate the threshold value based on the distance quantities of the normal condition. The shape of GEV distribution is equal to -0.0814, which refers to the Weibull-type EV distribution. Using the MLE technique, the shape, scale, and location of Weibull distribution are estimated and used in Eq. (4.27) to determine $\tau = 12.5673$ as the threshold limit for damage detection via the MD technique. Fig. 6.23 shows the results of damage detection in Cases 2-5, where the first 1000 MD values belong to the undamaged case, and the remaining distance quantities are associated with the damaged cases. It is apparent that the first 1000 distance quantities of the normal condition are below the threshold limit without any Type I error. This conclusion proves the ability of the EV statistics to estimate an accurate and reliable threshold limit. Moreover, the remaining distance quantities of Cases 2-4 in Fig. 6.23(a)-(c) exceed the threshold limit indicating the occurrence of damage with no Type II error. However, it is observed that there are numerous false-negatives (Type II=46.8%) in the distance values of Case 5. Therefore, the comparison between the proposed RMDS-based method and the conventional MD technique demonstrates that although both of them are successful in detecting damage and distinguishing the

damaged state from the normal condition, the proposed method outperforms the MD technique with fewer Type II errors.

Finally, Table 6.9 presents the numbers and percentages of Type I, Type II, and total errors in detecting early damage of the IASC-ASCE structure in all damaged cases by the proposed RMDS-based and the classical MD methods. In this comparison, the two threshold determination approaches (i.e. the EV statistics and the standard CI) are considered as well. As the data in Table 6.9 appears, the proposed RMDS-based method in conjunction with the EV statistics yields the best performance in terms of the smallest rates of the triple errors except for the Type II error in Case 5, which the only 3 points from 60 norm values fall below the threshold as shown in Fig. 6.20(d). The same conclusion can be reached for the MD technique. However, this feature classification approach suffers from an extremely large Type II error in Case 5 leading to a considerable total error as well. This conclusion proves the superiority of the proposed method over the classical MD technique. On the other hand, the numerical comparison between the EV statistics and the standard CI reveals that the latter, despite its inconsiderable Type II errors, is not a reliable approach to estimating an accurate threshold for early damage detection owing to large Type I and total errors in both feature classification methods. It is worth remarking that the good performance of the EV statistics depends directly on the use of a robust feature classification technique (e.g. the proposed RMDS-based method) with high damage detectability.

Table 6.9: *Performance evaluation of the feature classification methods using the EV statistics and standard CI for the threshold limit determination.*

Case no.	Method	Threshold	Type I	Type II	Total
2	RMDS	EV	0 (0%)	0 (0%)	0 (0%)
		Standard CI	21 (35%)	0 (0%)	21 (17.5%)
	MD	EV	0 (0%)	0 (0%)	0 (0%)
		Standard CI	40 (4%)	0 (0%)	40 (2%)
3	RMDS	EV	0 (0%)	0 (0%)	0 (0%)
		Standard CI	21 (35%)	0 (0%)	21 (17.5%)
	MD	EV	0 (0%)	0 (0%)	0 (0%)
		Standard CI	40 (4%)	0 (0%)	40 (2%)
4	RMDS	EV	0 (0%)	0 (0%)	0 (0%)
		Standard CI	21 (35%)	0 (0%)	21 (17.5%)
	MD	EV	0 (0%)	0 (0%)	0 (0%)
		Standard CI	40 (4%)	0 (0%)	40 (2%)
5	RMDS	EV	0 (0%)	3 (5%)	3 (2.5%)
		Standard CI	21 (35%)	0 (0%)	21 (17.5%)
	MD	EV	0 (0%)	468 (46.8%)	468 (23.4%)
		Standard CI	40 (4%)	64 (6.4%)	104 (5.2%)

6.2.2 Application to the Cable-Stayed Bridge

The Tianjin-Yonghe Bridge is one of the earliest cable-stayed bridges with continuous pre-stressed box-girder constructed in China, which was opened to traffic since December 1987. It consists of a total length of 514.40 m including the main span of 260 m and two side spans of 25.15 m and 99.85 m as depicted in Fig. 6.24. The bridge has 510 m long and 11 m wide including 9 m for vehicles and 2×1 m for pedestrians.

The concrete towers, connected by two transverse beams, include the height of 60.5 m. More details of the bridge are available in [196]. In 2005, after 19 years of operation, some serious cracks were found at the bottom of a girder segment over the mid-span. Additionally, some cables near the anchors were severely corroded. After a major rehabilitation program for replacing the damaged girder segment and all the cables between 2005 and 2007, a sophisticated SHM system organized by the Center of SMC at the Harbin Institute of Technology in China is applied to monitor the bridge in 2007. During a routine inspection in August 2008, new damage patterns were found in the girders of the bridge. Due to the availability of acceleration time histories of the health status of the bridge on January 17, 2008, and the damage status on July 31, 2008, it is possible to evaluate the performance of the proposed methods for early damage detection [196].
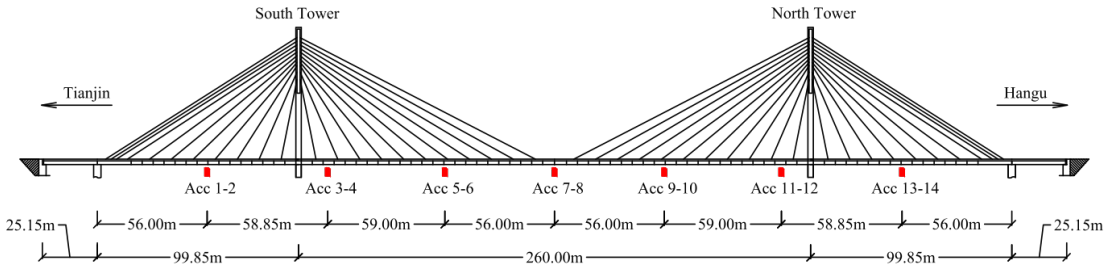
Figure 6.24: *The Tianjin-Yonghe Bridge [196]: (a) the general view, (b) the dimensions and sensors.*

The acceleration time histories of the normal and damaged conditions were acquired from 14 single-axis accelerometers during 24 hours ($nm = 24$) under the sampling frequency 100 Hz and time interval 0.01 Sec. On this basis, 360000 samples (nd) were measured by each accelerometer at each hour. According to initial data analysis on the acceleration datasets, it is found that the data of the 10th accelerometer is out of order due to meaningless measurement samples. Hence, the acceleration time series of the 13 accelerometers ($ns = 13$) are used to fit ARMA models to the vibration responses and extract the model residuals of the normal and damaged states as the high-dimensional DSFs. Similar to the previous application case, the signal pre-processing techniques including data detrending and standardizing are carried out to prepare the time series datasets for ARMA modeling. Using the iterative order determination algorithm based

on the Ljung-Box test under the 5% significance level, Table 6.10 lists the orders of ARMA models of the accelerometers 1-9 and 11-14 along with their p-values for the first test measurement on January 17, 2008 (the healthy state). As can be observed, all p-values are larger than 0.05, which means that the ARMA residuals of all accelerometers are uncorrelated. Furthermore, Fig. 6.25 illustrates the evolution of the p-values regarding the ARMA residuals of the 6th accelerometer in 23 iterations.

Table 6.10: *The orders of ARMA models and the p-values of the Ljung-Box test in the first test measurement on January 17, 2008.*

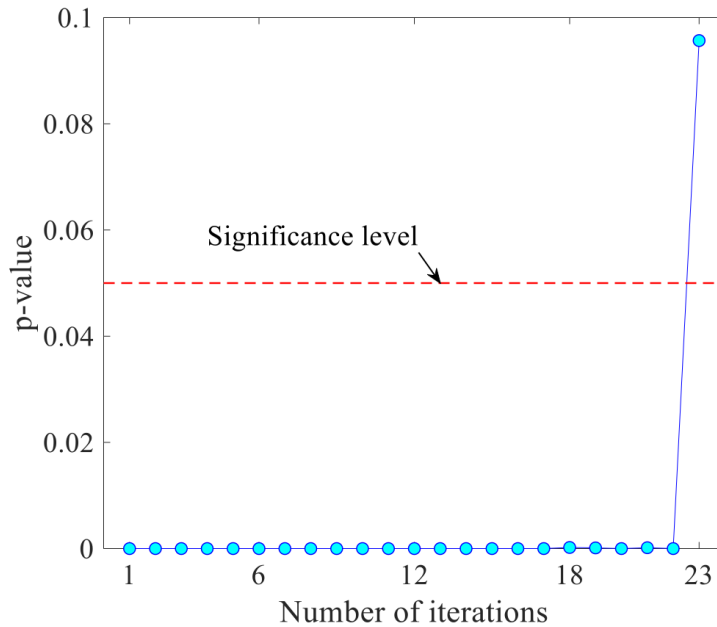| Sensor no.	Order no.		p-value
	na	*nc*	
1	30	30	0.1337
2	19	19	0.7840
3	31	31	0.9340
4	24	24	0.1158
5	16	16	0.3234
6	23	23	0.0956
7	25	25	0.8181
8	26	26	0.6483
9	15	15	0.8207
11	21	21	0.0820
12	30	30	0.4263
13	20	20	0.2804
14	19	19	0.6573

Figure 6.25: *The evolution of the p-values of the ARMA residuals regarding the 6th accelerometer.*

Having considered the ARMA orders, the model coefficients are estimated by the prediction-error technique. Subsequently, the uncorrelated residuals of the accelerometers 1-9 and 11-14 on January 17, 2008, are extracted as the DSFs of the normal

condition leading to the residual matrix $\mathbf{E} \in \mathbb{R}^{360000 \times 13}$ for each test measurement. Finally, the ARMA models including their orders and coefficients obtained from the normal condition are utilized to extract the model residuals of the accelerometers 1-9 and 11-14 on July 31, 2008, which makes the residual matrix $\bar{\mathbf{E}} \in \mathbb{R}^{360000 \times 13}$ for each test measurement. Note that there are 24 sets of the residual matrix for the normal and damaged conditions based on the number of test measurements. As a sample, Fig. 6.26 indicates the comparison between the residual samples at the 9th accelerometer regarding the normal and damaged states in the first test measurement.
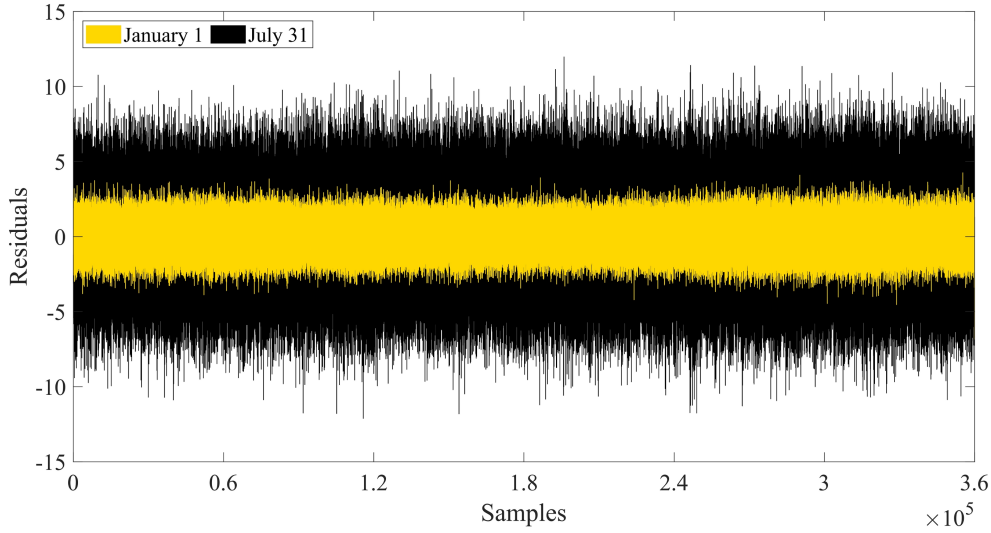
Figure 6.26: *The residual samples of ARMA models at the 9th accelerometer regarding the normal and damaged states in the first test measurement.*

The increases in the residuals of the ARMA model on July 31, 2008, demonstrate the occurrence of damage. The same conclusion is obtainable for the other accelerometers and other test measurements. However, the direct comparison of the high-dimensional residual samples at each sensor and each hour may cause a complex and time-consuming process. This limitation suggests the necessity of using a robust and efficient approach such as the proposed RMDS-based method for damage detection. Based on the first step of the proposed method, the residual matrices $\mathbf{E}$ and $\bar{\mathbf{E}}$ of each test measurement are divided into 200 partitions ($p = 200$); that is, ($\mathbf{E}_1^*, ..., \mathbf{E}_{200}^*$ and $\bar{\mathbf{E}}_1^*, ..., \bar{\mathbf{E}}_{200}^*$), each of which consists of 1800 rows ($np = 1800$) and 13 columns. Using the ESD technique, their distance matrices are ($\mathbf{D}_1^*, ..., \mathbf{D}_{200}^*$ and $\bar{\mathbf{D}}_1^*, ..., \bar{\mathbf{D}}_{200}^*$) of the size of 1800×1800. Subsequently, the RMDS method based on the MM approach is applied to obtain the embedding matrices ($\mathbf{U}_1, ..., \mathbf{U}_{200}$ and $\bar{\mathbf{U}}_1, ..., \bar{\mathbf{U}}_{200}^*$) of the size of 1800×2. The matrix vectorization technique is utilized to construct the vectors $\mathbf{u}_1, ..., \mathbf{u}_{200}$ and $\bar{\mathbf{u}}_1, ..., \bar{\mathbf{u}}_{200}$ with 3600 embedding samples. This process continues for all test measurements, which makes 24 sets of the vectors of $\mathbf{u}_1, ..., \mathbf{u}_{200}$ and $\bar{\mathbf{u}}_1, ..., \bar{\mathbf{u}}_{200}$. Finally, the vector $\mathbf{d_T}$ is determined by calculating the Euclidean norms of the 24 sets of embedding vectors. On this basis, this vector includes 9600 embedding norm values, where the first 4800 quantities belong to the healthy state and the remaining norm amounts are related to the damaged condition.
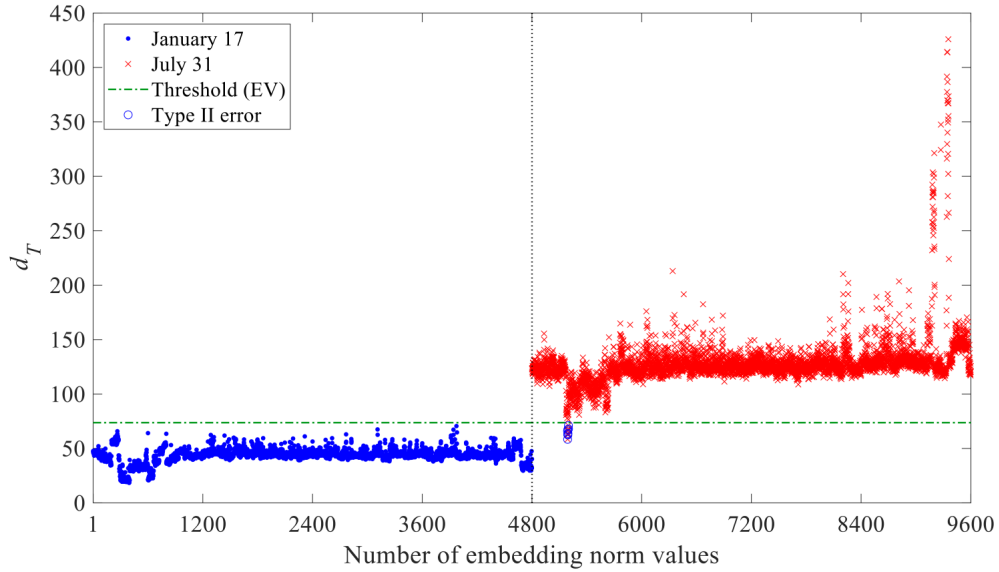
Figure 6.27: *Early damage detection of the Tianjin-Yonghe Bridge by the proposed RMDS-based method and the EV statistics.*

The GEV distribution is initially fitted to the first 4800 embedding norm values of $\mathbf{d_T}$ to estimate the shape parameter by the MLE technique and choose an appropriate EV distribution for the threshold limit determination. The shape of GEV distribution corresponds to 0.2338, which refers to the Fréchet-type EV distribution. By estimating the shape, scale, and location parameters of the Fréchet distribution, the threshold limit based on the 5% significance level is obtained from Eq. (4.26), which is identical to $\tau_2 = 73.6991$. For a comparative study, another threshold limit under the normality assumption of the same embedding norm values is determined by the standard CI. Applying the 5% significance level, the threshold limit based on the 95% CI is equal to 43.5110. Figs. 6.27 and 6.28 illustrate the results of early damage detection based on the proposed RMDS-based method in conjunction with the EV statistics and standard CI, respectively. In Fig. 6.27, the first 4800 embedding norm values do not exceed the threshold limit obtained from the EV statistics implying no false alarm. Moreover, the majority of the embedding norm quantities regarding the damaged state are larger than the threshold value indicating the occurrence of damage on July 31. However, the only eight norm values are under the threshold limit, which leads to the 0.17% Type II error. Although the observations in Fig. 6.28 appear that no false negative is available in the embedding norm values (4801-9600) on July 31, 2008, there are numerous false alarms in the first 4800 embedding norm values (Type I $= 56.60\%$).

For more evaluation, Fig. 6.29 indicates the normal probability of the embedding norm values 1-4800 along with the comparison between the EV theory and standard CI in terms of the rate of false alarm. It is apparent from Fig. 6.29(a) that the probability distribution embedding norm quantities is non-normal resulting from large deviations from the straight line. Therefore, it can be expected that the standard CI based on the normality assumption is not able to estimate an accurate and reliable threshold limit. In this regard, one can observe in Fig. 6.29(b) that the use of EV theory gives no false
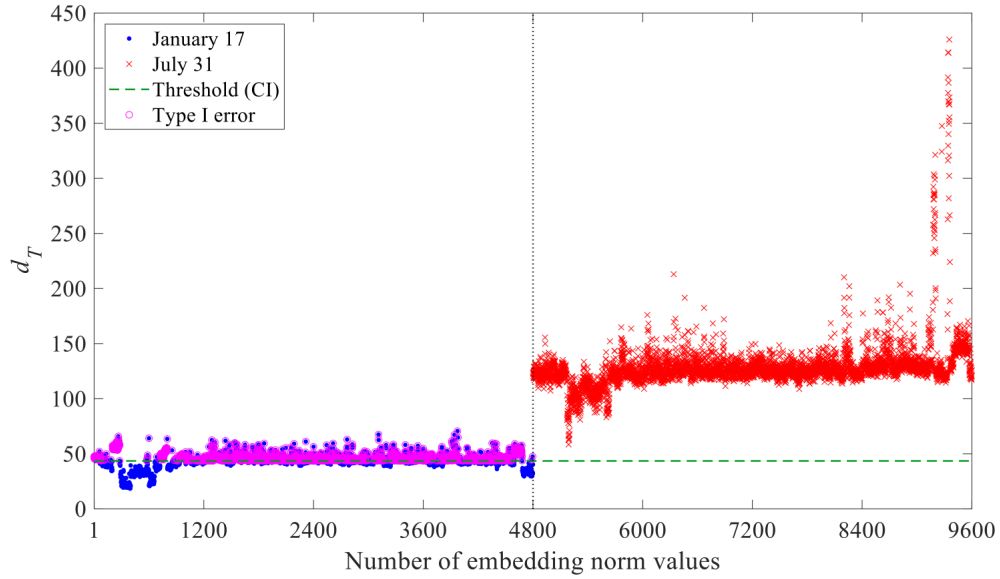
Figure 6.28: *Early damage detection of the Tianjin-Yonghe Bridge by the proposed RMDS-based method and the standard CI.*

alarm, whereas the standard CI suffers from the high rate of Type I error.
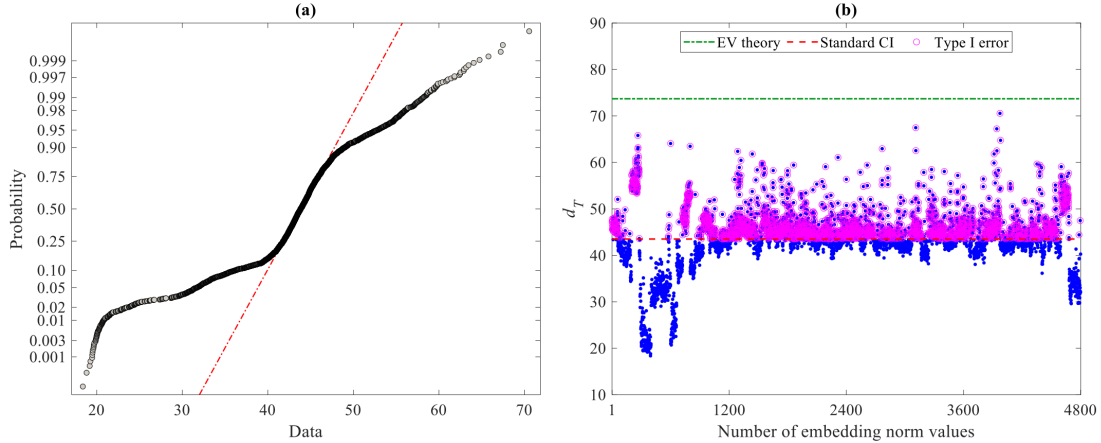
Figure 6.29: *(a) The normal probability plot of the first 4800 embedding norm values of d_T, (b) Comparison between the EV theory and standard CI for the threshold limit determination.*

Similar to the preceding application case, the performance of the proposed RMDS-based method is compared with the classical MD technique. For this purpose, the Euclidean norms of the residual matrices ($\mathbf{E}_1^*, ..., \mathbf{E}_{200}^*$ and $\bar{\mathbf{E}}_1^*, ..., \bar{\mathbf{E}}_{200}^*$) at all sensors and all measurements are calculated and collected to generate two multivariate feature datasets regarding the undamaged (January 17) and damaged (July 31) states. In this regard, both datasets are matrices of the size 360000×24, in which case the feature set of the undamaged state is considered to estimate the 24-dimensional mean vector and the covariance matrix of the size (24×24) needed for the MD metric. Using 360000 MD values of the undamaged condition, the EV statistics are utilized to deter-

75

mine a threshold limit. On this basis, the shape of the GEV distribution corresponds to -0.0524 implying the Weibull-type EV distribution. Under the 5% significance level, the threshold value from Eq. (4.27) is identical to $\tau_3 = 10.6540$. Fig. 6.30 illustrates the result of early damage detection in the bridge via the MD metric, where the first and second 360000 samples pertain to the undamaged and damaged states, respectively. It is seen that all the MD values regarding January 17 (the normal condition) fall below the threshold line without any Type I error. However, there are numerous erroneous results in the MD quantities of July 31 (the damaged condition) that are under the threshold value causing serious Type II errors. Apart from these conclusions, one of the limitations of utilizing the MD metric in this application case is related to its high-dimensional outputs. Unlike the IASC-ASCE structure (see Fig. 6.23), there are 720000 MD values for feature classification. In comparison with the result of early damage detection gained by the proposed RMDS-based method (see Fig. 6.27, where there are 9600 outputs for decision-making), one can conclude that the proposed RMDS-based method is more efficient than the classical MD technique.
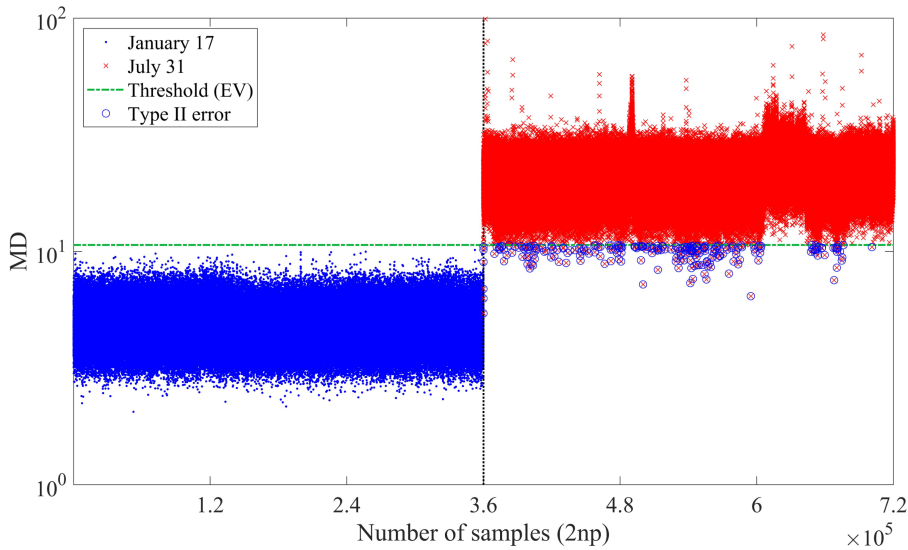
Figure 6.30: *Early damage detection in the Tianjin-Yonghe Bridge by the classical MD technique and the EV statistics.*

Eventually, the final comparison is concerned with the numerical evaluations of the performances of the proposed RMDS-based and classical MD methods based on Type I, Type II, and total errors. Using the two threshold determination approaches, Table 6.11 gives the numbers and percentages of these errors. As can be perceived, the best performance in terms of the smallest rates of Type I and total errors belongs to the proposed RMDS-based method in conjunction with the EV statistics. Furthermore, the EV theory is highly superior to the standard CI due to having smaller Type I and total errors. Although the standard CI provides smaller numbers and percentages of Type II error, the corresponding amounts concerning the proposed RMDS-based method are inconsiderable (i.e. the only 8 points from 4800 norm values fall below the threshold limit gained by the EV statistics). However, this conclusion is not valid for the outputs of the MD metric based on the EV theory. In summary, the numerical evaluations

in Table 6.11 confirm that the proposed RMDS-based method outperforms the classical MD technique and it is preferable to using the EV statistics for the threshold limit determination.

Table 6.11: *Performance evaluation of the feature classification methods using the EV statistics and standard CI for the threshold limit determination.*

Method	Threshold	Type I	Type II	Total
RMDS	EV	0 (0%)	8 (0.17%)	8 (0.08%)
	Standard CI	2717 (56.60%)	0 (0%)	2717 (28.30%)
MD	EV	0 (0%)	241 (0.06%)	241 (0.03%)
	Standard CI	13654 (3.79%)	3 ($\sim 0\%$)	13657 (1.89%)

6.2.3 Application to the Numerical Offshore Jacket Structure

The numerical offshore jacket structure which is described by Li et al. [198], shown in Fig. 6.31a. The platform consists of 36 steel tubular members which comprises 12 leg members, 12 horizontal brace members, and 12 diagonal brace members in vertical planes. All members have uniform outer diameter 17.8 cm and wall thickness 0.89 cm. The structure is fixed at the ground. The heights of the three stories are all 9.14 m, and the side lengths of the floors, from first to fourth, are 10.97, 8.53, 6.10, and 3.66 m, respectively. The material properties of the steel tubular members include: elastic modulus $E = 210$ GPa, Poisson's ratio $\nu = 0.3$, and mass density $\rho = 7850$ kg/m^3.
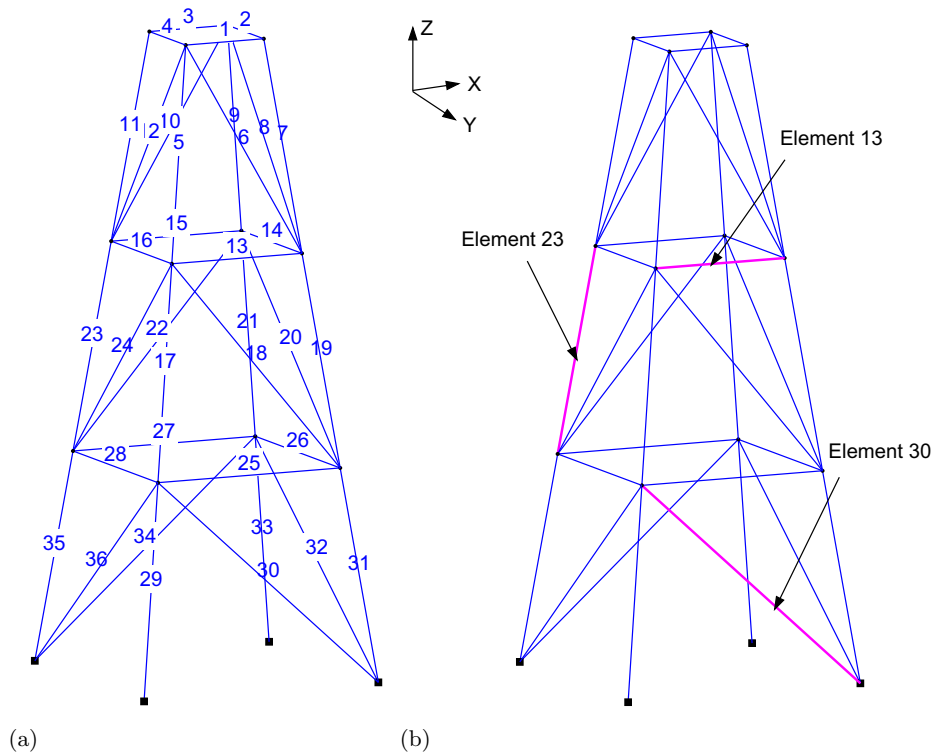
Figure 6.31: *(a) The sketch of the offshore structure, (b) The locations of damaged elements [198].*

The finite element model is developed in MATLAB environment to obtain structural responses in undamaged and damaged states. Moreover, Gaussian white noise signals are applied to the structure to excite the platform and simulate ambient vibration. Moreover, up to 5% noise in modulus of elasticity of elements are applied to consider environmental and operational effects. In this study, the damage severity is defined as the percentage stiffness loss of an element. Fig. 6.31b highlights the locations of those damaged elements. In addition, the damage scenarios are reported in Table 6.12.

Table 6.12: *The undamaged and damaged conditions of the numerical offshore jacket structure.*

Case no.	Structural Condition	Description
1	Undamaged	Baseline condition
2	Damaged	Damaged beam (Element 13) with 50% stiffness loss
3	Damaged	Damaged column (Element 23) with 40% stiffness loss
4	Damaged	Damaged brace (Element 30) with 60% stiffness loss
5	Damaged	All three damaged scenarios together

As it is mentioned, for early damage detection an appropriate threshold limit via the standard CI and the first 4500 embedding norm values of $\mathbf{d}$ regarding the undamaged state is defined. Having considered all embedding norm quantities of $\mathbf{d}$ and the threshold value of interest, Figs. 6.32 to 6.35 indicate the results of damage detection of the numerical offshore jacket structure in Cases 2-5. As can be seen, the first 4500 embedding norm values associated with the normal condition of the structure are under the threshold limit without any false alarms or Type I errors. In contrast, the majority of remaining 5000 embedding norm values in Figs. 6.32 to 6.35 are above the threshold limit implying the occurrence of damage in Cases 2-5. The number and percentages of Type I, Type II, and total errors for numerical offshore jacket structure are reported in Table 6.13.
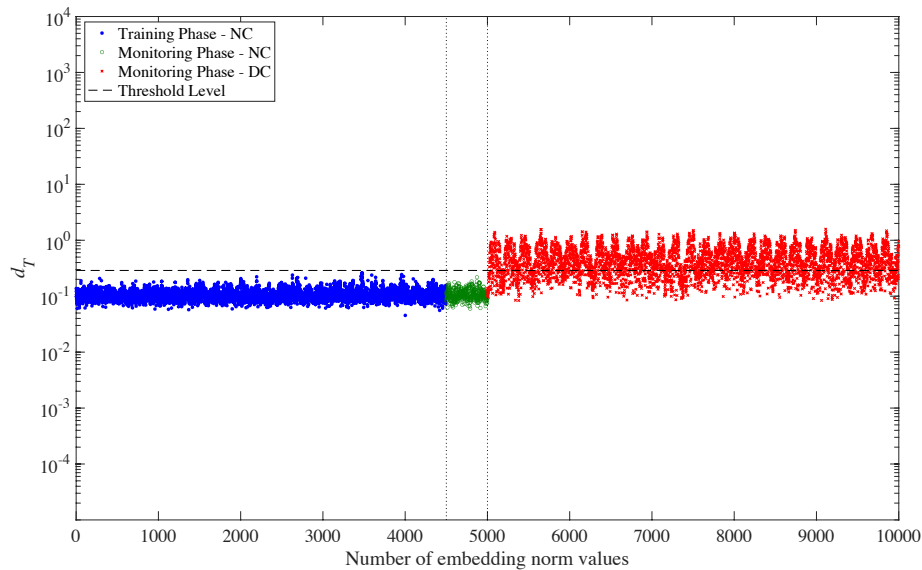
Figure 6.32: *Early damage detection of the numerical offshore jacket structure by the proposed RMDS-based method and the standard CI for damaged beam (Element 13).*
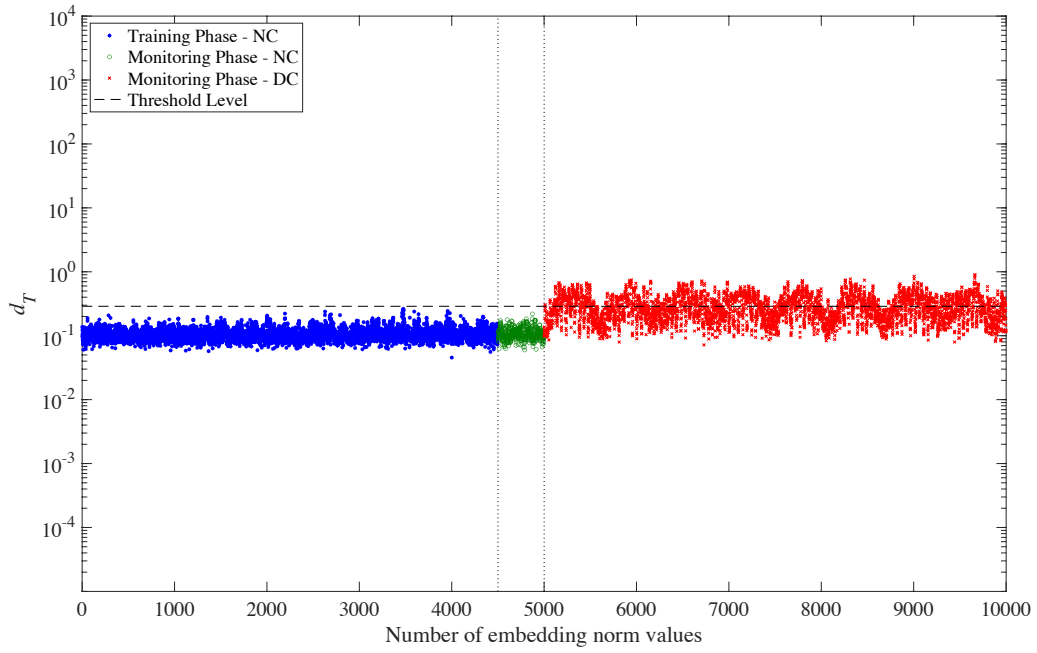
Figure 6.33: *Early damage detection of the numerical offshore jacket structure by the proposed RMDS-based method and the standard CI for damaged column (Element 23).*
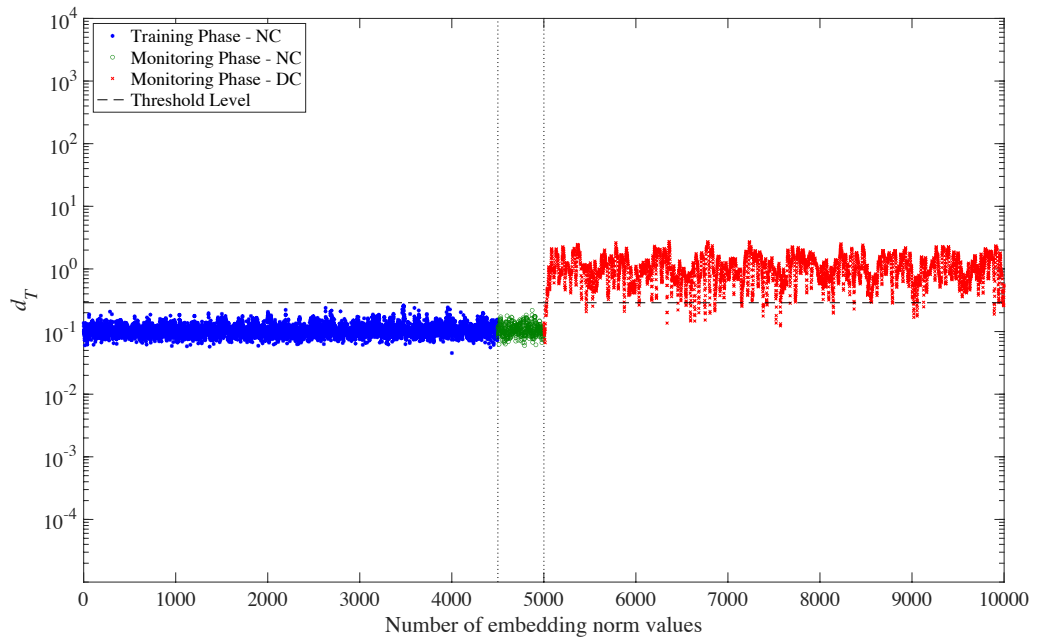
Figure 6.34: *Early damage detection of the numerical offshore jacket structure by the proposed RMDS-based method and the standard CI for damaged brace (Element 30).*
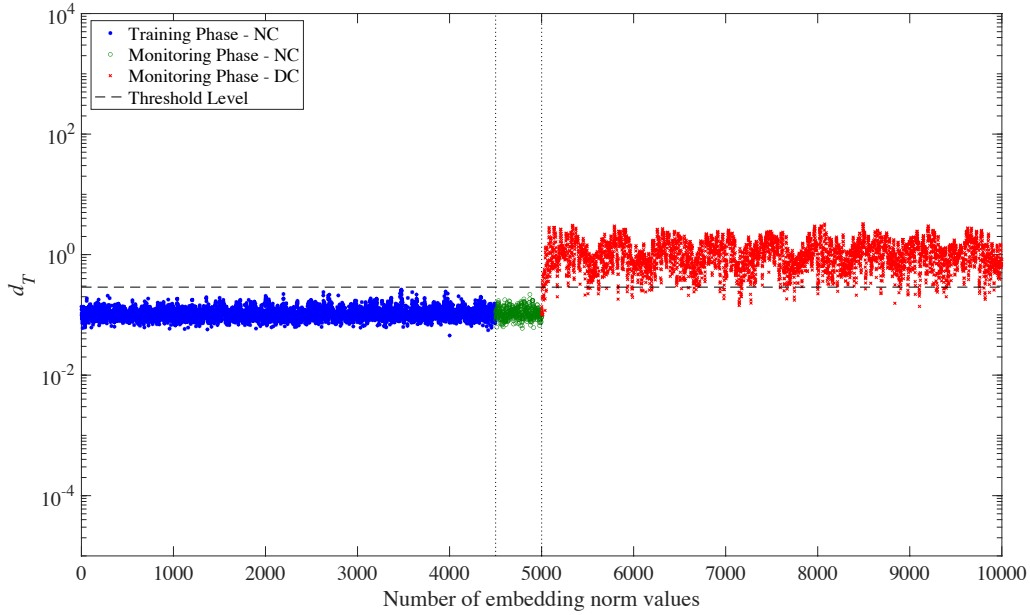
Figure 6.35: *Early damage detection of the numerical offshore jacket structure by the proposed RMDS-based method and the standard CI for all damaged scenarios together (Elements 13, 23 & 30).*

Table 6.13: *Numbers and percentages of Type I, Type II, and total errors in detecting damage for numerical offshore jacket structure.*

Case no.	Type I	Type II	Total
2	0(0%)	1591(31.82%)	1591(15.91%)
3	0(0%)	2852(57.04%)	2852(28.52%)
4	0(0%)	131(2.62%)	131(1.31%)
5	0(0%)	128(2.56%)	128(1.28%)

6.2.4 Conclusion

The novel data-driven method for SHM under ambient vibration and high-dimensional features explained in Chapter 4 was evaluated using the experimental datasets of the IASC-ASCE structure in Subsection 6.2.1, the Tianjin-Yonghe Bridge in Subsection 6.2.2, and the numerical offshore jacket structure in Subsection 6.2.3.

The proposed method has been developed from the RMDS algorithm and some computational approaches to deal with the main limitation of using high-dimensional DSFs for early damage detection. The process of feature extraction has been performed by ARMA modeling and the model residuals of the normal and damaged conditions have been extracted as the main DSFs. For accurately detecting damage without any false alarm, the EV theory has been used to determine a reliable threshold value. The shape of GEV distribution has also been considered to choose an appropriate EV distribution for the threshold limit determination.

The results have shown that the proposed RMDS-based method with the aid of the ARMA residuals and the EV theory is highly able to detect early damage without any false alarm error. It has been observed that the distribution of embedding norm val-

ues of the normal condition used in the threshold limit determination is not normal, in which case the standard CI based on the normality assumption suffers from numerous Type I errors. Therefore, it is recommended to utilize the EV statistics in the threshold limit determination when the outputs of the feature classification method regarding the undamaged condition are non-normal. The comparison between the proposed RMDS-based method and the well-known Mahalanobis distance has demonstrated that the former is superior to the latter in detecting small damage. Furthermore, the proposed RMDS-based method is more efficient than the Mahalanobis distance due to providing much fewer outputs for feature classification and decision-making.

6.3 Verification of Clustering-Based Novelty Detection Method

In order to validate the effectiveness and reliability of the proposed clustering-based method presented in Chapter 5, two examples including the well-known Z24 Bridge and an experimental offshore jacket platform are examined in this section.

6.3.1 Application to the Z24 Bridge

6.3.1.1 Bridge description

In this subsection, the accuracy and performance of the proposed methods are validated by the modal features of the Z24 Bridge [199]. Fig. 6.36(a)-(b) shows the general and close view of this bridge.
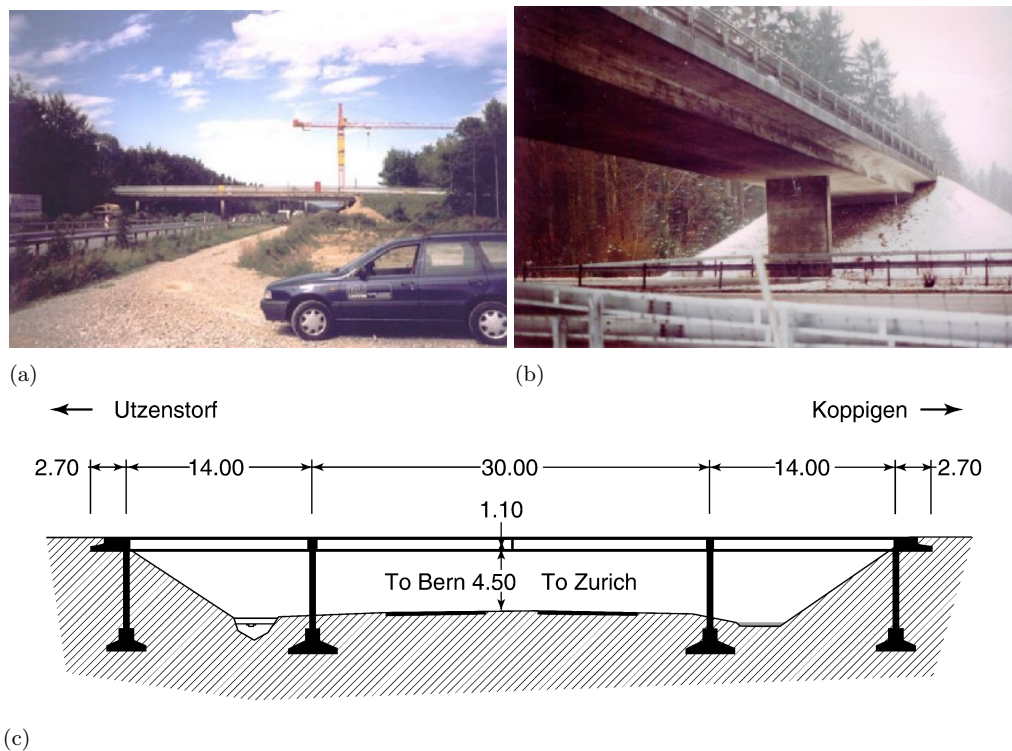
Figure 6.36: *(a) The general view of the Z24 Bridge, (b) the close view of the deck and one of the piers, (c) the longitudinal section.*

It was a classical post-tensioned concrete box-girder bridge located in Switzerland linking the villages of Koppigen and Utzenstorf as an $A1$ highway overpass between Bern and Zurich. The dimensions of the Z24 Bridge were the main span of 30 m and two side-spans of 14 m as shown in Fig. 6.36(c). In order to construct a new bridge with a larger side span, the Z24 Bridge was demolished at the end of 1998. Before the complete demolition, a long-term continuous monitoring test was performed to quantify the environmental variability components (e.g. temperature, wind characteristics, humidity, etc.) and acquire vibration data (acceleration time histories). Eventually, realistic damage patterns were gradually applied to the bridge in a controlled way during the month before complete demolition.

The modal features used in the process of early damage detection is a set of natural frequencies of four modes, which were obtained from the technique of frequency domain decomposition. This set consists of 3932 observations of the modal frequencies under varying actual environmental conditions. The first 3470 observations belong to the normal condition of the bridge and the last 462 observations are associated with the damaged state. Fig. 6.37 illustrates the natural frequencies of the Z24 Bridge in four modes. As can be seen, the obvious jumps in the modal frequencies of the normal condition are related to the changes in the asphalt layer in cold periods, which seriously affected the bridge stiffness and caused significant variations. In fact, these changes indicate high sensitivity of the measured natural frequencies to the environmental variability.
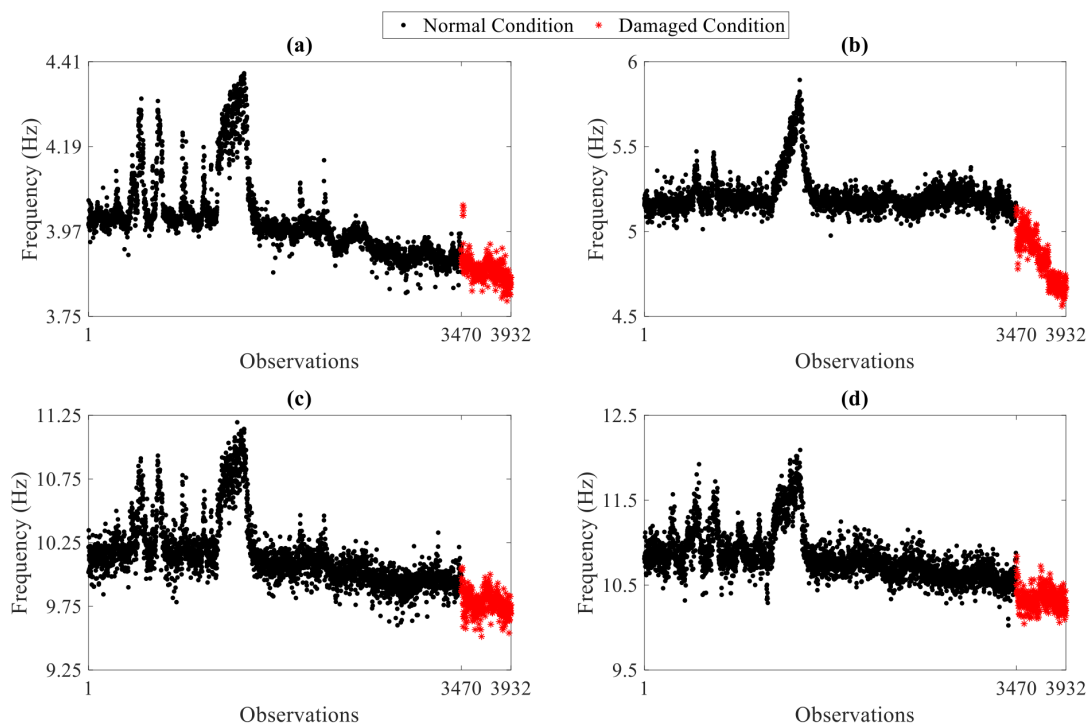
Figure 6.37: *The modal frequencies of the Z24 Bridge: (a) mode 1, (b) mode 2, (c) mode 3, (d) mode 4.*

Before detecting damage by the proposed clustering-based method, it is necessary to define the training and testing sets. On this basis, the training data consists of 90%

of the observations of the modal frequencies associated with the normal condition. In other words, it is a matrix with n observations and q variables, where $n = 3123$ and $q = 4$; that is, $\mathbf{X} = [\mathbf{x}_1, ..., \mathbf{x}_{3123}]$. On the other hand, the observations 3124-3470 (i.e. the remaining 10% of the modal frequencies of the normal condition), as well as the observations 3471-3932 regarding the damaged state, are applied to make the testing data, which is a matrix with 809 feature vectors ($m = 809$) and 4 variables; that is, $\mathbf{Z} = [\mathbf{z}_1, ..., \mathbf{z}_{809}]$.

6.3.1.2 Damage Detection

The first step of the proposed clustering-based method is to choose an $L_{p,r}$-distance measure or specify the amounts of p and r. Based on the definition of the $L_{p,r}$-distance measure, four metrics as the various values of the p and r are utilized to investigate different distance measures for early damage detection. These metrics are the Chebychev ($p = r = \infty$), Euclidean ($p = r = 2$), squared Euclidean ($p = 2$ and $r = 1$), and Manhattan ($p = r = 1$). However, the results of damage detection obtained from the Chebychev metric are illustrated due to its better performance than the other metrics. As mentioned, the measured modal frequencies of the Z24 Bridge, which are used as the main features for damage detection, are highly sensitive to the environmental variability. Based on the underlying idea of the proposed clustering-based method, one needs to deal with this problem by choosing an appropriate cluster number. According to the proposed cluster selection approach, 1500 sample clusters (K_{max}) are employed to incorporate into the algorithm of the *k*-medoids clustering and obtain 1500 variance amounts from 1500 sets of the DI values. Note that the calculated DI quantities are only related to the normal condition in the baseline phase. Fig. 6.38(a) indicates the 1500 variances of the DI sets, where the smallest variance amount is found at the 992nd cluster. In other words, one can realize that the most proper number of clusters for addressing the influences of the environmental variations is identical to 992. Using this number, the *k*-medoids algorithm yields the cluster sets $\mathbf{c}_1, ..., \mathbf{c}_{992}$, which are used to determine the DI values in the baseline and monitoring phases for obtaining the vectors $\mathbf{d_b}$ and $\mathbf{d_m}$.
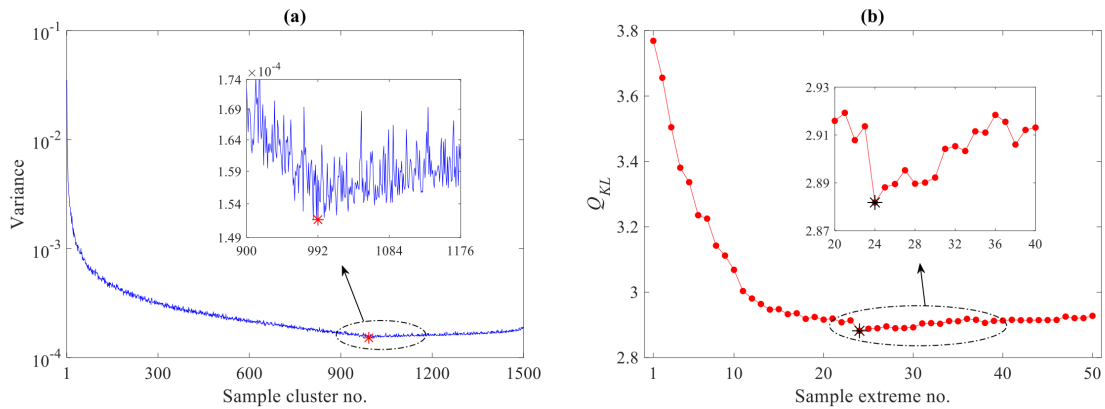
Figure 6.38: *(a) Determination of a proper cluster number for dealing with the environmental variability by the proposed cluster selection approach, (b) the values of Q_{KL} for choosing the most proper extreme samples.*

Having considered the vector $\mathbf{d_b} = [DI_1, ..., DI_{3123}]$, the proposed GOF method is applied to estimate an alarming threshold. Based on Fig. 5.2, the DI values of the vector $\mathbf{d_b}$ are arranged in descending order. The sample extreme number S and the variable h are set as 50 and 1560, respectively. Once, again, it should be clarified here that the variable h is the upper bound of $n/2$; that is, $h = \frac{n}{2} - 1$. In the problem of the Z24 Bridge, the number of training samples (n) is equal to 3123, in which case the upper bound of h corresponds to 1560.5. As described previously, the variable h should be a positive integer. Since the calculated value of h is not an integer, one should round it to 1560. Using the statistic of the Kullback-Leibler information, subsequently, one can obtain a set of 50 amounts of Q_{KL} as can be observed in Fig. 6.38(b). Considering that the optimal extreme number (s) is one that has provides the smallest Q_{KL} value, it is discerned in Fig. 6.38(b) that the proper value of s is equal to 24. Subsequently, the first 24 arranged DI values (i.e. $\hat{y}_1, ..., \hat{y}_{24}$, where $\hat{y}_1 = DI_{max}$) are extracted to fit a GEV distribution to these extreme samples. The shape (β), scale (σ), and location (μ) of this distribution estimated by the MLE technique are equal to 0.2793, 0.0035, and 0.0542, respectively. Under the 5% significance level ($\alpha = 0.05$), the alarming threshold τ_α is computed by Eq. (5.11), which corresponds to 0.0704.
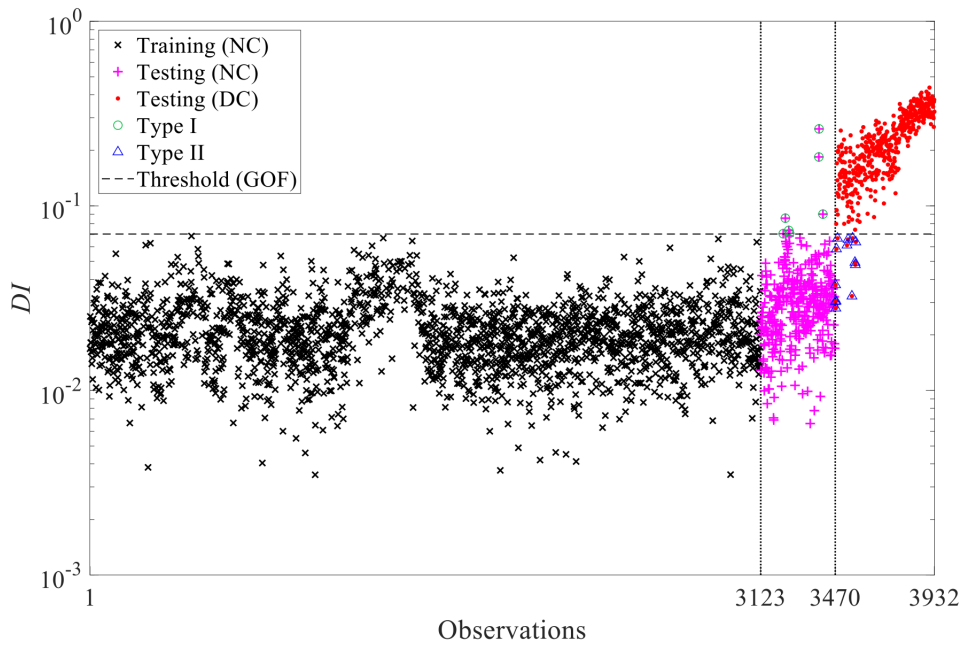
Figure 6.39: *Early damage detection by the proposed clustering-based method using the Chebychev metric as the $L_{p,r}$-distance measure and GOF for the threshold estimation (NC: Normal Condition, DC: Damaged Condition).*

Fig. 6.39 shows the result of early damage detection in the Z24 Bridge using the Chebychev distance metric, where the horizontal dashed line is indicative of the threshold limit gained by the proposed GOF method. From Fig. 6.39, it is clear that no DI values of the observations 1-3123 (i.e. the training samples) exceed the threshold limit indicating the good performance of the proposed GOF method in estimating a proper threshold without any false alarm in the baseline phase. Moreover, most of the DI

values of the observations 3124-3470, which are used in the monitoring stage and treat as the validation samples, fall below the threshold limit and roughly have the same DI quantities as the training observations. In contrast, the majority of the DI values of the damaged state related to the observations 3471-3923 are over the threshold, which these outputs accurately imply the occurrence of damage. Therefore, one can conclude that the proposed clustering-based method in conjunction with the proposed GOF approach is successful in detecting damage even under the strong and nonlinear environmental variations. Regardless of the alarming threshold, it is perceived that there are clear differences between the DI values of the normal and damaged conditions. This conclusion also proves the high damaged detectability of the Chebychev distance metric.

6.3.1.3 Comparisons

In order to demonstrate the superiority of the proposed clustering-based method, it is compared with the classical clustering-based technique as discussed in Subsection 5.1.2. Although both the classical and proposed methods utilize the *k*-medoids clustering algorithm, their differences pertain to the number of clusters used in this algorithm. For the classical technique, the number of clusters is determined by the conventional Silhouette value technique. In this regard, 30 sample clusters are considered to calculate their Silhouette values as shown in Fig. 6.40(a). The most suitable cluster number is one that provides the largest Silhouette value. From this figure, it is apparent that the mentioned cluster number is identical to 2. Without considering any threshold limit, Fig. 6.40(b) indicates the result of early damage detection by the classical clustering-based technique using the Chebychev metric as the $L_{p,r}$-distance measure. It can be observed that the DI amounts of many observations of the normal condition are larger than the maximum DI value of the damaged state.This result indicates the poor performance and low damage detectability of the classical clustering-based technique. Moreover, one can realize that although the proposed clustering-based method is able to address the effects of the environmental variability and increase the detectability of damage, the classical technique fails in providing reliable results. This conclusion also confirms the accuracy of the idea behind the proposed approach to selecting an appropriate cluster number with the smallest variance.

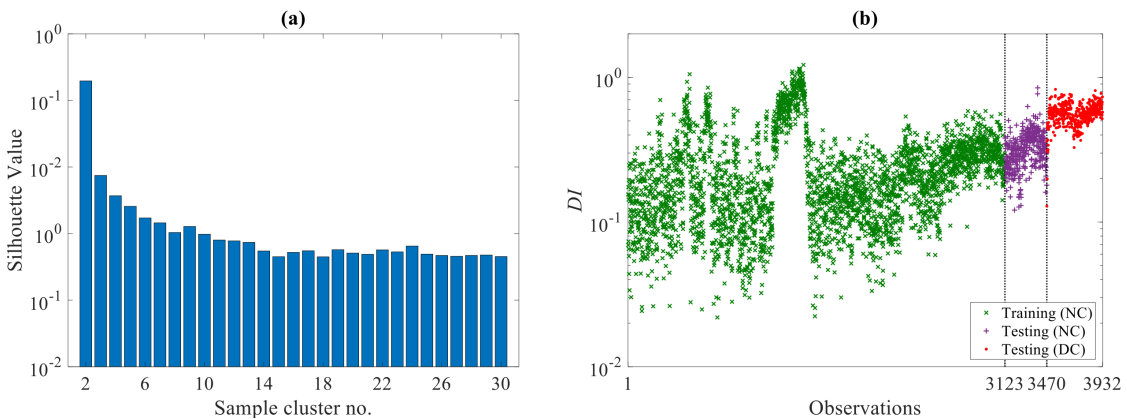**Figure 6.40:** *(a) Determination of the number of clusters for the k-medoids clustering by the Silhouette value, (b) Early damage detection by the classical clustering-based method using the Chebychev metric as the $L_{p,r}$-distance measure (NC: Normal Condition, DC: Damaged Condition).*

In the following, the distance metrics Chebychev, Euclidean, squared Euclidean, and Manhattan are compared to investigate their performances in detecting damage. This comparative study is based on evaluating the numbers and percentages of Type I, Type II, and total (misclassification) errors as presented in Table 6.14. As can be seen, the best performance in terms of the smallest misclassification rate is related to the Chebychev distance metric. Conversely, both the Euclidean and the Manhattan metrics have the worst performances in the misclassification rate. Note that the Euclidean distance is a widely used metric in most of the clustering-based damage detection methods. Although the squared Euclidean distance has the smallest Type I error, it suffers from a relatively large Type II error. On the other hand, the range of Type I errors in the distance metrics is approximately similar. Accordingly, it can be concluded that the Chebychev distance outperforms the other metrics, particularly in the total error.

Table 6.14: *Numbers and percentages of Type I, Type II, and total errors in detecting damage by different distance metrics using GOF for the threshold estimation.*

Distance metrics	Type I	Type II	Total
Chebychev	7(0.20%)	13(2.81%)	20(0.51%)
Euclidean	11(0.31%)	19(4.11%)	30(0.76%)
Squared Euclidean	4(0.11%)	24(5.19%)	28(0.71%)
Manhattan	6(0.17%)	24(5.19%)	30(0.76%)

The other comparative study is concerned with the evaluation of the performances of the threshold estimation techniques. For this purpose, the misclassification rate (total error) in detecting damage based on the proposed clustering-based approach is applied to compare GOF, BM, and POT. Because the selections of an adequate block number for the BM method and an optimal threshold for choosing sufficient exceedances in the POT technique are critical issues, various block and exceedance numbers are utilized to compute different misclassification errors for these techniques. Fig. 6.41 illustrates the rates of misclassification between GOF vs. BM and GOF vs. POT. In this comparison, the significance level is equal toset at 0.05. An obvious indication in this figure is that the proposed GOF method possesses a smaller misclassification rate than the BM and POT techniques in all sample blocks and exceedances. This conclusion, thus, proves the superiority of the proposed GOF method over the mentioned conventional techniques.

In all the previous results, the process of early damage detection has been implemented by using 90% of the modal frequencies regarding the normal condition in an effort to make the feature vectors of training data with 3123 observations. As the other comparison, the percentage for obtaining the training matrix is reduced to assess the effect of small training samples on the performance of the proposed clustering-based method. Accordingly, two different percentages including 75% and 60% are considered to define new training matrices with 2602 and 2082 observations. Under such circumstances, the remaining 25% and 40% of the modal frequencies of the normal condition and all modal frequencies of the damaged state are utilized to make two testing datasets. Having implemented all the steps of the proposed clustering-based method using the Chebychev distance metric and GOF approach for the threshold estimation, Fig. 6.42 shows the results of damage detection under the reduced training samples.

In addition, Table 6.15 lists the numbers and percentages of Type I, Type II, and total errors in detecting damage using the reduced training samples. As can be ob-
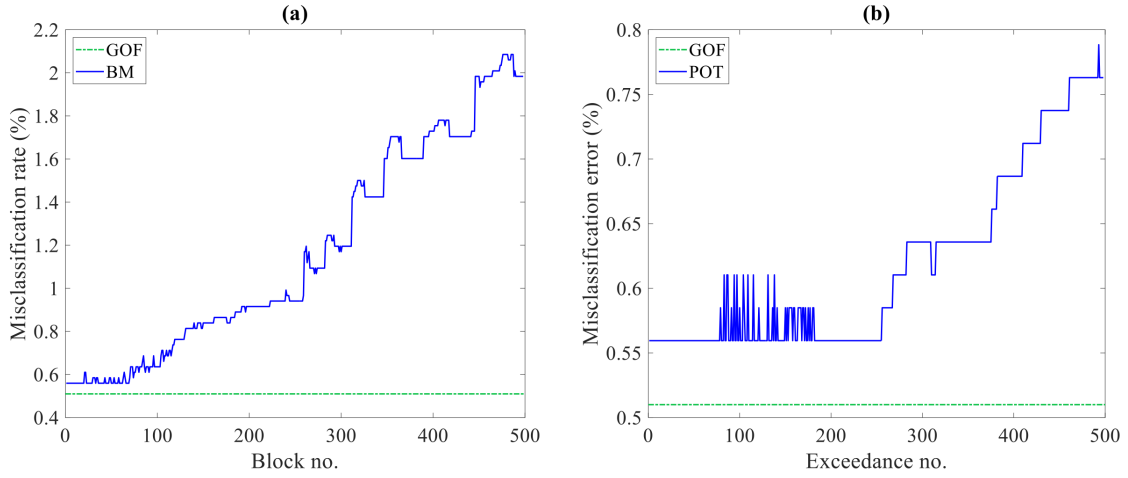
Figure 6.41: *Comparison of the threshold estimation methods in terms of the misclassification error (a) GOF vs. BM, (b) GOF vs. POT.*
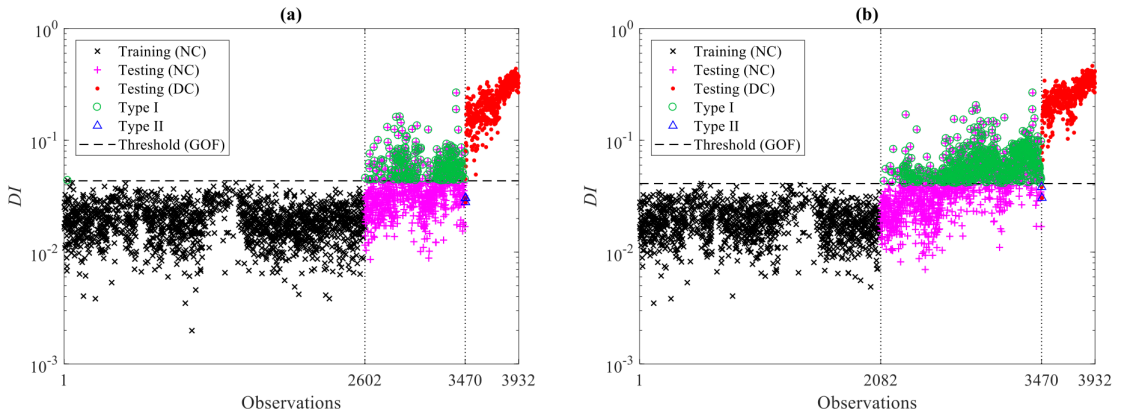
Figure 6.42: *Early damage detection by the proposed clustering-based method using the Chebychev metric as the $L_{p,r}$-distance measure and GOF for the threshold estimation under reduced training samples: (a) 75%, (b) 60%.*

served, all DI values of the training data are below the threshold limits. This confirms the reliability of the proposed GOF method in yielding an appropriate threshold limit even under reduced training samples. However, there are numerous false alarms in the validation samples (i.e. the remaining 25% and 40% of the observations of the modal frequencies associated with the normal condition). It can be seen that the rate of Type I error increases by decreasing the training samples.

Table 6.15: *Numbers and percentages of Type I, Type II, and total errors in detecting damage by the proposed method using the Chebychev metric and GOF under different training samples.*

Percentage of training samples	Type I	Type II	Total
90	7(0.20%)	13(2.81%)	20(0.51%)
75	301(8.67%)	3(0.64%)	304(7.73%)
60	748(21.55%)	2(0.43%)	750(19.07%)

From Table 6.15, it is obvious that the use of 60% training samples causes the worst

performance in terms of Type I error. Although this percentage reduces Type II error, it suffers from high misclassification rate. The same conclusion is observable when using the 75% of training samples. In fact, as the size (percentage) of training samples reduces, the misclassification rate and false alarm error increase as well. Despite the high damage detectability of the proposed clustering-based method, one can conclude that the use of adequate training samples is a significant issue and it is necessary to capture a wide range of environmental variations in the baseline phase.

In order to evaluate the performance of the proposed clustering-based method without using all available data in the training phase, limited amounts of the modal frequencies regarding the normal condition are considered in two scenarios [146]. First, one supposes that there are smaller observations of the normal condition for the training procedure than the main problem. On this basis, it is assumed that the first 1735 observations of the modal frequencies are only available instead of utilizing all 3470 samples. Taking the 90% of 1735 observations of the normal condition, the new training matrix consists of 1561 feature vectors; that is, $\mathbf{X} \in \Re^{4\times1561}$. Moreover, the observations 1562-1735, which serve as the validation samples, and all modal frequencies of the damaged state (the same 462 observations) are used to make the new testing matrix $\mathbf{Z} \in \Re^{4\times636}$.

Second, the daily observations of the normal and damaged states are incorporated to define new small training and testing matrices. Accordingly, the number of observations of the modal frequencies decreases to 235, where the observations 1-198 belong to the normal condition and the observations 199-235 are associated with the damaged state [146]. Hence, the training matrix is obtained from 90% of the daily observations of the modal frequencies concerning the normal condition; that is, $\mathbf{X} \in \Re^{4\times178}$. On the other hand, the remaining 10% of the daily observations of the normal condition, which serve as the validation samples, along with all daily observations of the damaged state are gathered to generate the testing matrix $\mathbf{Z} \in \Re^{4\times57}$. The results of early damage detection by the proposed clustering-based method, the Chebychev distance metric, and GOF approach under the above-mentioned scenarios are shown in Fig. 6.43. It needs to clarify that the optimal cluster numbers regarding the first and second scenarios are equal to 305 and 28, respectively.

As can be observed in Fig. 6.43(a) regarding the reduced version of the normal feature samples, most of the DI values in the observations 1-1735 fall below the threshold limit, except for only one point (Type I) among 174 validation samples. On the other hand, one can discern that the majority of the DI quantities of the damaged state exceed the threshold limit indicting accurate damage detection. However, the only three points (Type II) among 462 samples are under the threshold. The same conclusions with the different and small rates of Type I and Type II errors can be seen in Fig. 6.43(b) concerning the daily samples. Therefore, one can conclude that the proposed clustering-based method with the aids of the Chebychev distance metric and GOF approach is successful in accurately detecting damage using the small and daily feature samples.

To evaluate the performance of the Chebychev distance and compare it with the other statistical measures, Table 6.16 lists the numbers and percentages of Type I, Type II, and total errors in the first and second scenarios. In the first scenario, one can realize that the Chebychev distance still outperforms the other metrics in terms of all three errors.

(a)

(b)
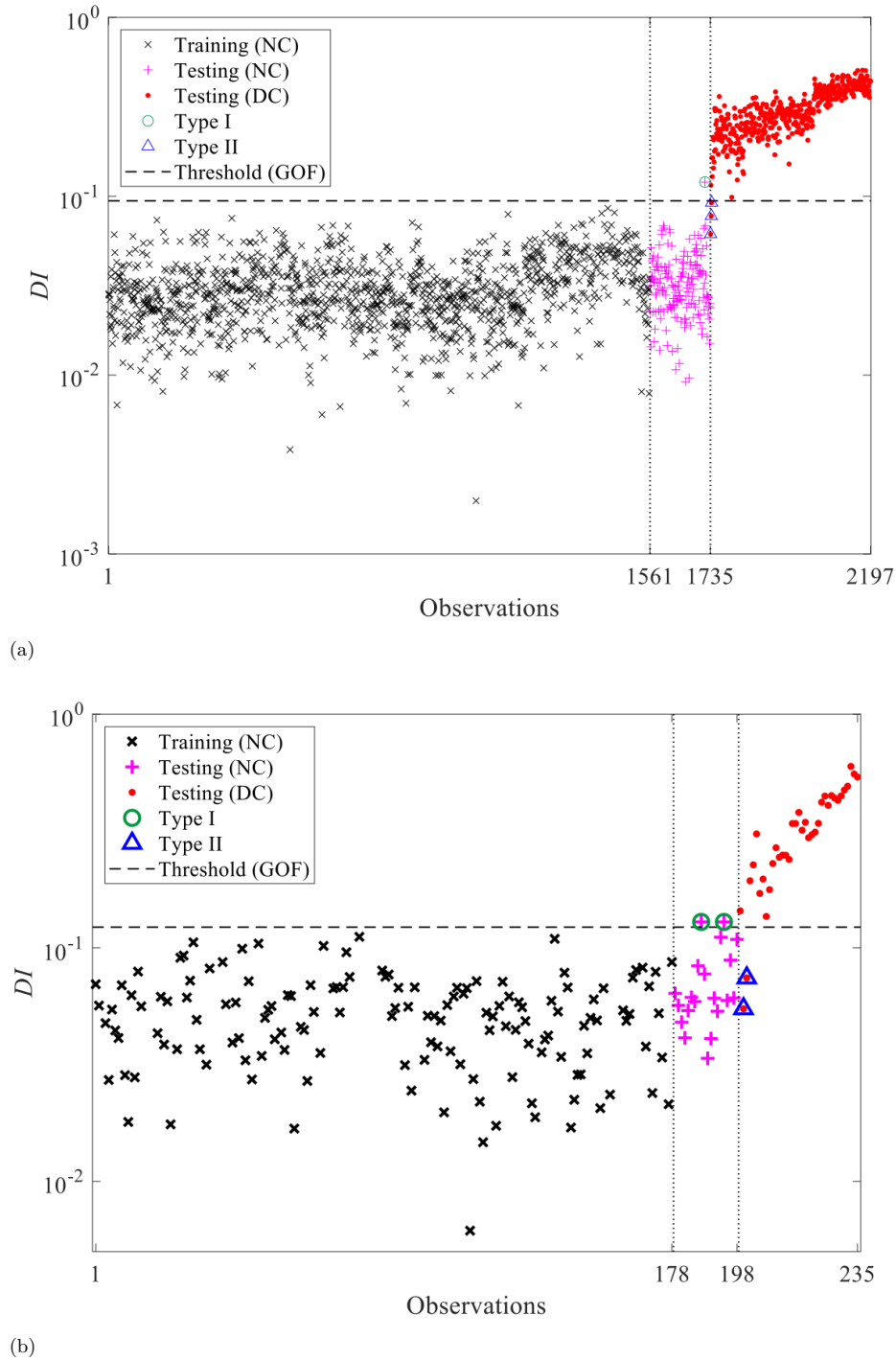
Figure 6.43: *Early damage detection by the proposed clustering-based method and GOF: (a) the small samples of the normal condition, (b) the daily samples.*

Moreover, the error rates of the Euclidean, Squared Euclidean, and Manhattan are close to each other. In the second scenario, the amounts in Table 6.16 reveal that all statistical divergence measures approximately have the same performances. The comparison

89

between the error rates in Table 6.14 and Table 6.16 demonstrates that the divergence measures roughly yield similar results when the number of feature samples is small (e.g. the second scenario regarding the daily samples). Nonetheless, the Chebychev distance outperforms the other measures when there are relatively large samples.

Table 6.16: *Numbers and percentages of Type I, Type II, and total errors in detecting damage by different distance metrics and GOF using the small and daily feature samples.*

Distance metrics	Small samples			Daily samples		
	Type I	Type II	Total	Type I	Type II	Total
Chebychev	1(0.06%)	3(0.64%)	4(0.18%)	2(1.01%)	2(5.40%)	4(1.70%)
Euclidean	4(0.23%)	5(1.08%)	9(0.18%)	2(1.01%)	3(8.10%)	5(2.12%)
Squared Euclidean	1(0.06%)	8(1.73%)	9(0.18%)	2(1.01%)	2(5.40%)	4(1.70%)
Manhattan	3(0.23%)	7(1.51%)	10(2.16%)	3(1.51%)	3(8.10%)	6(2.55%)

All the previous results have been based on the *k*-medoids clustering. In the context of SHM by machine learning, there are other widely-used techniques, which have broadly been applied to detect damage. On this basis, the final comparison is carried out by evaluating the performance of the proposed method by the well-known MSD [146, 200] and PCA [180] in terms of damage detectability without considering any alarming threshold. For this comparison, the training and testing data sets are based on the main problem (i.e. $\mathbf{X} \in \Re^{4 \times 3123}$ and $\mathbf{Z} \in \Re^{4 \times 809}$). Fig. 6.44 illustrates the results of early damage detection by the above-mentioned conventional techniques, where DI_m and DI_p refer to the outputs of the MSD and PCA. Note that the number of principal components required for the PCA-based damage detection method is equal to 2. This number has been determined by using the average eigenvalue criterion or Kaiser's criterion [200]. From Fig. 6.44(a) and Fig. 6.44(b) regarding the MSD and PCA methods, respectively, one can observe that the sudden jump in the distance values of the normal condition is still available. Moreover, some distance values of the normal condition are equal or larger than the corresponding values associated with the damaged state. These conclusions demonstrate the serious influence of environmental variability and poor performances of the conventional MSD and PCA methods for early damage detection.
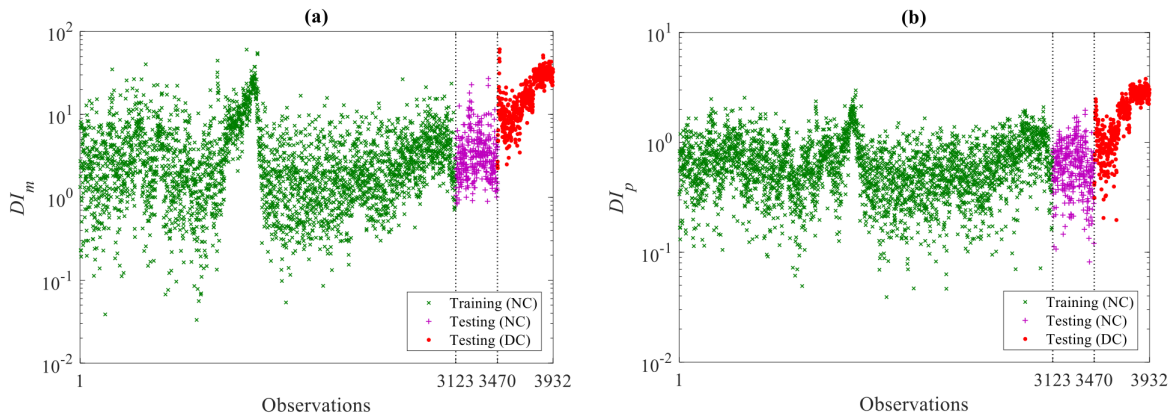
Figure 6.44: *Early damage detection without threshold values (NC: Normal Condition, DC: Damaged Condition): (a) MSD, (b) PCA.*

6.3.2 Application to the Experimental Offshore Jacket Platform

The tested structure is a laboratory jacket-type offshore platform which is inspired by the real offshore jacket platform located in Persian Gulf. The platform includes four main legs, horizontal and diagonal bracing members, as shown in Fig. 6.45. The platform was made by welded-aluminum pipes which were welded to the top aluminum plate as the deck of jacket. The main legs have pipe cross-section with outer-diameter of 22 mm and 3.5 mm thickness, while bracing members have 15.8 mm outer-diameter and 2 mm thickness. The deck is an aluminum plate of 2 mm and Young modulus is 67 GPa for all members. The effects of environmental and operational variability are investigated by adding mass on the deck of Jacket Platform. Several damage scenarios are simulated in the tests. The damage scenarios are including single damage case and double damage cases as listed in Table 6.17. In order to induce damage in the platform some bracing members are removable as shown in Fig 6.45. Additionally, the location of damaged elements are highlighted in Fig 6.46.

Figure 6.45: *The overall view of the experimental offshore jacket platform.*

Figs. 6.47 and 6.48 depict the results of early damage detection in the experimental offshore jacket platform using the Chebychev distance metric for damage scenarios 4 and 5 respectively, where the horizontal dashed line is indicative of the threshold limit gained by the standard CI method. From Figs. 6.47 and 6.48, it is clear that no DI
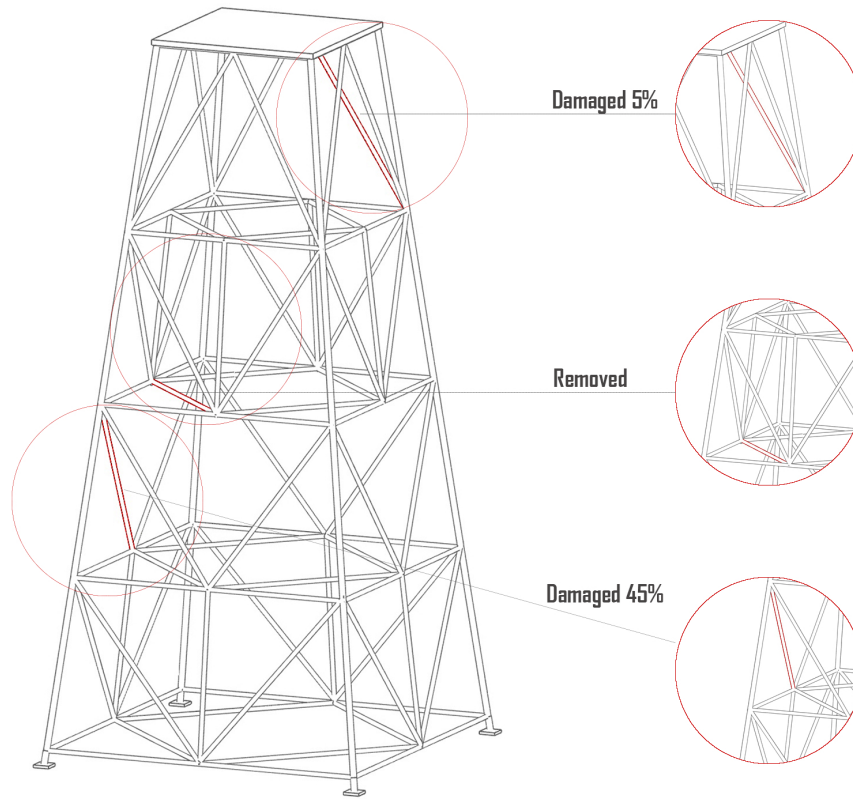
Figure 6.46: *The locations of the damaged members of the experimental offshore jacket platform.*

Table 6.17: *The undamaged and damaged conditions of the experimental offshore jacket platform.*

Case no.	Structural Condition	Description
1	Undamaged	Baseline
2	Undamaged	Baseline + Added 40 kg on deck
3	Undamaged	Baseline + Added 80 kg on deck
4	Damaged	Removing horizontal member in 3rd level + Added 80 kg on deck
5	Damaged	Inducing 5% damage in diagonal member of 5th level and 45% damage in diagonal member of 3rd level + Added 80 kg on deck

values of the observations 1-9000 (i.e. the training samples) exceed the threshold limit indicating the good performance of the proposed clustering-based method without any false alarm in the baseline phase. Moreover, most of the DI values of the observations 9001-10000, which are used in the monitoring stage and treat as the validation samples, fall below the threshold limit. In contrast, the majority of the DI values of the damaged state related to the observations 1001-20000 are over the threshold, which these outputs accurately imply the occurrence of damage. Therefore, one can conclude that the proposed clustering-based method is successful in detecting damage in the offshore jacket structures. In addition, the number and percentages of Type I, Type II, and total errors for experimental offshore jacket structure are listed in Table 6.18.
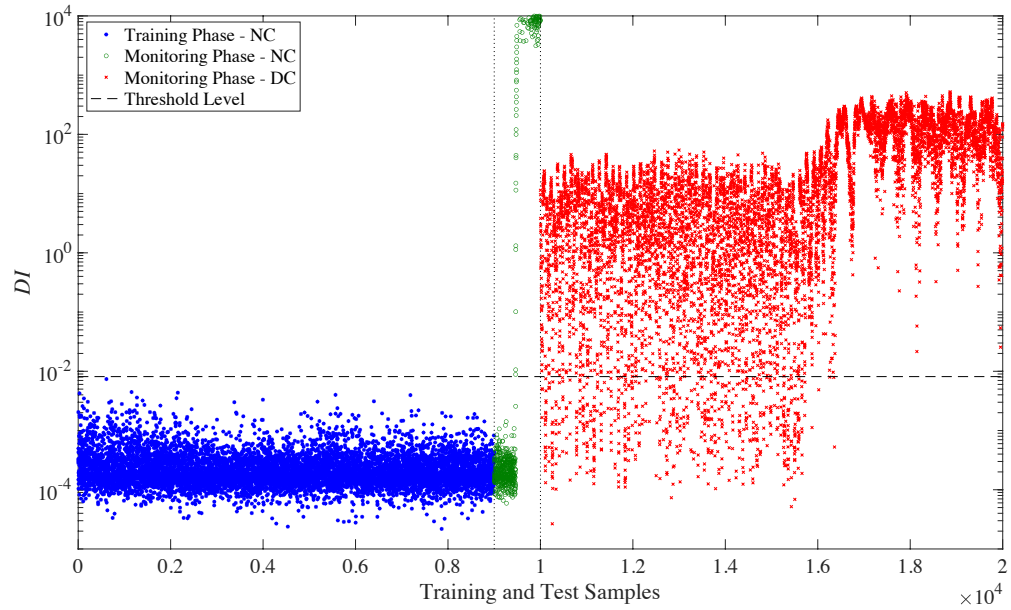
(a)
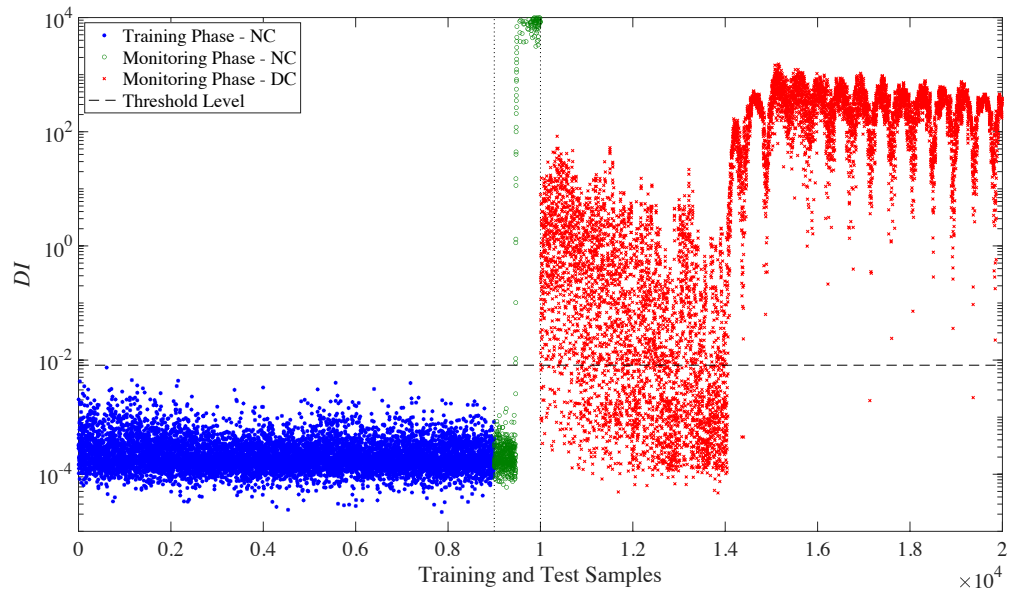
(b)

Figure 6.47: *Early damage detection by the proposed clustering-based method using the Chebychev metric as the $L_{p,r}$-distance measure and standard CI for the threshold estimation (NC: Normal Condition, DC: Damaged Condition) for damage case no. 4. a) measurement no. 1 b) measurement no. 15*

93
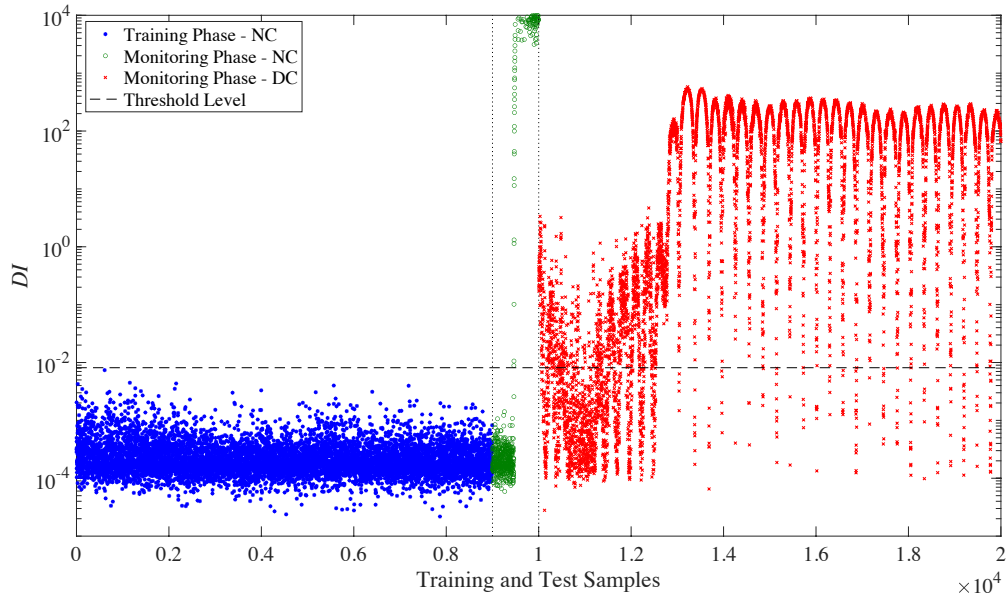
(a)
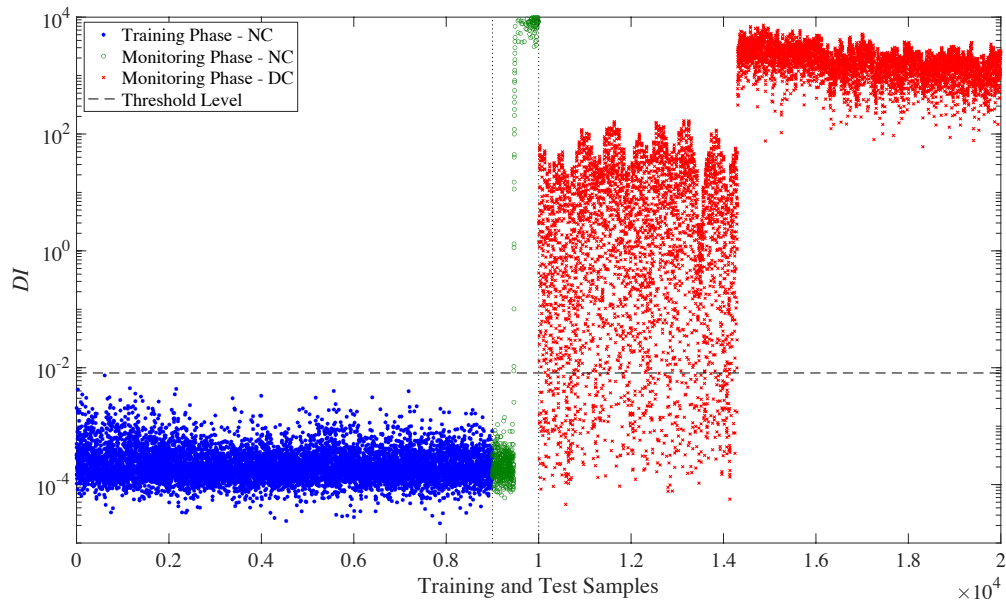
(b)

Figure 6.48: *Early damage detection by the proposed clustering-based method using the Chebychev metric as the $L_{p,r}$-distance measure and standard CI for the threshold estimation (NC: Normal Condition, DC: Damaged Condition) for damage case no. 5. a) measurement no. 1 b) measurement no. 15*

6.3.3 Conclusion

The new clustering and threshold estimation methods presented in Chapter 5 was verified by utilizing the modal frequencies of the well-known Z24 Bridge in Subsection

Table 6.18: *Numbers and percentages of Type I, Type II, and total errors in detecting damage for experimental offshore jacket structure.*

Case no.	Type I	Type II	Total
4 (measurement no. 1)	537(5.37%)	656(6.52%)	1193(5.965%)
4 (measurement no. 15)	537(5.37%)	1480(14.80%)	2017(10.085%)
5 (measurement no. 1)	537(5.37%)	1476(14.76%)	2013(10.065%)
5 (measurement no. 15)	537(5.37%)	1276(12.76%)	1813(9.065%)

6.3.1 and acceleration data of the experimental offshore jacket platform in Subsection 6.3.2. The proposed clustering-based method has been developed from the k-medoids algorithm with a new approach to select an appropriate cluster number for dealing with the effects of environmental variations. To increase the detectability of damage, this study has presented the application of the $L_{p,r}$-distance metric to the algorithm of the k-medoids clustering. A novel threshold estimation method called GOF based on the EVT and GEV distribution modeling has also been proposed to define a reliable alarming threshold for early damage detection.

The results demonstrated that the proposed clustering-based method in conjunction with the proposed GOF approach highly succeeds in detecting damage under strong environmental variations. This conclusion is also valid for the scenarios of using the small and daily feature samples for early damage detection. The comparison among different $L_{p,r}$-distance measures has indicated that the Chebychev metric outperforms the other distance measures, particularly the Euclidean and squared Euclidean distances, which are widely used in the clustering-based damage detection techniques. When the size of feature samples is small, it has been demonstrated that the statistical distances roughly have the same performances in terms of the rates of Type I, Type II, and total errors. It has been observed that the k-medoids clustering with a relatively large cluster number, which yields the smallest rate of variance, is able to deal with the negative effects of environmental variability conditions and increase the detectability of damage. The comparison between the proposed and classical clustering-based methods by considering the k-medoids algorithm and the Chebychev distance metric has revealed that the former prevails over the latter. Furthermore, the proposed clustering-based method has been superior to the conventional MSD and PCA techniques in terms of damage detectability and SHM under strong environmental variability.

Furthermore, the comparisons between the proposed GOF method and the conventional BM and POT techniques have demonstrated that GOF not only facilitates the process of threshold estimation but also provides more reliable results owing to a smaller misclassification rate compared to the other techniques. Eventually, it has been seen that the use of small training samples considerably increases the false alarms and misclassification rates. This conveys that the proposed clustering-based method is sensitive to the number of samples needed for the training process. Therefore, it is preferable to apply a wide range of training samples that cover all possible environmental variability conditions in the baseline phase. For further research, it is recommended to develop an algorithm to determine the adequate number of training samples.

Conclusions and Further Development

T HE research presented in this dissertation focused on the application of statistical pattern recognition paradigm in order to address some issues in SHM. Due to the complexity and cost of conventional inspection and maintenance methods, the offshore environment provides a challenging and fruitful field in which to implement SHM approaches. In this chapter the main contribution of this dissertation and obtained results are summarized. Furthermore, some interesting topics for further investigation which will motivate future work in this area are presented.

The main challenge of many methods in the statistical pattern recognition paradigm is to assess damage identification process when environmental and operational variability (EOV) are present. Hence, in this dissertation a damage identification process by proposing an iterative feature extraction technique using time series modeling and some machine learning methods for dealing with the EOV conditions is proposed. The proposed iterative technique is to identify the most consistent time series model with raw vibration time-domain data based on Box-Jenkins methodology. Moreover, the proposed technique aims at fitting a model that is able to produce uncorrelated residuals.

Dealing with the problem of large volumes of high-dimensional features and detecting damage under ambient vibration are critical to structural health monitoring. To address these challenges, this dissertation proposes a novel data-driven method for early damage detection of civil engineering structures by robust multidimensional scaling. The proposed method consists of some simple but effective computational parts including a segmentation process, a pairwise distance calculation, an iterative algorithm regarding robust multidimensional scaling, a matrix vectorization procedure, and a Euclidean norm computation. AutoRegressive Moving Average models are fitted to vibration time-domain responses caused by ambient excitations to extract the model

residuals as high-dimensional features. In order to increase the reliability of damage detection and avoid any false alarm, the extreme value theory is considered to determine a reliable threshold limit. However, the selection of an appropriate extreme value distribution is crucial and troublesome. To cope with this limitation, this study introduces the generalized extreme value distribution and its shape parameter for choosing the best extreme value model among Gumbel, Fréchet, and Weibull distributions.

In addition, environmental variability is a major challenging issue in structural health monitoring of offshore structures and bridges because these structures are more prone to such variability than other civil structures. To deal with this challenge, this dissertation proposes a new machine learning method for early damage detection under environmental variability by means of the *k*-medoids clustering, a new damage indicator, and an innovative approach for selecting a proper cluster number. Estimation of a reliable alarming threshold is another important challenge for early damage detection via most of the machine learning methods. On this basis, a novel probabilistic approach by using the theory of extreme value and a goodness-of-fit measure is proposed to estimate an alarming threshold.

Lastly, two numerical examples, three experimental benchmark structures, and two real structures were investigated to validate the effectiveness and performance of the above-mentioned approaches along with several comparative studies.

7.1 Overall Summary

According to the results of implementing the iterative feature extraction technique based on time series modeling to the numerical model of the concrete beam and the benchmark model of the laboratory frame one can conclude that the method was able to identify the best time series model for the raw vibration time-domain data according to Box-Jenkins methodology and choose an optimal order for the identified model to produce uncorrelated residuals. Moreover, The results of machine learning technique indicated that they are capable of identifying any possible damage, even in the presence of the operational and environmental variability. Furthermore, they are appropriately able to estimate the extent of damage in the structures.

The application of the proposed robust multidimensional scaling algorithm on the IASC-ASCE benchmark structure, the Tianjin-Yonghe Bridge, and the numerical offshore jacket structure demonstrated the ability of method to detect early damage without any false alarm error. In addition, it has been found that the distribution of embedding norm values of the normal condition utilized in threshold limit estimation is not normal, and resulting in numerous Type I errors in the standard CI based on the normality assumption. As a result, it is advisable to use the EV statistics in the threshold limit estimation when the outputs of the feature classification method regarding the undamaged condition are non-normal. Furthermore, the comparison between the proposed RMDS-based method and the Mahalanobis distance has shown that the former is superior to the latter in detecting small damage. Besides, the proposed RMDS-based method is more efficient than the Mahalanobis distance due to providing much fewer outputs for feature classification and decision-making.

Finally, the proposed clustering and threshold estimation methods were applied to the well-known Z24 Bridge and the experimental offshore jacket platform. The clus-

tering technique was developed from the k-medoids algorithm to select an appropriate cluster number for dealing with the effects of environmental variations. However, in order to increase the detectability of damage, the application of the $L_{p,r}$-distance metric to the algorithm of the k-medoids clustering, and a reliable alarming threshold for early damage detection using GOF based on the EVT and GEV distribution modeling was proposed. The results confirmed that clustering-based method in conjunction with the proposed GOF method highly succeeds in detecting damage under strong environmental variations. According to the comparison of different $L_{p,r}$-distance measurements, it is shown that Chebychev metric outperforms the other $L_{p,r}$-distance measures. Additionally, when the size of feature samples is small, it was demonstrated that the statistical distances roughly have the same performances in terms of the rates of Type I, Type II, and total errors. Moreover, it can be observed that the use of small training samples considerably increases the false alarms and misclassification rates.

7.2 Recommendations for Further Research

In this section some suggestions for future works are presented as follow:

- Since the use of small training samples considerably increases the false alarms and misclassification rates. Therefore, it is preferable to apply a wide range of training samples that cover all possible environmental variability conditions in the baseline phase. Hence, for further research, it is recommended to develop an algorithm to determine the adequate number of training samples.

- The statistical correlation-based methods between extracted damage-sensitive features are not only able to detect early damage by high-dimensional features but also capable of estimating the level of damage severity.

- As sensor placement has an important role in the damage localization process, therefore, it is recommended to pay more attention to the problem of sensor placement in the damage localization process.

- Based on the statistical similarity method, the sensor location from dense sensor networks regarding the largest value that exceeds the threshold limit is identified as the location of damage in structures.

- Multi-stage algorithms are highly suitable for extracting damage-sensitive features from non-stationary and stationary vibration signals when unmeasurable and unknown ambient excitations are subjected to the civil and mechanical systems.

Bibliography

[1] H. Vestli, H. G. Lemu, B. T. Svendsen, O. Gabrielsen, and S. C. Siriwardane, "Case studies on structural health monitoring of offshore bottom-fixed steel structures," in *The 27th International Ocean and Polar Engineering Conference*, OnePetro, 2017.

[2] T. J. Rogers, *Towards Bayesian system identification: with application to SHM of offshore structures*. PhD thesis, University of Sheffield, 2019.

[3] K. Worden and J. M. Dulieu-Barton, "An overview of intelligent fault detection in systems and structures," *Structural Health Monitoring*, vol. 3, no. 1, pp. 85–98, 2004.

[4] A. Rytter, *Vibrational based inspection of civil engineering structures*. PhD thesis, Aalborg, 1993.

[5] R. J. Barthorpe, *On model-and data-based approaches to structural health monitoring*. PhD thesis, University of Sheffield, 2010.

[6] C. R. Farrar and K. Worden, "An introduction to structural health monitoring," *Philosophical Transactions of the Royal Society A: Mathematical, Physical and Engineering Sciences*, vol. 365, no. 1851, pp. 303–315, 2007.

[7] C. R. Farrar and K. Worden, *Structural health monitoring: a machine learning perspective*. John Wiley & Sons, 2012.

[8] C. R. Farrar and N. A. Lieven, "Damage prognosis: the future of structural health monitoring," *Philosophical Transactions of the Royal Society A: Mathematical, Physical and Engineering Sciences*, vol. 365, no. 1851, pp. 623–632, 2007.

[9] C. Papadimitriou and E. Ntotsios, "Structural model updating using vibration measurements," 2009.

[10] B. Weber and P. Paultre, "Damage identification in a truss tower by regularized model updating," *Journal of structural engineering*, vol. 136, no. 3, pp. 307–316, 2010.

[11] J. E. Mottershead, M. Link, and M. I. Friswell, "The sensitivity method in finite element model updating: A tutorial," *Mechanical systems and signal processing*, vol. 25, no. 7, pp. 2275–2296, 2011.

[12] B. Moaveni, A. Stavridis, G. Lombaert, J. P. Conte, and P. B. Shing, "Finite-element model updating for assessment of progressive damage in a 3-story infilled rc frame," *Journal of Structural Engineering*, vol. 139, no. 10, pp. 1665–1674, 2013.

[13] S. Sehgal and H. Kumar, "Structural dynamic model updating techniques: a state of the art review," *Archives of Computational Methods in Engineering*, vol. 23, no. 3, pp. 515–533, 2016.

[14] D. Giagopoulos, A. Arailopoulos, V. Dertimanis, C. Papadimitriou, E. Chatzi, and K. Grompanopoulos, "Structural health monitoring and fatigue damage estimation using vibration measurements and finite element model updating," *Structural Health Monitoring*, vol. 18, no. 4, pp. 1189–1206, 2019.

[15] S. Mariani, F. Caimmi, G. Capellari, and S. E. Azam, "Online damage detection and model updating via proper orthogonal decomposition and recursive bayesian filters," 2021.

[16] M. Rezaiee-Pajand, A. Entezami, and H. Sarmadi, "A sensitivity-based finite element model updating based on unconstrained optimization problem and regularized solution methods," *Structural Control and Health Monitoring*, vol. 27, no. 5, p. e2481, 2020.

Bibliography

[17] O. Markogiannaki, A. Arailopoulos, D. Giagopoulos, and C. Papadimitriou, "Vibration-based damage detection framework of large-scale structural systems," in *Model Validation and Uncertainty Quantification, Volume 3*, pp. 179–186, Springer, 2022.

[18] A. Entezami and H. Shariatmadar, "Damage detection in structural systems by improved sensitivity of modal strain energy and tikhonov regularization method," *International Journal of Dynamics and Control*, vol. 2, no. 4, pp. 509–520, 2014.

[19] C. Zhang and Y. Xu, "Comparative studies on damage identification with tikhonov regularization and sparse regularization," *Structural control and health monitoring*, vol. 23, no. 3, pp. 560–579, 2016.

[20] A. Entezami, H. Shariatmadar, and H. Sarmadi, "Structural damage detection by a new iterative regularization method and an improved sensitivity function," *Journal of Sound and Vibration*, vol. 399, pp. 285–307, 2017.

[21] M. Rezaiee-Pajand, H. Sarmadi, and A. Entezami, "A hybrid sensitivity function and lanczos bidiagonalization-tikhonov method for structural model updating: Application to a full-scale bridge structure," *Applied Mathematical Modelling*, vol. 89, pp. 860–884, 2021.

[22] B. Weber, P. Paultre, and J. Proulx, "Consistent regularization of nonlinear model updating for damage identification," *Mechanical Systems and Signal Processing*, vol. 23, no. 6, pp. 1965–1985, 2009.

[23] M. I. Friswell, "Damage identification using inverse methods," in *Dynamic methods for damage detection in structures*, pp. 13–66, Springer, 2008.

[24] K. Worden and M. I. Friswell, "Modal–vibration-based damage identification," *Encyclopedia of Structural Health Monitoring*, 2009.

[25] C.-P. Fritzen, D. Jennewein, and T. Kiefer, "Damage detection based on model updating methods," *Mechanical systems and signal processing*, vol. 12, no. 1, pp. 163–186, 1998.

[26] V. Karbhari and L. S.-W. Lee, "Vibration-based damage detection techniques for structural health monitoring of civil infrastructure systems," in *Structural health monitoring of civil infrastructure systems*, pp. 177–212, Elsevier, 2009.

[27] M. G. Limongelli, M. Domaneschi, and L. Martinelli, "Vibration-based damage severity estimation basing on a non-model damage feature," in *IALCCE*, pp. 347–354, 2017.

[28] A. Entezami, H. Shariatmadar, and A. Karamodin, "Data-driven damage diagnosis under environmental and operational variability by novel statistical pattern recognition methods," *Structural Health Monitoring*, vol. 18, no. 5-6, pp. 1416–1443, 2019.

[29] C. Papadimitriou, E. N. Chatzi, S. E. Azam, and V. K. Dertimanis, "Fatigue monitoring and remaining lifetime prognosis using operational vibration measurements," in *Model Validation and Uncertainty Quantification, Volume 3*, pp. 133–136, Springer, 2019.

[30] A. Entezami, H. Shariatmadar, and S. Mariani, "Early damage assessment in large-scale structures by innovative statistical pattern recognition methods based on time series modeling and novelty detection," *Advances in Engineering Software*, vol. 150, p. 102923, 2020.

[31] E. Akintunde, S. E. Azam, A. Rageh, and D. G. Linzell, "Unsupervised machine learning for robust bridge damage detection: Full-scale experimental validation," *Engineering Structures*, vol. 249, p. 113250, 2021.

[32] R. Schalkoff, "Pattern recognition: Statistical, structural and neural approaches, john wiley & sons," *Inc. New York, NY*, 1992.

[33] C. R. Farrar, S. W. Doebling, and D. A. Nix, "Vibration–based structural damage identification," *Philosophical Transactions of the Royal Society of London. Series A: Mathematical, Physical and Engineering Sciences*, vol. 359, no. 1778, pp. 131–149, 2001.

[34] M. L. Wang, J. P. Lynch, and H. Sohn, *Sensor Technologies for Civil Infrastructures, Volume 1: Sensing Hardware and Data Collection Methods for Performance Assessment.* Elsevier, 2014.

[35] G. Capellari, E. Chatzi, and S. Mariani, "Cost-benefit optimization of sensor networks for shm applications," in *Multidisciplinary digital publishing institute proceedings*, vol. 2, p. 132, 2017.

[36] J. P. Lynch, "An overview of wireless structural health monitoring for civil structures," *Philosophical Transactions of the Royal Society A: Mathematical, Physical and Engineering Sciences*, vol. 365, no. 1851, pp. 345–372, 2007.

[37] H. Sohn, "Effects of environmental and operational variability on structural health monitoring," *Philosophical Transactions of the Royal Society A: Mathematical, Physical and Engineering Sciences*, vol. 365, no. 1851, pp. 539–560, 2007.

[38] G. Park and D. J. Inman, "Structural health monitoring using piezoelectric impedance measurements," *Philosophical Transactions of the Royal Society A: Mathematical, Physical and Engineering Sciences*, vol. 365, no. 1851, pp. 373–392, 2007.

[39] M. D. Todd, J. M. Nichols, S. T. Trickey, M. Seaver, C. J. Nichols, and L. N. Virgin, "Bragg grating-based fibre optic sensors in structural health monitoring," *Philosophical Transactions of the Royal Society A: Mathematical, Physical and Engineering Sciences*, vol. 365, no. 1851, pp. 317–343, 2007.

[40] A. Entezami, *Structural Health Monitoring by Time Series Analysis and Statistical Distance Measures*. Springer, 2021.

[41] S. W. Doebling, C. R. Farrar, M. B. Prime, and D. W. Shevitz, "Damage identification and health monitoring of structural and mechanical systems from changes in their vibration characteristics: a literature review," 1996.

[42] H. Sohn, C. R. Farrar, F. M. Hemez, D. D. Shunk, S. Stinemates, B. R. Nadler, and J. J. Czarnecki, "A review of structural health monitoring literature form 1996-2001," *Los Alamos National Laboratory*, 2004.

[43] D. Wisch, "Fixed steel offshore structure design-past, present & future," in *Offshore technology conference*, OnePetro, 1998.

[44] J. Nichols, "Structural health monitoring of offshore structures using ambient excitation," *Applied Ocean Research*, vol. 25, no. 3, pp. 101–114, 2003.

[45] C. R. Farrar and K. Worden, "New trends in vibration based structural health monitoring," *An introduction to structural health monitoring*, pp. 1–17, 2010.

[46] S. Wang, F. Liu, and M. Zhang, "Modal strain energy based structural damage localization for offshore platform using simulated and measured data," *Journal of Ocean University of China*, vol. 13, no. 3, pp. 397–406, 2014.

[47] N. Dervilis, K. Worden, and E. Cross, "On robust regression analysis as a means of exploring environmental and operational conditions for shm data," *Journal of Sound and Vibration*, vol. 347, pp. 279–296, 2015.

[48] E. J. Cross, K. Worden, and Q. Chen, "Cointegration: a novel approach for the removal of environmental trends in structural health monitoring data," *Proceedings of the Royal Society A: Mathematical, Physical and Engineering Sciences*, vol. 467, no. 2133, pp. 2712–2732, 2011.

[49] E. Cross, *On structural health monitoring in changing environmental and operational conditions*. PhD thesis, University of Sheffield, 2012.

[50] J. L. Beck and L. S. Katafygiotis, "Updating models and their uncertainties. i: Bayesian statistical framework," *Journal of Engineering Mechanics*, vol. 124, no. 4, pp. 455–461, 1998.

[51] G. Steenackers and P. Guillaume, "Finite element model updating taking into account the uncertainty on the modal parameters estimates," *Journal of Sound and Vibration*, vol. 296, no. 4-5, pp. 919–934, 2006.

[52] B. Peeters and G. De Roeck, "One-year monitoring of the z24-bridge: environmental effects versus damage events," *Earthquake engineering & structural dynamics*, vol. 30, no. 2, pp. 149–171, 2001.

[53] A. Iliopoulos, W. Weijtjens, D. Van Hemelrijck, and C. Devriendt, "Fatigue assessment of offshore wind turbines on monopile foundations using multi-band modal expansion," *Wind Energy*, vol. 20, no. 8, pp. 1463–1479, 2017.

[54] A. Skafte, U. T. Tygesen, and R. Brincker, "Expansion of mode shapes and responses on the offshore platform valdemar," in *Dynamics of Civil Structures, Volume 4*, pp. 35–41, Springer, 2014.

[55] N. Perišić and U. T. Tygesen, "Cost-effective load monitoring methods for fatigue life estimation of offshore platform," in *International Conference on Offshore Mechanics and Arctic Engineering*, vol. 45431, p. V04BT02A005, American Society of Mechanical Engineers, 2014.

[56] N. Perišić, P. H. Kirkegaard, and U. T. Tygesen, "Load identification of offshore platform for fatigue life estimation," in *Structural Health Monitoring, Volume 5*, pp. 99–109, Springer, 2014.

[57] L. Ziegler, S. Voormeeren, S. Schafhirt, and M. Muskulus, "Design clustering of offshore wind turbines using probabilistic fatigue load estimation," *Renewable Energy*, vol. 91, pp. 425–433, 2016.

[58] K. Maes, A. Iliopoulos, W. Weijtjens, C. Devriendt, and G. Lombaert, "Dynamic strain estimation for fatigue assessment of an offshore monopile wind turbine using filtering and modal expansion algorithms," *Mechanical Systems and Signal Processing*, vol. 76, pp. 592–611, 2016.

[59] J. F. Wilson, *Dynamics of offshore structures*. John Wiley & Sons, 2003.

Bibliography

[60] T. Nogami, J. Otani, K. Konagai, and H.-L. Chen, "Nonlinear soil-pile interaction model for dynamic lateral motion," *Journal of Geotechnical Engineering*, vol. 118, no. 1, pp. 89–106, 1992.

[61] L. M. Bryant and H. M. Matlock, "Three-dimensional analysis of framed structures with nonlinear pile foundations," in *Offshore Technology Conference*, OnePetro, 1977.

[62] L. V. Andersen, M. Vahdatirad, M. T. Sichani, and J. D. Sørensen, "Natural frequencies of wind turbines on monopile foundations in clayey soils—a probabilistic approach," *Computers and Geotechnics*, vol. 43, pp. 1–11, 2012.

[63] S. Bisoi and S. Haldar, "Dynamic analysis of offshore wind turbine in clay considering soil–monopile–tower interaction," *Soil Dynamics and Earthquake Engineering*, vol. 63, pp. 19–35, 2014.

[64] D. M. Duggan, E. R. Wallace, and S. R. Caldwell, "Measured and predicted vibrational behavior of gulf of mexico platforms," in *Offshore Technology Conference*, OnePetro, 1980.

[65] R. M. Kenley and C. J. Dodds, "West sole we platform: Detection of damage by structural response measurements," in *Offshore technology conference*, OnePetro, 1980.

[66] H. Crohas and P. Lepert, "Damage-detection monitoring method for offshore platforms is field-tested," *Oil Gas J.;(United States)*, vol. 80, no. 8, 1982.

[67] R. Nataraja, "Structural integrity monitoring in real seas," in *Offshore Technology Conference*, OnePetro, 1983.

[68] T. Whittome and C. Dodds, "9 monitoring offshore structures by vibration techniques," in *Design in Offshore Structures*, pp. 93–100, Thomas Telford Publishing, 1983.

[69] R. D. Begg, A. C. Mackenzie, C. J. Dodds, and O. D. Loland, "Structural integrity monitoring using digital processing of vibration siqnals," in *Offshore Technology Conference*, OnePetro, 1976.

[70] J. C. Yang, N. G. Dagalakis, and M. Hirt, "Application of the random decrement technique in the detection of an induced crack on an offshore platform model," in *Computational Methods for Offshore Structures. The winter annual meeting of the American Society of Mechanical Engineers*, vol. 37, pp. 55–67, American Society of Mechanical Engineers, New York, 1980.

[71] R. Osegueda, P. Dsouza, and Y. Qiang, "Damage evaluation of offshore structures using resonant frequency shifts," *Serviceability of Petroleum, Process, and Power Equipment, ASME PVP*, vol. 239, pp. 31–37, 1992.

[72] M. d. C. Feijóo, Y. Zambrano, Y. Vidal, and C. Tutivén, "Unsupervised damage detection for offshore jacket wind turbine foundations based on an autoencoder neural network," *Sensors*, vol. 21, no. 10, p. 3333, 2021.

[73] J. K. Vandiver, "Detection of structural failure on fixed platforms by measurement of dynamic response," in *Offshore Technology Conference*, OnePetro, 1975.

[74] O. Loland and C. J. Dodds, "Experiences in developing and operating integrity monitoring systems in the north sea," in *Presented at the Eighth Annual Offshore Technology Conference, Houston, Texas, May 3-6, 1976.*, no. V2, OTC 2551 Proceeding, 1976.

[75] M. E. Wojnarowski, S. G. Stiansen, and N. E. Reddy, "Structural integrity evaluation of a fixed platform using vibration criteria," in *Offshore Technology Conference*, OnePetro, 1977.

[76] R. Coppolino and S. Rubin, "Detectability of structural failures in offshore platforms by ambient vibration monitoring," in *Offshore Technology Conference*, OnePetro, 1980.

[77] P. Lepert, M. Chay, J. Y. Heas, and P. Narzul, "Vibro-detection applied to offshore platforms," in *Offshore Technology Conference*, OnePetro, 1980.

[78] J.-T. Kim and N. Stubbs, "Damage detection in offshore jacket structures from limited modal information," *International Journal of Offshore and Polar Engineering*, vol. 5, no. 01, 1995.

[79] N. Roitman and P. F. Viero, "Detection and location of damages in offshore platforms: An application of some methods using eigenvectors," in *Proceedings-SPIE the international society for optical engineering*, pp. 1124–1131, SPIE International society for optical, 1997.

[80] H. Yang, H. Li, and W. Huang, "Experimental modal analysis of offshore platform under operational conditions," *Journal of vibration and shock*, vol. 24, no. 2, pp. 129–133, 2005.

[81] S. Wang, H. Li, and J. Han, "Damage detection of an offshore jacket structure from partial modal information: numerical study," in *The Seventh ISOPE Pacific/Asia Offshore Mechanics Symposium*, OnePetro, 2006.

[82] X. Shi, T. Matsui, H. J. Li, and C. Gong, "A damage detection algorithm based on partial measurement for offshore jacket platforms," in *The Seventeenth International Offshore and Polar Engineering Conference*, OnePetro, 2007.

[83] Y.-s. Cheng and Z. Wang, "Detecting damage to offshore platform structures using the time-domain data," *Journal of Marine Science and Application*, vol. 7, no. 1, pp. 7–14, 2008.

[84] B. Asgarian, M. Amiri, and A. Ghafooripour, "Damage detection in jacket type offshore platforms using modal strain energy," *Structural Engineering and Mechanics*, vol. 33, no. 3, pp. 325–337, 2009.

[85] A. A. Elshafey, M. R. Haddara, and H. Marzouk, "Damage detection in offshore structures using neural networks," *Marine Structures*, vol. 23, no. 1, pp. 131–145, 2010.

[86] A. J. Hillis and C. Courtney, "Structural health monitoring of fixed offshore structures using the bicoherence function of ambient vibration measurements," *Journal of sound and vibration*, vol. 330, no. 6, pp. 1141–1152, 2011.

[87] Y. S. Diao, Q. L. Zhang, and D. M. Meng, "Structural damage identification based on acceleration response vibration transmissibility," in *Applied Mechanics and Materials*, vol. 236, pp. 640–645, Trans Tech Publ, 2012.

[88] S. Wang, "Damage detection in offshore platform structures from limited modal data," *Applied Ocean Research*, vol. 41, pp. 48–56, 2013.

[89] P. Kraemer and H. Friedmanna, "Vibration-based structural health monitoring for offshore wind turbines-experimental validation of stochastic subspace algorithms," *Wind & structures*, vol. 21, no. 6, pp. 693–707, 2015.

[90] J.-H. Yi, "Laboratory tests on local damage detection for jacket-type offshore structures using optical fbg sensors based on statistical approaches," *Ocean Engineering*, vol. 124, pp. 94–103, 2016.

[91] W. Kim, J.-H. Yi, and J.-S. Park, "Structural damage detection for hybrid offshore wind and tidal current turbine," in *8th Conference on Smart Structures and Materials, SMART 2017 and 6th International Conference on Smart Materials and Nanotechnology in Engineering*, pp. 247–254, International Center for Numerical Methods in Engineering, 2017.

[92] G. Oliveira, F. Magalhães, Á. Cunha, and E. Caetano, "Vibration-based damage detection in a wind turbine using 1 year of data," *Structural Control and Health Monitoring*, vol. 25, no. 11, p. e2238, 2018.

[93] Y. Vidal Seguí, J. L. Rubias, and F. Pozo Montero, "Wind turbine health monitoring based on accelerometer data," in *9th ECCOMAS Thematic Conference on Smart Structures and Materials*, pp. 1604–1611, 2019.

[94] Z. Jiang, M. Bjørnholm, J. Guo, W. Dong, Z. Ren, and A. S. Verma, "Damage identification of a jacket support structure for offshore wind turbines," in *2020 15th IEEE Conference on Industrial Electronics and Applications (ICIEA)*, pp. 995–1000, IEEE, 2020.

[95] Y. Vidal, G. Aquino, F. Pozo, and J. E. M. Gutiérrez-Arias, "Structural health monitoring for jacket-type offshore wind turbines: Experimental proof of concept," *Sensors*, vol. 20, no. 7, p. 1835, 2020.

[96] B. Puruncajas, Y. Vidal, and C. Tutivén, "Vibration-response-only structural health monitoring for offshore wind turbine jacket foundations via convolutional neural networks," *Sensors*, vol. 20, no. 12, p. 3429, 2020.

[97] X. Bao, T. Fan, C. Shi, and G. Yang, "One-dimensional convolutional neural network for damage detection of jacket-type offshore platforms," *Ocean Engineering*, vol. 219, p. 108293, 2021.

[98] X. Bao, Z. Wang, and G. Iglesias, "Damage detection for offshore structures using long and short-term memory networks and random decrement technique," *Ocean Engineering*, vol. 235, p. 109388, 2021.

[99] X. Bao, T. Fan, C. Shi, and G. Yang, "Deep learning methods for damage detection of jacket-type offshore platforms," *Process Safety and Environmental Protection*, vol. 154, pp. 249–261, 2021.

[100] A. Entezami, H. Shariatmadar, and A. Karamodin, "Improving feature extraction via time series modeling for structural health monitoring based on unsupervised learning methods," *Scientia Iranica*, vol. 27, no. 3, pp. 1001–1018, 2020.

[101] H. Sohn and C. R. Farrar, "Damage diagnosis using time series analysis of vibration signals," *Smart materials and structures*, vol. 10, no. 3, p. 446, 2001.

[102] M. Rezaiee-Pajand, A. Entezami, and H. Shariatmadar, "An iterative order determination method for time-series modeling in structural health monitoring," *Advances in Structural Engineering*, vol. 21, no. 2, pp. 300–314, 2018.

[103] A. Entezami, H. Sarmadi, M. Salar, A. Behkamal, A. Arslan, and C. De Michele, "A novel structural feature extraction method via time series modelling and machine learning techniques for early damage detection in civil and architectural buildings," in *International conference on emerging technologies in architectural design (ICETAD2019)*, 2019.

[104] B. Monavari, T. H. Chan, A. Nguyen, D. P. Thambiratnam, and K.-D. Nguyen, "Structural deterioration localization using enhanced autoregressive time-series analysis," *International Journal of Structural Stability and Dynamics*, vol. 20, no. 10, p. 2042013, 2020.

[105] A. Entezami, "Feature extraction in time-frequency domain for non-stationary data," in *Structural Health Monitoring by Time Series Analysis and Statistical Distance Measures*, pp. 47–57, Springer, 2021.

[106] A. Entezami, S. Mariani, and H. Shariatmadar, "Damage detection in largely unobserved structures under varying environmental conditions: An autoregressive spectrum and multi-level machine learning methodology," *Sensors*, vol. 22, no. 4, p. 1400, 2022.

[107] H. Sohn, J. A. Czarnecki, and C. R. Farrar, "Structural health monitoring using statistical process control," *Journal of structural engineering*, vol. 126, no. 11, pp. 1356–1363, 2000.

[108] M. L. Fugate, H. Sohn, and C. R. Farrar, "Vibration-based damage detection using statistical process control," *Mechanical systems and signal processing*, vol. 15, no. 4, pp. 707–721, 2001.

[109] H. Sohn, C. R. Farrar, N. F. Hunter, and K. Worden, "Structural health monitoring using statistical pattern recognition techniques," *J. Dyn. Sys., Meas., Control*, vol. 123, no. 4, pp. 706–711, 2001.

[110] K. K. Nair, A. S. Kiremidjian, and K. H. Law, "Time series-based damage detection and localization algorithm with application to the asce benchmark structure," *Journal of Sound and Vibration*, vol. 291, no. 1-2, pp. 349–368, 2006.

[111] M. Gul and F. N. Catbas, "Structural health monitoring and damage assessment using a novel time series analysis methodology with sensor clustering," *Journal of Sound and Vibration*, vol. 330, no. 6, pp. 1196–1210, 2011.

[112] A. M. Ay and Y. Wang, "Structural damage identification based on self-fitting armax model and multi-sensor data fusion," *Structural Health Monitoring*, vol. 13, no. 4, pp. 445–460, 2014.

[113] A. A. Mosavi, D. Dickey, R. Seracino, and S. Rizkalla, "Identifying damage locations under ambient vibrations utilizing vector autoregressive models and mahalanobis distances," *Mechanical systems and signal processing*, vol. 26, pp. 254–267, 2012.

[114] G. E. Box, G. M. Jenkins, G. C. Reinsel, and G. M. Ljung, *Time series analysis: forecasting and control*. John Wiley & Sons, 2015.

[115] G. Kitagawa, *Introduction to time series modeling*. CRC press, 2010.

[116] O. R. de Lautour and P. Omenzetter, "Damage classification and estimation in experimental structures using time series analysis and pattern recognition," *Mechanical Systems and Signal Processing*, vol. 24, no. 5, pp. 1556–1569, 2010.

[117] R. Yao and S. N. Pakzad, "Autoregressive statistical pattern recognition algorithms for damage detection in civil structures," *Mechanical Systems and Signal Processing*, vol. 31, pp. 355–368, 2012.

[118] E. P. Carden and J. M. Brownjohn, "Arma modelled time-series classification for structural health monitoring of civil infrastructure," *Mechanical systems and signal processing*, vol. 22, no. 2, pp. 295–314, 2008.

[119] Z. Wang and K. Ong, "Autoregressive coefficients based hotelling's t2 control chart for structural health monitoring," *Computers & structures*, vol. 86, no. 19-20, pp. 1918–1935, 2008.

[120] J. L. Zapico-Valle, M. García-Diéguez, M. P. González-Martínez, and K. Worden, "Experimental validation of a new statistical process control feature for damage detection," *Mechanical Systems and Signal Processing*, vol. 25, no. 7, pp. 2513–2525, 2011.

[121] M. Gul and F. N. Catbas, "Statistical pattern recognition for structural health monitoring using time series modeling: Theory and experimental verifications," *Mechanical Systems and Signal Processing*, vol. 23, no. 7, pp. 2192–2204, 2009.

[122] B. Zima and M. Rucka, "Guided waves for monitoring of plate structures with linear cracks of variable length," *Archives of civil and mechanical engineering*, vol. 16, no. 3, pp. 387–396, 2016.

[123] E. Figueiredo, G. Park, C. R. Farrar, K. Worden, and J. Figueiras, "Machine learning algorithms for damage detection under operational and environmental variability," *Structural Health Monitoring*, vol. 10, no. 6, pp. 559–572, 2011.

[124] H. Sohn, K. Worden, and C. R. Farrar, "Statistical damage classification under changing environmental and operational conditions," *Journal of intelligent material systems and structures*, vol. 13, no. 9, pp. 561–574, 2002.

[125] J. Kullaa, "Is temperature measurement essential in structural health monitoring?," in *Proceedings of the 4th International Workshop on Structural Health Monitoring, Stanford, CA., September 1517, 2003*, p. 717724, 2003.

[126] C. K. Oh and H. Sohn, "Damage diagnosis under environmental and operational variations using unsupervised support vector machine," *Journal of sound and vibration*, vol. 325, no. 1-2, pp. 224–239, 2009.

[127] V. Papakos and S. Fassois, "Multichannel identification of aircraft skeleton structures under unobservable excitation: a vector ar/arma framework," *Mechanical Systems and Signal Processing*, vol. 17, no. 6, pp. 1271–1290, 2003.

[128] P. C. Mahalanobis, "On the generalized distance in statistics," National Institute of Science of India, 1936.

[129] K. G. Jöreskog, "A general approach to confirmatory maximum likelihood factor analysis," *Psychometrika*, vol. 34, no. 2, pp. 183–202, 1969.

[130] S. Sharma, *Applied multivariate techniques*. John Wiley & Sons Inc., 1996.

[131] M. J. Zaki, W. Meira Jr, and W. Meira, *Data mining and analysis: fundamental concepts and algorithms*. Cambridge University Press, 2014.

[132] A. Sophian, G. Y. Tian, D. Taylor, and J. Rudlin, "A feature extraction technique based on principal component analysis for pulsed eddy current ndt," *NDT & e International*, vol. 36, no. 1, pp. 37–41, 2003.

[133] L. Zhong, H. Song, and B. Han, "Extracting structural damage features: Comparison between pca and ica," in *Intelligent Computing in Signal Processing and Pattern Recognition*, pp. 840–845, Springer, 2006.

[134] S. Park, J.-J. Lee, C.-B. Yun, and D. J. Inman, "Electro-mechanical impedance-based wireless structural health monitoring using pca-data compression and k-means clustering algorithms," *Journal of intelligent material systems and structures*, vol. 19, no. 4, pp. 509–520, 2008.

[135] D. A. Tibaduiza, L. E. Mujica, J. Rodellar, and A. Güemes, "Structural damage detection using principal component analysis and damage indices," *Journal of Intelligent Material Systems and Structures*, vol. 27, no. 2, pp. 233–248, 2016.

[136] J. P. Amezquita-Sanchez and H. Adeli, "Signal processing techniques for vibration-based health monitoring of smart structures," *Archives of Computational Methods in Engineering*, vol. 23, no. 1, pp. 1–15, 2016.

[137] L. D. Avendaño-Valencia, E. N. Chatzi, K. Y. Koo, and J. M. Brownjohn, "Gaussian process time-series models for structures under operational variability," *Frontiers in Built Environment*, vol. 3, p. 69, 2017.

[138] A. Liu, L. Wang, L. Bornn, and C. Farrar, "Robust structural health monitoring under environmental and operational uncertainty with switching state-space autoregressive models," *Structural Health Monitoring*, vol. 18, no. 2, pp. 435–453, 2019.

[139] A. G. Poulimenos and J. S. Sakellariou, "A transmittance-based methodology for damage detection under uncertainty: An application to a set of composite beams with manufacturing variability subject to impact damage and varying operating conditions," *Structural Health Monitoring*, vol. 18, no. 1, pp. 318–333, 2019.

[140] A. Entezami, H. Sarmadi, B. Behkamal, and S. Mariani, "Big data analytics and structural health monitoring: a statistical pattern recognition-based approach," *Sensors*, vol. 20, no. 8, p. 2328, 2020.

[141] A. Entezami and H. Shariatmadar, "An unsupervised learning approach by novel damage indices in structural health monitoring for damage localization and quantification," *Structural Health Monitoring*, vol. 17, no. 2, pp. 325–345, 2018.

[142] M. Döhler, F. Hille, L. Mevel, and W. Rücker, "Structural health monitoring with statistical methods during progressive damage test of s101 bridge," *Engineering Structures*, vol. 69, pp. 183–193, 2014.

[143] A. Entezami, H. Shariatmadar, and S. Mariani, "Structural health monitoring for condition assessment using efficient supervised learning techniques," in *Multidisciplinary Digital Publishing Institute Proceedings*, vol. 42, p. 17, 2019.

[144] A. Entezami, H. Shariatmadar, and S. Mariani, "Fast unsupervised learning methods for structural health monitoring with large vibration data from dense sensor networks," *Structural Health Monitoring*, vol. 19, no. 6, pp. 1685–1710, 2020.

[145] M. Yeager, B. Gregory, C. Key, and M. Todd, "On using robust mahalanobis distance estimations for feature discrimination in a damage detection scenario," *Structural Health Monitoring*, vol. 18, no. 1, pp. 245–253, 2019.

[146] H. Sarmadi and A. Karamodin, "A novel anomaly detection method based on adaptive mahalanobis-squared distance and one-class knn rule for structural health monitoring under environmental effects," *Mechanical Systems and Signal Processing*, vol. 140, p. 106495, 2020.

Bibliography

[147] C. Modarres, N. Astorga, E. L. Droguett, and V. Meruane, "Convolutional neural networks for automated damage recognition and damage type identification," *Structural Control and Health Monitoring*, vol. 25, no. 10, p. e2230, 2018.

[148] D. B. Verstraete, E. L. Droguett, V. Meruane, M. Modarres, and A. Ferrada, "Deep semi-supervised generative adversarial fault diagnostics of rolling element bearings," *Structural Health Monitoring*, vol. 19, no. 2, pp. 390–411, 2020.

[149] S. Chen, S. Zhou, C. Chen, Y. Li, and S. Zhai, "Detection of double defects for plate-like structures based on a fuzzy c-means clustering algorithm," *Structural Health Monitoring*, vol. 18, no. 3, pp. 757–766, 2019.

[150] G. V. Demarie and D. Sabia, "A machine learning approach for the automatic long-term structural health monitoring," *Structural Health Monitoring*, vol. 18, no. 3, pp. 819–837, 2019.

[151] D. A. Tibaduiza, L. E. Mujica, and J. Rodellar, "Damage classification in structural health monitoring using principal component analysis and self-organizing maps," *Structural Control and Health Monitoring*, vol. 20, no. 10, pp. 1303–1316, 2013.

[152] V. Meruane, C. Espinoza, E. L. Droguett, and A. Ortiz-Bernardin, "Impact identification using nonlinear dimensionality reduction and supervised learning," *Smart Materials and Structures*, vol. 28, no. 11, p. 115005, 2019.

[153] N. L. Khoa, B. Zhang, Y. Wang, F. Chen, and S. Mustapha, "Robust dimensionality reduction and damage detection approaches in structural health monitoring," *Structural Health Monitoring*, vol. 13, no. 4, pp. 406–417, 2014.

[154] G. San Martin, E. López Droguett, V. Meruane, and M. das Chagas Moura, "Deep variational auto-encoders: A promising tool for dimensionality reduction and ball bearing elements fault diagnosis," *Structural Health Monitoring*, vol. 18, no. 4, pp. 1092–1128, 2019.

[155] C. Mylonas, I. Abdallah, and E. Chatzi, "Deep unsupervised learning for condition monitoring and prediction of high dimensional data with application on windfarm scada data," in *Model Validation and Uncertainty Quantification, Volume 3*, pp. 189–196, Springer, 2020.

[156] A. Entezami, H. Sarmadi, and S. Mariani, "An unsupervised learning approach for early damage detection by time series analysis and deep neural network to deal with output-only (big) data," in *Engineering Proceedings*, vol. 2, p. 17, Multidisciplinary Digital Publishing Institute, 2020.

[157] I. Lopez and N. Sarigul-Klijn, "Distance similarity matrix using ensemble of dimensional data reduction techniques: vibration and aerocoustic case studies," *Mechanical Systems and Signal Processing*, vol. 23, no. 7, pp. 2287–2300, 2009.

[158] L. E. Mujica, J. Vehí, M. Ruiz, M. Verleysen, W. Staszewski, and K. Worden, "Multivariate statistics process control for dimensionality reduction in structural assessment," *Mechanical Systems and Signal Processing*, vol. 22, no. 1, pp. 155–171, 2008.

[159] M. REBILLAT and N. MECHBAL, "Dimension reduction algorithms in the damage indexes space for damage size quantification in aeronautic composite structures," *Structural Health Monitoring 2019*, 2019.

[160] H. Sarmadi and A. Entezami, "Application of supervised learning to validation of damage detection," *Archive of Applied Mechanics*, vol. 91, no. 1, pp. 393–410, 2021.

[161] A. Deraemaeker and K. Worden, "A comparison of linear approaches to filter out environmental effects in structural health monitoring," *Mechanical systems and signal processing*, vol. 105, pp. 1–15, 2018.

[162] M. Rebillat, O. Hmad, F. Kadri, and N. Mechbal, "Peaks over threshold–based detector design for structural health monitoring: Application to aerospace structures," *Structural Health Monitoring*, vol. 17, no. 1, pp. 91–107, 2018.

[163] H. Sarmadi and K.-V. Yuen, "Early damage detection by an innovative unsupervised learning method based on kernel null space and peak-over-threshold," *Computer-Aided Civil and Infrastructure Engineering*, 2021.

[164] A. Entezami and H. Shariatmadar, "Damage localization under ambient excitations and non-stationary vibration signals by a new hybrid algorithm for feature extraction and multivariate distance correlation methods," *Structural Health Monitoring*, vol. 18, no. 2, pp. 347–375, 2019.

[165] I. Borg and P. J. Groenen, *Modern multidimensional scaling: Theory and applications.* Springer Science & Business Media, 2005.

[166] P. A. Forero and G. B. Giannakis, "Robust multi-dimensional scaling via outlier-sparsity control," in *2011 Conference Record of the Forty Fifth Asilomar Conference on Signals, Systems and Computers (ASILOMAR)*, pp. 1183–1187, IEEE, 2011.

[167] A. Entezami, H. Sarmadi, B. Behkamal, and S. Mariani, "Health monitoring of large-scale civil structures: An approach based on data partitioning and classical multidimensional scaling," *Sensors*, vol. 21, no. 5, p. 1646, 2021.

[168] S. Coles, J. Bawa, L. Trenner, and P. Dorazio, *An introduction to statistical modeling of extreme values*, vol. 208. Springer, 2001.

[169] G. Salvadori, C. De Michele, N. T. Kottegoda, and R. Rosso, *Extremes in nature: an approach using copulas*, vol. 56. Springer Science & Business Media, 2007.

[170] Y. Xia, B. Chen, S. Weng, Y.-Q. Ni, and Y.-L. Xu, "Temperature effect on vibration properties of civil structures: a literature review and case studies," *Journal of civil structural health monitoring*, vol. 2, no. 1, pp. 29–46, 2012.

[171] Q. Han, Q. Ma, J. Xu, and M. Liu, "Structural health monitoring research under varying temperature condition: a review," *Journal of Civil Structural Health Monitoring*, pp. 1–25, 2020.

[172] H.-Q. Mu and K.-V. Yuen, "Modal frequency-environmental condition relation development using long-term structural health monitoring measurement: Uncertainty quantification, sparse feature selection and multivariate prediction," *Measurement*, vol. 130, pp. 384–397, 2018.

[173] O. Avci, O. Abdeljaber, S. Kiranyaz, M. Hussein, M. Gabbouj, and D. J. Inman, "A review of vibration-based damage detection in civil structures: From traditional methods to machine learning and deep learning applications," *Mechanical systems and signal processing*, vol. 147, p. 107077, 2021.

[174] A. Entezami, H. Shariatmadar, and C. De Michele, "Non-parametric empirical machine learning for short-term and long-term structural health monitoring," *Structural Health Monitoring*, p. 14759217211069842, 2022.

[175] J. P. Santos, C. Crémona, L. Calado, P. Silveira, and A. D. Orcesi, "On-line unsupervised detection of early damage," *Structural Control and Health Monitoring*, vol. 23, no. 7, pp. 1047–1069, 2016.

[176] A. Diez, N. L. D. Khoa, M. M. Alamdari, Y. Wang, F. Chen, and P. Runcie, "A clustering approach for structural health monitoring on bridges," *Journal of Civil Structural Health Monitoring*, vol. 6, no. 3, pp. 429–445, 2016.

[177] R. de Almeida Cardoso, A. Cury, and F. Barbosa, "Automated real-time damage detection strategy using raw dynamic measurements," *Engineering Structures*, vol. 196, p. 109364, 2019.

[178] H. Sarmadi, A. Entezami, M. Salar, and C. De Michele, "Bridge health monitoring in environmental variability by new clustering and threshold estimation methods," *Journal of Civil Structural Health Monitoring*, vol. 11, no. 3, pp. 629–644, 2021.

[179] S. da Silva, M. D. Junior, V. L. Junior, and M. J. Brennan, "Structural damage detection by fuzzy clustering," *Mechanical Systems and Signal Processing*, vol. 22, no. 7, pp. 1636–1649, 2008.

[180] E. Figueiredo and E. Cross, "Linear approaches to modeling nonlinearities in long-term monitoring of bridges," *Journal of Civil Structural Health Monitoring*, vol. 3, no. 3, pp. 187–194, 2013.

[181] C. Yang, Y. Liu, and Y. Sun, "Damage detection of bridges considering environmental temperature effect by using cluster analysis," *Procedia engineering*, vol. 161, pp. 577–582, 2016.

[182] J. Wu, *Advances in K-means clustering: a data mining thinking*. Springer Science & Business Media, 2012.

[183] G. Gan, C. Ma, and J. Wu, *Data clustering: theory, algorithms, and applications*. SIAM, 2020.

[184] C. C. Aggarwal and C. K. Reddy, "Data clustering," *Algorithms and applications. Chapman&Hall/CRC Data mining and Knowledge Discovery series, Londra*, 2014.

[185] D. J. Weller-Fahy, B. J. Borghetti, and A. A. Sodemann, "A survey of distance and similarity measures used within network intrusion anomaly detection," *IEEE Communications Surveys & Tutorials*, vol. 17, no. 1, pp. 70–91, 2014.

[186] M. M. Deza and E. Deza, *Encyclopedia of Distances*. Springer, 2016.

[187] J. Abello, P. M. Pardalos, and M. G. Resende, *Handbook of massive data sets*, vol. 4. Springer, 2013.

[188] M. Krit, O. Gaudoin, and E. Remy, "Goodness-of-fit tests for the weibull and extreme value distributions: A review and comparative study," *Communications in Statistics-Simulation and Computation*, pp. 1–24, 2019.

[189] P. Perez-Rodriguez, H. Vaquera-Huerta, and J. A. Villaseñor-Alva, "A goodness-of-fit test for the gumbel distribution based on kullback–leibler information," *Communications in Statistics—Theory and Methods*, vol. 38, no. 6, pp. 842–855, 2009.

Bibliography

[190] A. Khennane, *Introduction to finite element analysis using MATLAB® and abaqus*. CRC Press, 2013.

[191] M. I. Friswell and J. E. Penny, "Crack modeling for structural health monitoring," *Structural health monitoring*, vol. 1, no. 2, pp. 139–148, 2002.

[192] P. Paultre, *Dynamics of structures*. John Wiley & Sons, 2013.

[193] O. Chavez, J. Millan-Almaraz, R. Pérez-Enríquez, J. Arzate-Flores, A. Kotsarenko, J. Cruz-Abeyro, and E. Rojas, "Detection of ulf geomagnetic signals associated with seismic events in central mexico using discrete wavelet transform," *Natural Hazards and Earth System Sciences*, vol. 10, no. 12, pp. 2557–2564, 2010.

[194] E. Figueiredo, G. Park, J. Figueiras, C. Farrar, and K. Worden, "Structural health monitoring algorithm comparisons using standard data sets," tech. rep., Los Alamos National Lab.(LANL), Los Alamos, NM (United States), 2009.

[195] S. J. Dyke, D. Bernal, J. Beck, and C. Ventura, "Experimental phase ii of the structural health monitoring benchmark problem," in *Proceedings of the 16th ASCE engineering mechanics conference*, 2003.

[196] S. Li, H. Li, Y. Liu, C. Lan, W. Zhou, and J. Ou, "Smc structural health monitoring benchmark problem using monitored data from an actual cable-stayed bridge," *Structural Control and Health Monitoring*, vol. 21, no. 2, pp. 156–172, 2014.

[197] A. Entezami, H. Sarmadi, M. Salar, C. De Michele, and A. N. Arslan, "A novel data-driven method for structural health monitoring under ambient vibration and high-dimensional features by robust multidimensional scaling," *Structural Health Monitoring*, p. 1475921720973953, 2020.

[198] H. Li, J. Wang, and S.-L. J. Hu, "Using incomplete modal data for damage detection in offshore jacket structures," *Ocean Engineering*, vol. 35, no. 17-18, pp. 1793–1799, 2008.

[199] J. Maeck and G. De Roeck, "Description of z24 benchmark," *Mechanical Systems and Signal Processing*, vol. 17, no. 1, pp. 127–131, 2003.

[200] H. Sarmadi, A. Entezami, B. Saeedi Razavi, and K.-V. Yuen, "Ensemble learning-based structural health monitoring by mahalanobis distance metrics," *Structural Control and Health Monitoring*, vol. 28, no. 2, p. e2663, 2021.